

**Synthesis and characterization of inorganic nanoparticles,
and analysis of their uptake by cells and plants for
in vitro and *in vivo* imaging**

Dissertation

zur Erlangung des Doktorgrades

der Naturwissenschaften

(Dr.rer.nat)

dem

Fachbereich Chemie

der Universität Hamburg

vorgelegt von

Yang Liu

aus

Jilin, China

Hamburg, 2022

The presented work conducted under the supervision of Prof. Wolfgang Parak and Dr. Neus Feliu at the Center for Hybrid Nanostructures (CHyN) of the University of Hamburg, Germany (from September 2018 to March 2022).

Thesis Committee:

Prof. Dr. Wolfgang Parak

Prof. Dr. Florian Grüner

Evaluation Committee:

Prof. Dr. Wolfgang Parak

Prof. Dr. Tobias Beck

Prof. Dr. Michael Fröba

Disputation date:

20.05.2022

Index

Abstract.....	1
Zusammenfassung	2
1. Introduction	3
1.1 Nanoparticles application	3
1.2. Techniques used for investigating NPs in plant and animals.....	4
1.2.1. Transmission electron microscopy (TEM) or scanning electron microscopy (SEM)	4
1.2.2. Inductively coupled plasma mass spectrometry (ICP-MS).....	6
1.2.3. X-ray fluorescence imaging (XFI)	7
1.2.4. Multi techniques together used for investigating NPs in plant or animal	9
1.3. Motivation of the study.....	11
1.3.1. Research intention.....	11
1.3.2. Research significance.....	12
2. Size-dependent transport of nanoparticles in matricaria chamomilla investigated with ICP-MS and XFI	13
2.1. Introduction.....	13
2.2. Major reagents	13
2.3. Key instruments	14
2.4. Experiments and methods	14
2.4.1. Synthesis of different size nanoparticles.....	14
2.4.2. Daisy flower incubation with different size Au NPs and iodine	17
2.4.3. Flower uptake to different size NPs study by ICP-MS.....	20
2.4.4 In vivo synchrotron-based XFI of different size NPs in flower	21
2.5. Results and discussion.....	22
2.5.1. Characterization of Au NPs.....	22
2.5.2. Distribution study of different size Au NPs in daisy flower by ICP-MS	27
2.5.3. In vivo distribution study of NPs in flower by XFI.....	41
2.5.4. Conclusion	43
3. Cell labeled by Iohexol, Pd NPs, QDs and Ag NPs for <i>in vitro</i> XFI	45
3.1. Introduction.....	45
3.2. Major reagents	45
3.3. Key instrument	46
3.4. Experiments and methods	46
3.4.1. Synthesis of NPs.....	46

3.4.2. Colloidal stability of NPs	48
3.4.3. Cell culture	48
3.4.4. Cell cytotoxicity study by Resazurin experiment.....	49
3.4.5. Cell viability study by cell live/dead staining experiment	50
3.4.6. Cell uptake study	50
3.4.7. Cell proliferation study	51
3.4.8. Cell migration study.....	53
3.4.9. Cell exocytosis study.....	54
3.4.10. Cell growth.....	55
3.4.11. Cell area	55
3.4.12. <i>In vitro</i> synchrotron-based XFI by mouse.....	55
3.5. Result and discussion	56
3.5.1. NPs synthesis and characterization	56
3.5.2 Colloidal stability of Pd NPs, QDs and Ag NPs	59
3.5.3. Cell viability of iohexol, Pd NPs, QDs and Ag NPs.....	61
3.5.4. Cellular live/dead staining experiment	63
3.5.5. Cellular uptake studied by ICP-MS	66
3.5.6. Cellular proliferation study.....	68
3.5.7. Cell exocytosis study.....	70
3.5.8. Cell growth and area	73
3.5.9. Transwell migration study	74
3.5.10. <i>In vitro</i> synchrotron-based XFI	75
3.6. Conclusion	77
References	79
Publications.....	84
Acknowledgement	86
Abbreviation.....	87
List of hazardous substances	89
Declaration on oath	99

Abstract

Nanoparticles (NPs) are widely used in agriculture as nanofertilizer or insect pesticide. Due to their physical dimensions, NPs can penetrate biomembranes and subsequently accumulate and translocate in plants to cause the serious biological hazards and environment problems. Thus, it is essential to understand the interaction of NPs with plant. However, the interaction study of NPs with plants is highly dependent on the development of analytical techniques. Synchrotron-based X-ray fluorescence imaging (XFI), as a powerful tool for tracing elements, was applied to monitoring the NPs biodistribution *in situ*. Herein, we are going to explore tracing NPs in plant by XFI and investigate the transportation and distribution of a series Au NPs size from 1 to 100 nm in matricaria chamomilla by inductively coupled plasma mass spectrometry (ICP-MS) and XFI. Results indicated XFI possessed effectively nondestructive imaging, allowing potentially for recording *in situ/in vivo* biodistribution.

Cell therapy is with great promises for the preclinical application. Tracking cell migration is very important for understand in cell therapy. Thus noninvasive cell tracing is widely investigated. Synchrotron-based XFI is promising technique for tracing cell labeled by contrast agent. Herein, palladium NPs, quantum dots, silver NPs and iohexol (a commercial small molecule contrast agent) were employed as the contrast agent. Cell lineage macrophage (MHS) and T cell (CTLL-2) were used and labeled by palladium nanoparticles, quantum dots, silver nanoparticles and iohexol. Cell uptake results indicated MHS and CTLL-2 could be effectively labeled by NPs and iohexol. Systematically cell study and XFI result showed the cells after labeled were in health state and could be effectively detected by XFI. Our discovery indicated XFI possessed effectively nondestructive imaging and could be potentially *for in situ/in vivo* biodistribution in animals.

Zusammenfassung

Nanopartikel (NP) werden in der Landwirtschaft häufig als Nanodünger oder Insektenbekämpfungsmittel eingesetzt. Aufgrund ihrer physikalischen Abmessungen können sie Biomembranen durchdringen und sich anschließend in Pflanzen anreichern und verlagern, was zu ernsthaften biologischen Gefahren und Umweltproblemen führt. Daher ist es wichtig, die Wechselwirkung von NPs mit Pflanzen zu verstehen. Die Untersuchung der Interaktion von NPs mit Pflanzen hängt jedoch in hohem Maße von der Entwicklung analytischer Techniken ab. Die Synchrotron-basierte Röntgenfluoreszenz-Bildgebung (XFI), ein leistungsfähiges Instrument zur Rückverfolgung von Elementen, wurde zur Überwachung der NPs-Biodistribution in situ eingesetzt. In diesem Artikel werden wir die Verfolgung von NPs in Pflanzen mittels XFI erforschen und den Transport und die Verteilung einer Reihe von Au NPs mit einer Größe von 1 bis 100 nm in *Matricaria chamomilla* mittels induktiv gekoppelter Plasmamassenspektrometrie (ICP-MS) und XFI untersuchen. Die Ergebnisse deuten darauf hin, dass XFI eine effektiv zerstörungsfreie Bildgebung ermöglicht, so dass die Biodistribution in situ/in vivo aufgezeichnet werden kann.

Die Zelltherapie ist für die präklinische Anwendung sehr vielversprechend. Die Verfolgung der Zellmigration ist für das Verständnis der Zelltherapie sehr wichtig. Daher wird die nichtinvasive Zellverfolgung umfassend untersucht. Synchrotron-basiertes XFI ist eine vielversprechende Technik zur Verfolgung von Zellen, die mit Kontrastmitteln markiert sind. In diesem Projekt wurden Palladium-NP, Quantenpunkte, Silber-NP und Iohexol (ein kommerzielles niedermolekulares Kontrastmittel) als Kontrastmittel eingesetzt. Es wurden Makrophagen (MHS) und T-Zellen (CTLL-2) verwendet, die mit Palladium-Nanopartikeln, Quantenpunkten, Silber-Nanopartikeln und Iohexol markiert wurden. Die Ergebnisse der Zellaufnahme zeigten, dass MHS und CTLL-2 durch NPs und Iohexol effektiv markiert werden konnten. Systematische Zellstudien und XFI-Ergebnisse zeigten, dass sich die Zellen nach der Markierung in einem gesunden Zustand befanden und durch XFI effektiv nachgewiesen werden konnten. Unsere Entdeckung deutet darauf hin, dass XFI eine effektive zerstörungsfreie Bildgebung ermöglicht und möglicherweise für die In-situ-/In-vivo-Biodistribution bei Tieren eingesetzt werden kann.

1. Introduction

1.1 Nanoparticles application

Nanoparticles (NPs) are widely used in many fields as shown in Figures 1-1 and 1-2¹⁻². Based on their excellent properties, many applications were developed for humans as contrast agent³⁻⁷, therapeutic agent⁸⁻¹², cosmetics¹³⁻¹⁴, and drug delivery¹⁵⁻¹⁷. It also can be designed for plant as fertilizer¹⁸⁻¹⁹, nano-based target delivery approach (gene transfer)²⁰⁻²² and nanopesticides²³⁻²⁴. However, due to their physical dimensions, NPs can penetrate biomembranes and subsequently accumulate and translocate in living matters to cause the serious biological hazards and environment problems²⁵⁻²⁷. Thus, it is essential to understand the interaction of NPs with living matters. However, the interaction study of NPs with plants and animals is highly dependent on the development of analytical techniques. In the past decades, some advanced techniques have been used in detection of NPs in plants and animals.

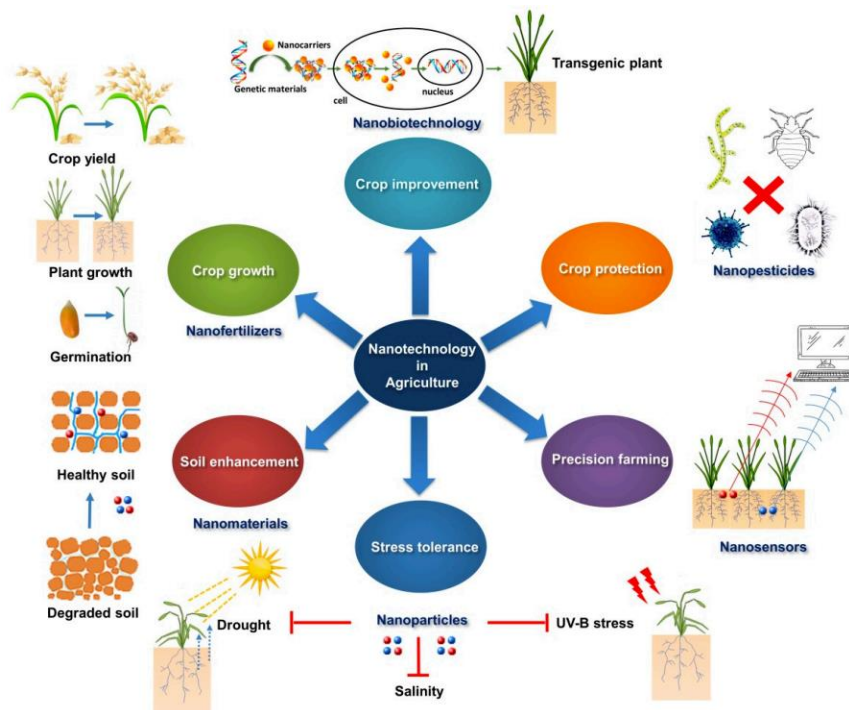


Figure 1-1. Applications of nanotechnology in agriculture. Controlled released nanofertilizers, nano-based target delivery approach (gene transfer), nanopesticides etc. Cited from reference².

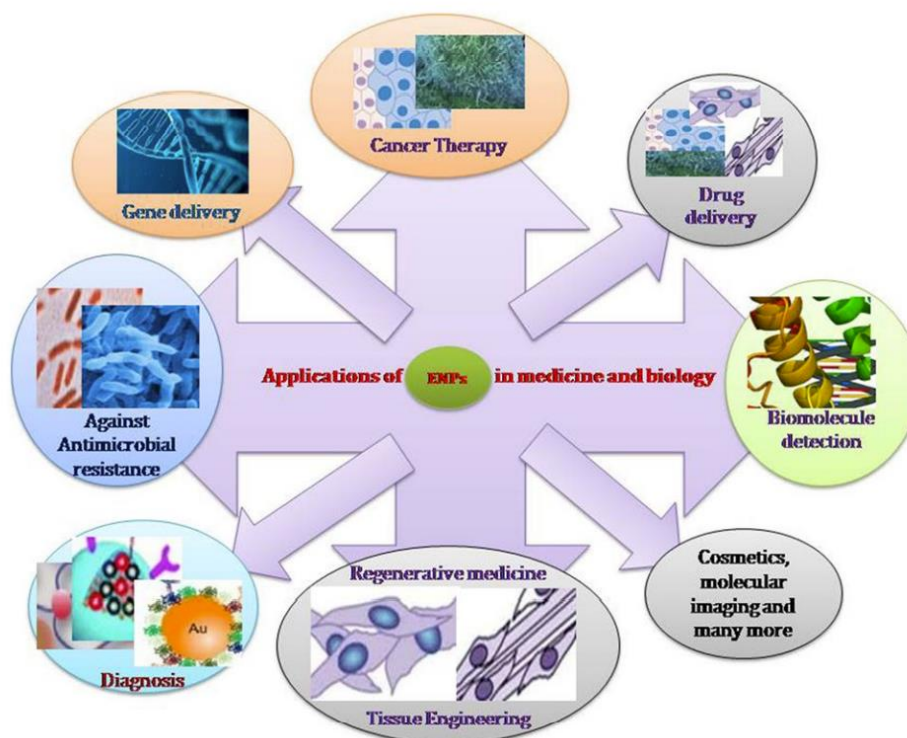


Figure 1-2. Applications of nanoparticles in different fields of medicine and biology. Cited from reference¹.

1.2. Techniques used for investigating NPs in plant and animals

1.2.1. Transmission electron microscopy (TEM) or scanning electron microscopy (SEM)

TEM or SEM, as useful characterization method, can be directly used to observe the NPs morphology and location in tissue or organ with extremely high resolution *ex vivo*²⁸. Thus, it can be used to study the uptake and translocation of plant to NPs. Wei-Ning Wang *et al.* studied MgO NPs by foliar uptake in living watermelon as shown in Figure 1-3²⁹. It indicated that MgO NPs were present inside the vein system. This was the direct evidence of nanoparticle transport through the stomatal pathway. No NPs were observed inside the mesophyll cells and chloroplast. TEM also can be used to observe the NPs in animal tissue and organs *ex vivo*. Katrin Loeschner *et al.* investigated the silver NPs (Ag NPs) distribution in rat by oral administration³⁰. In the Ag NPs exposed rats, mostly spherical, but aggregated Ag NPs were found in the lysosomes of macrophages within the lamina propria (Figures 1-4a-c) and individual NPs in the basal lamina of the epithelium (Figures 1-4d-f).

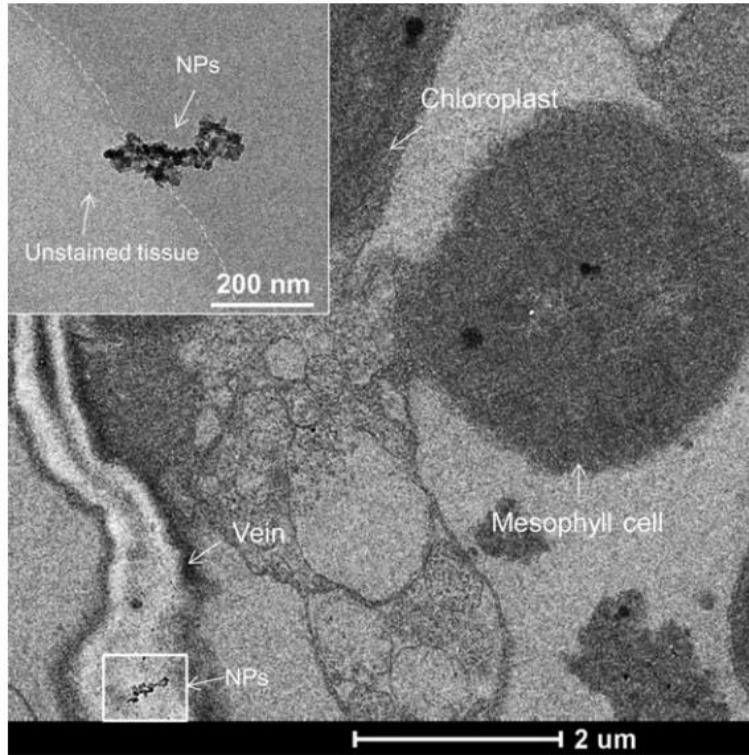


Figure 1-3. Example TEM images of MgO NPs inside the leaf after applying nanoparticles for three d. The inset is the high contrast image of NPs inside the leaf using an unstained sample. Cited from reference²⁹.

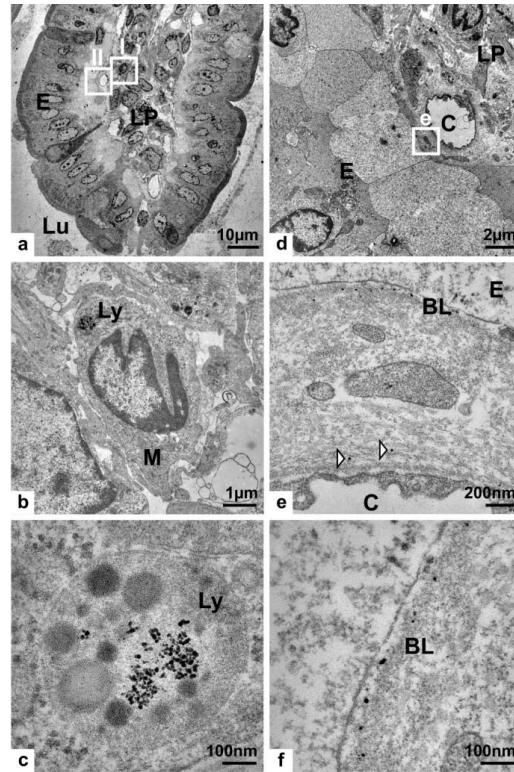


Figure 1-4. TEM of an intestinal villus (ileum) from Ag NPs exposed rat. TEM of ultra-thin sections showing a) overview of an intestinal villus (LU = lumen) highlighting two regions of interest (I and II) in the lamina propria (LP) as well as in a region between lamina propria and the epithelium (E), respectively; b-c) details of region I showing granules in a lysosome (Ly) within a macrophage (M); d-f) details of region II showing granules in close proximity to a capillary (C) within the lamina propria and in the basal lamina (BL) of the epithelium. The region of interest highlighted in d) is presented in e), whereas f) is showing the basal lamina in more detail. Cited from reference³⁰.

1.2.2. Inductively coupled plasma mass spectrometry (ICP-MS)

ICP-MS was widely used in quantitative detection with good detection limitation³¹⁻³³. It also allowed element-specific detection and was convenient technique to investigate the biodistribution of NPs *ex vivo*. Jonathan D. Judy *et al.* studied the tobacco to 5, 10, and 15 nm Au NPs uptake and investigated the potential for trophic transfer by ICP-MS as shown in Figure 1-5³⁴. Au content can be directly detected in primary producer (tobacco) and primary consumer (hornworms). Philipp Nold *et al.* investigated the migratory capacity of MSC labeled

by Au NPs in mouse³⁵. As shown in Figure 1-6, the amount of Au in liver, lung, spleen, kidney, and blood can be determined via ICP-MS to study the distribution of MSC labeled by Au NPs.

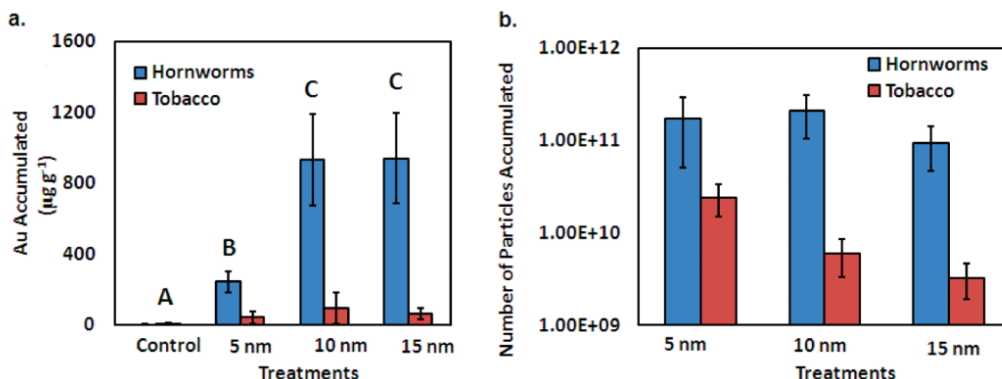


Figure 1-5. Au concentration reported as mean (one standard error for tobacco and hornworms based on (a) mass and (b) particle number. Groups with the same letter are not significantly different from each other. Cited from reference³⁴.

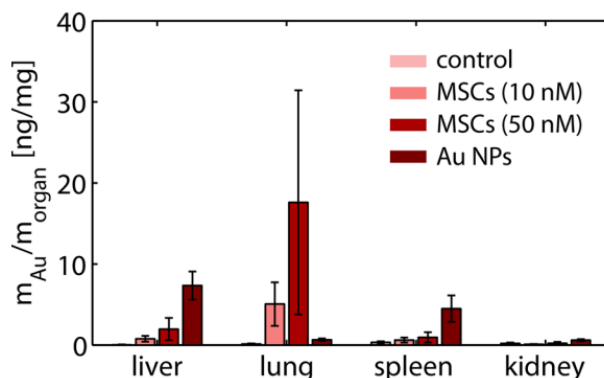


Figure 1-6. In vivo tissue distribution of MSCs labeled with Au NPs at concentrations of 10 and 50 nM for 48 h. Mice were injected in their tail vein with 50 μ L of Au NP labeled MSCs (i.e. 10^6 cells, which had been incubated with 10 or 50 nM Au NPs for 48 h). Alternatively, mice were injected in their tail vein with 50 μ L of Au NPs at a concentration of 1300 nM. After 72 h, mice were sacrificed and the amount m_{Au} of Au in the different organs was determined with ICP-MS. Cited from reference³⁵.

1.2.3. X-ray fluorescence imaging (XFI)

XFI was found to be able to detect exogenous elements with higher sensitivity and low background signal³⁶⁻³⁷. Jose A. Hernandez-Viezcas *et al.* investigated the Ce and Zn elements

within soybean tissues, including the reproductive organ, and analyzes the possible transfer of nanoceria and ZnO NPs into the food chain by synchrotron XFI³⁸. As shown in Figure 1-7, Zn, Ca and K elements were directly observed in plant tissue and the fluorescence intensity indicated the element relative amount. Nivedh Manohar *et al.* studied the high-sensitivity imaging and quantification of intratumoral distributions of gold nanoparticles by benchtop XFI³⁹. As shown in Figure 1-8, it showed the biodistribution of Au NPs within an *ex vivo* tumor sample. The result indicated that XFI could be useful for detecting Au NPs within *ex vivo* samples in highly sensitive detection and imaging.

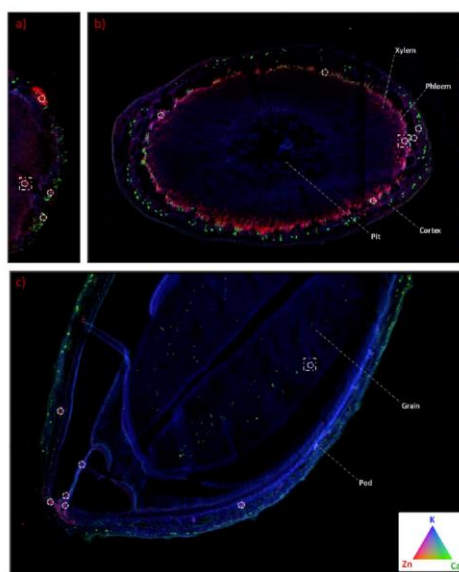


Figure 1-7. Tricolor XFI maps (red = Zn, green = Ca, blue = K): (a) nodule, (b) stem, and (c) pod maps. Cited from reference³⁸.

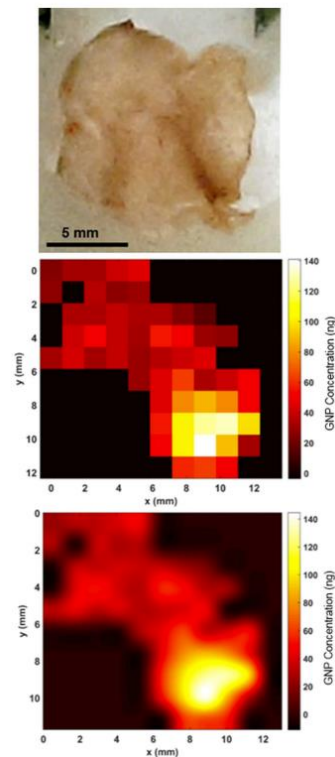


Figure 1-8. Photograph of the detector point of view of the extracted tissue sample (top panel). Raw XFI mapping of the Au NPs concentration (middle panel). Smoothed 2D XFI image of the Au NPs concentration (bottom panel). Cited from reference³⁹.

1.2.4. Multi techniques together used for investigating NPs in plant or animal

Single technique exist its own drawbacks for measure the specimens. Based on research purposes, different techniques were used to measure. Thus, Multi techniques together was developed to investigate NPs in plant or animal according to research necessity. Jitao Lv *et al.*^{40,42} used X-ray absorption spectroscopy (XAS) and micro-X-ray fluorescence microscopy (μ -XRF), optical fluorescence microscopic to track labeled ZnO NPs, transmission electron microscopy (TEM) used to study the uptake pathway, accumulation and cellular localization of ZnO NPs in maize as shown in Figure 1-9. Giulia Veronesi *et al.*⁴¹ used X-ray fluorescence imaging (XRF) coupled with *in situ* X-ray absorption near edge structure (XANES) spectroscopy to probe biodistribution and chemical state of InP-based core and core/shell QDs in *Hydra vulgaris* as shown in Figure 1-10.

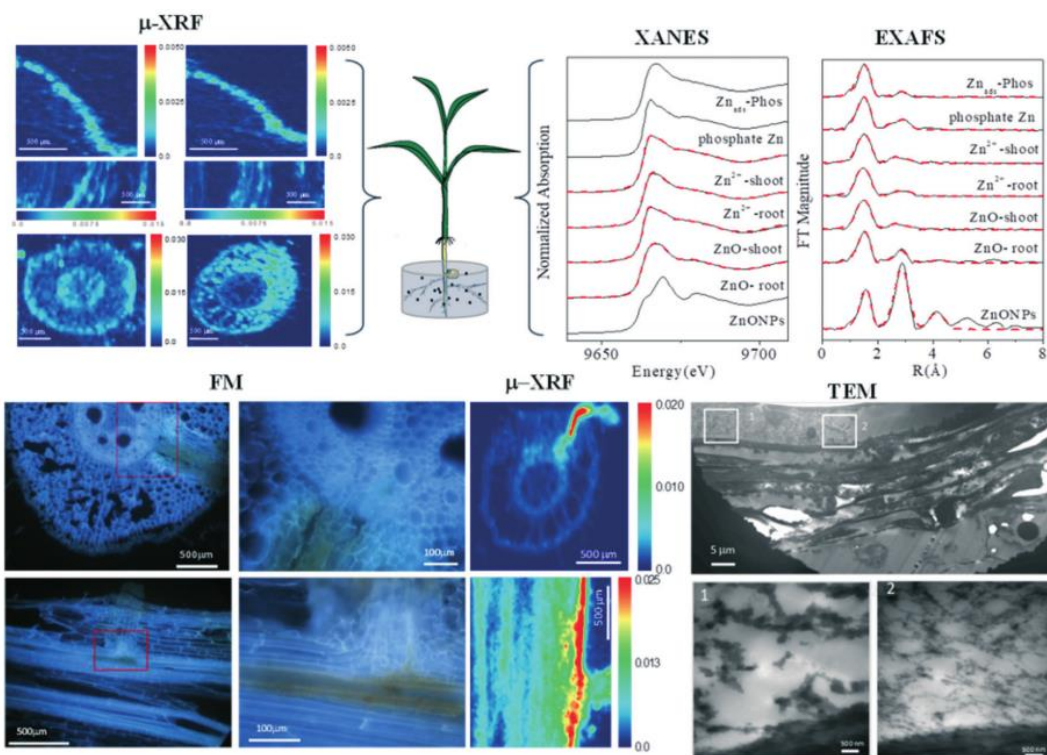


Figure 1-9. Combining micro-X-ray fluorescence microscopy (μ -XRF), X-ray absorption near edge structure (XANES), extended X-ray absorption fine structure (EXAFS), fluorescence microscopy (FM) and transmission electron microscopy (TEM) to study the uptake, translocation and transformation of ZnO NPs in maize plants. Cited from reference^{40, 42}.

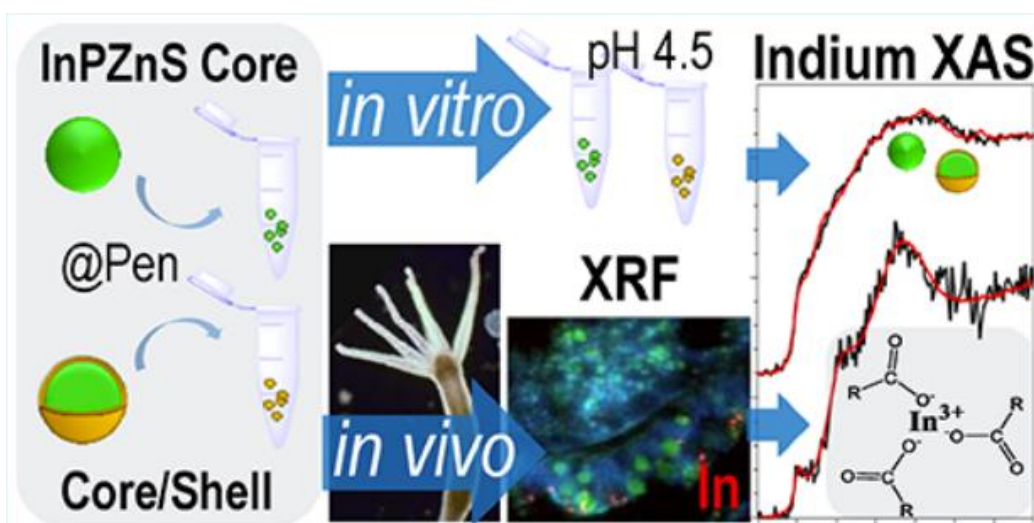


Figure 1-10. XRF coupled with in situ X-ray absorption near edge structure (XANES) spectroscopy to highlight the biodistribution and chemical state of InP-based core and

*core/shell QDs in the model organism Hydra vulgaris. Cited from reference*⁴¹.

Moreover, magnetic resonance imaging (MRI)⁴³⁻⁴⁸, computed tomography (CT)⁴⁹⁻⁵¹, fluorescence imaging (FL)⁵²⁻⁵³ and single photon emission computed tomography (SPECT)⁵⁴⁻⁵⁶ etc. also were contrast-dependent imaging techniques and can be used to investigate the interaction of NPs with plant or animals. However, those techniques have restrictions such as which type NPs can be used, in the imaging in specimens with macroscopic dimensions or the sample destroyed during measurements etc. Therefore, it is necessary to apply *in situ* techniques for monitoring the NPs biodistribution for *in vivo* imaging.

1.3. Motivation of the study

1.3.1. Research intention

1.3.1.1. Size-dependent transport of nanoparticles in matricaria chamomilla investigated with ICP-MS and XFI

Many elements have distinct X-ray fluorescence and thus can be distinguished⁵⁷⁻⁵⁹. But it is difficult to record fluorescence due to their own scattering in biological tissue. Florian *et al.*⁶⁰ developed a method to reduce the background by use of X-ray with high brilliance, in combination with advanced spatial and spectral filtering. Thus, XFI would be possible for deep tissue imaging. Considering the radiation damage, it is feasible for effectively nondestructive imaging to allow potentially for recording *in situ/in vivo* biodistribution namely synchrotron-based XFI for recording *in vivo* biodistribution by tracking of NPs. In order to prove the feasibility, an easy model system was applied which is ink flower experiment. Daisy flower was incubated in a pot of ink, and the ink was uptake by the plant. The petals of flower changed to the color of the ink. Such a scenario inspired us that thinking of the distribution of NPs as fertilizers, or of NPs contaminating the soil in crops. Plant-based experimental set-up does not exist ethical aspects, in particular consider radiation damage, we have chosen to demonstrate the possibility of XFI. As scientific question, apart from demonstrating the XFI technique, we wanted to investigate if there is a size dependence of the NPs for their transport within flowers. In our study, one library of Au NPs from 1-100 nm was synthesized and recorded their distribution in matricaria chamomilla by ICP-MS as well as real-time *in vivo* distribution in

matricaria chamomilla by XFI *in situ*.

1.3.1.2. Cell labeled by iohexol, Pd NPs, QDs and Ag NPs for XFI

As we all know, cell therapy has potentially provided the new opportunity to treat disease and is with great promises for the preclinical application⁶¹. It is necessary to understand the cell how to migrate and distribute in the whole body. Thus, tracing cell is imperative in their working process⁶². Based on 1.3.1.1 design, synchrotron-based XFI is an effective and feasible technique to study the NPs *in vivo* distribution in plant *in situ*. The key of XFI is the contrast agent which can be effectively detected. Thus, it inspired us to monitor cell labeled contrast agent for *in vivo* distribution in mouse by XFI *in situ*. Meanwhile, the interaction of cell with the contrast agent are essential to investigate. In order to realize *in vivo* tracing immune cell, the preliminary explore work is necessary. In our study, the Pd NPs and Ag NPs were synthesized. Moreover, QDs and iohexol (a commercial small molecule iodine contrast agent) was used to label the macrophage (MHS) and T cell (CTLL-2) cell. And interaction of cell with the contrast agent was systematically studied. XFI was employed for imaging in mouse to evaluate the contrast agent imaging effect.

1.3.2. Research significance

In the first study, a library of Au NPs from 1 to 100 nm was synthesized and recorded their real-time *in vivo* distribution in matricaria chamomilla by XFI *in situ*. To address if there is a size dependence of the NPs for their transport within flowers. Thereby providing valuable information for future possible NPs as carrier in plant study.

In the second study, the Pd NPs, QDs, Ag NPs and iohexol were used to label the macrophage (MHS) and T cell (CTLL-2) cell. XFI was employed for imaging in mouse to compare these contrast agents imaging effect. It can provide the valuable information for future *in situ/ in vivo* XFI.

2. Size-dependent transport of nanoparticles in *matricaria chamomilla* investigated with ICP-MS and XFI

2.1. Introduction

Colloidal NPs have been used in various fields due to its excellent properties. Especially in agriculture, a huge amount NPs were used in fertilizer^{18-19, 63} and insecticide^{2, 23-24, 64-65}. However, only small amount of them worked with the plants⁶⁶. The others nanoparticles will be exposed in the environment and potentially cause the environment pollution²⁶. Thus, it is essential to study the interaction between the nanoparticles and plant⁴². A lot of studies have been done about the nanoparticles with plant^{25, 67-71}. However, the NPs transport in the plant is rarely studied. Florian *et al.*⁶⁰ developed the method to reduce the background by use of X-ray with high brilliance, in combination with advanced spatial and spectral filtering. It makes XFI possible for deep tissue imaging. In this study, Au NPs 1 - 100 nm were chosen as the model NPs and *matricaria chamomilla* flower was chosen as the model plant as shown in Figure 2-1. Meanwhile, ICP-MS and synchrotron based X-ray fluorescence image were used to study the distribution and transportation of different size Au NPs in flower *in vitro* and *in vivo*.

2.2. Major reagents

Name	Purity	Company	Function
Trisodium citrate	≥ 99 %	Sigma Aldrich	For AuNPs synthesis
Gold (III) chloride trihydrate	≥ 99.9 %	Sigma Aldrich	For AuNPs synthesis
Bovine serum albumin	≥ 96 %	Sigma Aldrich	For AuNPs synthesis
Sodium hydroxide	>98 %	Roth	
6-aza-2-thiothymine		Alfa Aesar	For AuNPs synthesis
Acetylcysteine	99 %	Sigma Aldrich	For AuNPs synthesis
Acetic acid	≥ 99 %	Alfa Aesar	For AuNPs synthesis
Methanol	98 %	Roth	For AuNPs synthesis

Tetraoctylammonium bromide	≥ 98 %	Sigma Aldrich	For AuNPs synthesis
Sodium borohydride	>98 %	Sigma Aldrich	For AuNPs synthesis
poly(isobutylene-alt-maleic anhydride)	85 %	Sigma Aldrich	For AuNPs synthesis
1- dodecanethiol	98 %	Sigma Aldrich	For AuNPs synthesis
dodecylamine	90 %	Sigma Aldrich	For AuNPs synthesis
CHO-PEG-SH 2000		Rapp Polymere	For AuNPs synthesis

2.3. Key instruments

Name	Model	Company	Function
Dynamic light scattering (DLS)	NANO ZS	Malvern	NPs characterization
UV–Vis absorption spectrophotometer	Agilent 8453	Agilent technologies	Absorption spectra measurement
Inductively coupled plasma mass spectrometry	7700 Series studies	Agilent	For daisy flower uptake
Transmission electron microscopy (TEM)	JEM- 1400PLUS	JEOL	For NPs morphology visualization

2.4. Experiments and methods

2.4.1. Synthesis of different size nanoparticles

2.4.1.1. Synthesis of 1.4 nm 6-aza-2-thiothymine (ATT)-capped Au NPs

As previously reported⁷², the ATT was added into the freshly prepared NaOH (0.2 M, 10 mL) to form the 80 mM concentration. The H₂AuCl₄ (10 mg mL⁻¹, 10 mL) freshly prepared was added into the above solution and stirred for overnight. Then the solution was collected and centrifuged by centrifugal filter (3000 Da) at 6000 rpm for 10 min. Discard the filtration solution and add the Milli-Q water 3 mL to wash for 3 times. After characterization by TEM, NPs are termed ATT@Au NPs (1.4 nm) hereafter.

2.4.1.2. Synthesis of 1.6 nm acetylcysteine-(ACC)-capped Au NPs

Following a published protocol⁷³, freshly prepared HAuCl₄ (0.10 mol L⁻¹, 0.4 mL) and ACC (0.10 mol L⁻¹, 0.6 mL) were mixed in a solution (1.6 mL) of MeOH/glacial acetic acid (6:1, v/v) and stirred for 30 min at 25 °C. The color of the above solution changed from yellow to orange and some white suspension shown in the solution. The Milli-Q water (8.7 mL) was added to the mixture and the mixture was heated to 70 °C reflux for 24 h. The gold nanocluster formed and has orange fluorescence emission. Finally, the solution was purified by centrifugal filter (3000 Da) and centrifuged for 10 min at 6000 rpm. Discard the filtration solution and add the Milli-Q water 3 mL to wash for 3 times. After characterization by TEM, NPs are termed in the following ACC@Au NPs (1.6 nm).

2.4.1.3. Synthesis of 10 nm bovin serum albumin (BSA)-capped Au NPs

Following a published protocol⁷⁴, freshly prepared BSA (50 mg mL⁻¹, 10 mL) and HAuCl₄ (0.01 mol L⁻¹, 10 mL) were stirred for 2 min. Then NaOH (1 M, 1 mL) was added and stirred for overnight at 37 °C. Finally, it was dialyzed against Milli-Q water for 3 d by cellulose ester dialysis membrane (35k Da). After characterization by TEM, NPs are termed in the following BSA@Au NPs (10 nm).

2.4.1.4. Synthesis of 5 nm poly (isobutylene–alt–maleic anhydride)–graft dodecyl (PMA)-overcoated Au NPs

Au NPs of around 5 nm core size, capped with 1-dodecanethiol (DDT) a were synthesized according to previously published protocols⁷⁵. HAuCl₄ (36 μmol mL⁻¹, 25 mL) in Milli-Q water and tetraoctylammonium bromide (TOAB, 48.75 μmol mL⁻¹, 80 mL) in toluene were freshly prepared. These two solutions were mixed in the 500 mL separation funnel and shaken vigorously for 5 min. The mixture was transferred to the 250 mL flask with the freshly prepared sodium borohydride (NaBH₄, 13.36 mg mL⁻¹, 25 mL) dropped in 1 min and keep stirring for 1 h at room temperature. After 1 h, the mixture was transferred to the separation funnel and discard the aqueous phase. Then the organic phase was washed by HCl (10 mM, 25 mL)

aqueous solution, NaOH (10 mM, 25 mL) and Milli-Q water (25 mL) for 3 times. After finishing the washing steps, the mixture was transferred into the 250 mL flask with stirred overnight. 10 mL of DDT added into the flask and heated to 60 °C for 2 h to facilitate ligand exchange. After 2 h, the mixture was centrifuged at 900 rcf to remove the large agglomeration. Then it was transferred into the 40 mL glass vial and add the methanol till the cloudy phenomenon appearance to centrifuge at 900 rcf for 5 min. The sedimentation was collected and dispersed in the chloroform. The methanol was added again like last step to induce turbidity followed by centrifuge at 900 rcf for 5 min and the precipitation was collected to disperse in the chloroform to form the DDT-Au NPs. Then PMA was added in the ratio (C_{PMA}/C_{NP}) of 100⁷⁵. The PMA and Au NPs were mixed in 100 mL chloroform in flask and evaporate by rotary evaporation. This evaporation was repeat 3 times. The SSB buffer (pH = 12) was added into the dry flask till dissolved all nanoparticles from flask wall. It was centrifuged at 137,000 rcf for 30 min. The supernatant containing excess polymer was discarded and the pelleted Au NPs was washed 3 times with Milli-Q water (10 mL). Finally, the NPs were redissolved in Milli-Q water (2 mL). After characterization by TEM, NPs are termed PMA@Au NPs (5 nm).

2.4.1.5. Synthesis of 15 nm - 100 nm PMA-overcoated Au NPs

Au NPs of different core size ranging from around 15 - 100 nm diameter capped with citric acid were synthesized according to previously published protocols⁷⁵. Milli-Q water (146.7 mL) with freshly prepared sodium citrate (60 mM, 3.3 mL) was boiled for 5 min. The freshly prepared HAuCl₄ (25 mM, 1.5 mL) was added into the solution and boiled for another 15 min to form the 15 nm Au NPs. It was cooled down to the room temperature. Then 15 nm Au NPs as seed to cool down to 90 °C. The freshly prepared HAuCl₄ (25 mM, 1 mL) was added into the flask for 30 min and repeat this step another twice as generation 0 (g_0). After that, 55 mL was taken out and add the Milli-Q water (52 mL) and sodium citrate (60 mM, 2 mL) into the above solution with stirring for 15 min. Then repeat above growth step till the UV absorption to determine the NPs size. PEG2000 with sulfhydryl was added into the above Au NPs solution in the specific ratio overnight. For the 18 nm, 25 nm, 50 nm and 100 nm Au NPs, the ratio (C_{PEG}/C_{NP}) of PEG2000 was added in 3×10^4 , 3×10^4 , 20×10^4 and 50×10^4 , respectively. Then the

dodecylamine (DDA) was dissolved in chloroform and added into the Au NPs after PEGylation in the ratio (C_{DDA}/C_{NP}) of 10×10^6 , 13×10^6 , 20×10^6 and 40×10^6 overnight, respectively. Then the organic phase was collected by separation funnel. To remove the free DDA, the organic phase was centrifuged and the precipitation was collected. Then the precipitation was dispersed in 20 mL chloroform to wash for another twice. The centrifuge rcf is 10950 rcf for 30 min, 8650 rcf for 20 min, 8650 rcf for 20 min and 540 rcf for 20 min for 18 nm, 25 nm, 50 nm and 100 nm Au NPs respectively. In order to stabilize the Au NPs, the resulting DDA capped Au NPs was further coated by polymer. For the Au 18 nm, 25 nm, 50 nm and 100 nm NPs, the PMA was added in the ratio (C_{PMA}/C_{NP}) of 3000^{75-76} . The PMA and Au NPs were mixed in 100 mL chloroform in flask and evaporate by rotary evaporation. This evaporation was repeat 3 times. The SSB buffer (pH = 12) was added into the dry flask till dissolved all NPs from flask wall. Finally, the NPs were purified by centrifugation for 10950 rcf for 30 min, 8650 rcf for 20 min, 8650 rcf for 20 min, and 540 rcf for 20 min for NPs of around 18 nm, 25 nm, 50 nm and 100 nm Au NPs diameter, respectively. After pelleting the supernatant was discarded and the NP pellet was washed 3 times by Milli-Q water (10 mL), before the NPs finally were redissolved in Milli-Q water. After characterization by TEM, these NPs are termed PMA@Au NPs (14, 31, 54, 94 nm).

2.4.2. Daisy flower incubation with different size Au NPs and iodine

Daisy flower was chosen as the model plant because it is easy to culture and easily available and was gotten from the flower shop as shown in Figure 2-1. The daisy flowers were incubated in the above synthesized Au NPs. Meanwhile, potassium iodide (KI) and iohexol (small molecule with 821.138 molecular weight) were chosen as inner reference. Flower also was incubated in $HAuCl_4$, KI and iohexol respectively as the control experiment. As shown in Figure 2-2 and Figure 2-3, flowers were incubated in mixed solution of Au element concentration ($100 \mu\text{g}/\text{mL}$) and I element concentration ($100 \mu\text{g}/\text{mL}$) for 6 h, 12 h, 24 h and 48 h. The flower was cut with stem length around 4 cm. Three flowers were incubated per Eppendorf (2 mL) with 1 mL incubation solution as shown in Table 2-1. The stem was soaped in the solution around 0.5 cm. For the 50 and 100 nm Au NPs, due to the gravity, the NPs will precipitate to

the tube bottom. Thus, the solution will be dispersed every 3 h to make sure the flower can always touch the Au NPs.

Table 2-1. Concentration C_x of different size Au NPs, HAuCl₄, KI or iohexol; X = Au, I. The concentrations are exhibited as mass concentration ($\mu\text{g/mL}$).

Sample	C_x [$\mu\text{g/mL}$]
HAuCl ₄	100
KI	100
iohexol	100
ATT@Au NPs (1.4 nm)	100
ACC@Au NPs (1.6 nm)	100
BSA@Au NPs (10 nm)	100
PMA@Au NPs (5 nm)	100
PMA@Au NPs (14 nm)	100
PMA@Au NPs (31 nm)	100
PMA@Au NPs (54 nm)	100
PMA@Au NPs (94 nm)	100



Figure 2-1. Full (A) and Partial (B) picture of matricaria chamomilla.

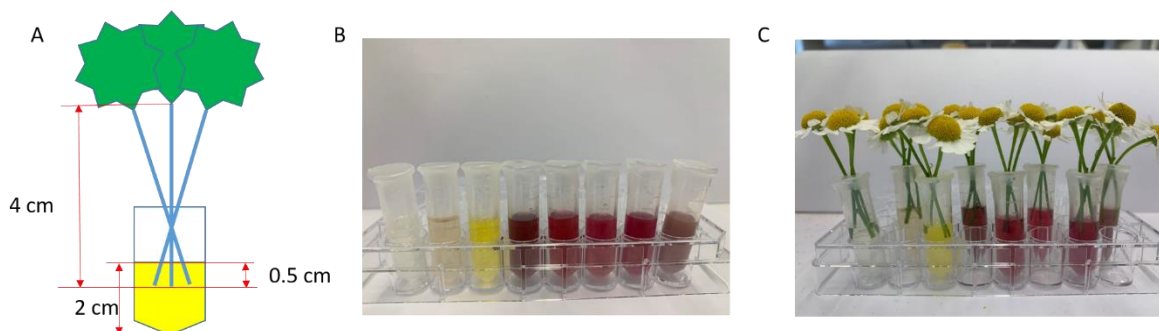


Figure 2-2. (A) The incubation sketch of daisy flower in Eppendorf tube. (B) Solutions of $V_{sol} = 1$ mL of Au NPs of different size with an elemental Au concentration (as determined by ICP-MS) of $100 \mu\text{g/mL}$. From left to right: ACC@Au NPs (1.6 nm), BSA@Au NPs (10 nm), ATT@Au NPs (1.4 nm), PMA@Au NPs (5 nm), PMA@Au NPs (14 nm), PMA@Au NPs (31 nm), PMA@Au NPs (54 nm), PMA@Au NPs (94 nm). (C) Picture for flowers directly after having put them in the NP solutions ($t = 0$). The same image shown in Figure 2-3B.

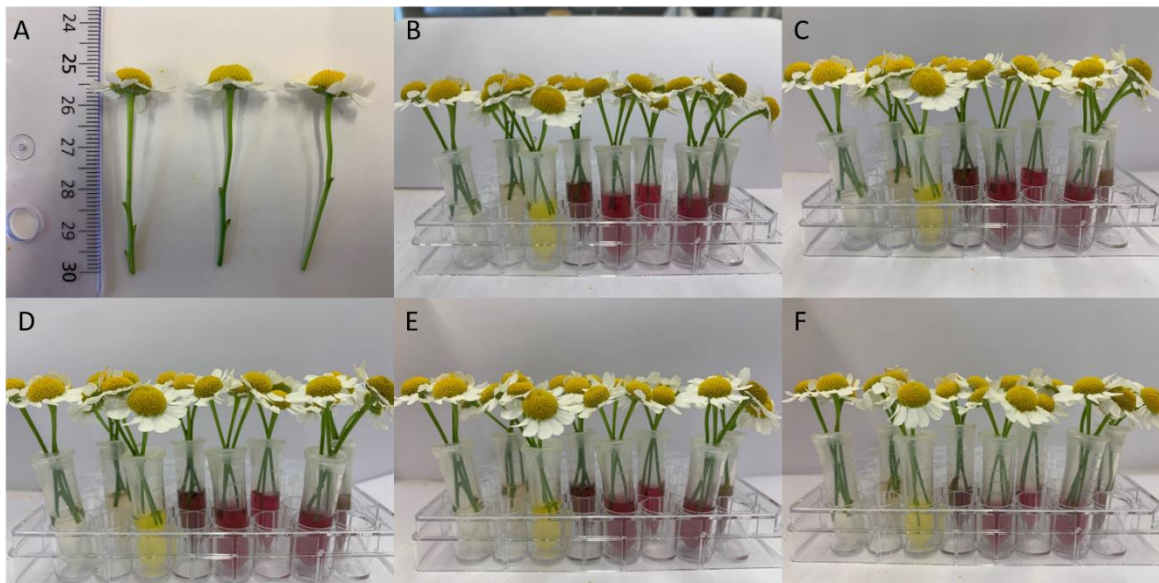


Figure 2-3. (A) Picture of flowers, which were cut to a stem length of 4 cm. The flowers were incubated with 3 flowers per tube in 1 mL solutions containing Au NPs of different size (100 $\mu\text{g/mL}$ elemental Au; containing optionally also KI or iohexol). The stems were inserted approximately 0.5 cm below the liquid surface. Photos of the flowers after (B) 0 h, (C) 6 h, (D) 12 h, (E) 24 h, and (F) 48 h are shown. Even after 48 h of incubation the flowers are visually in good conditions. In each image incubation in the different NP solutions are shown. From left to right: ACC@Au NPs (1.6 nm), BSA@Au NPs (10 nm), ATT@Au NPs (1.4 nm), PMA@Au NPs (5 nm), PMA@Au NPs (14 nm), PMA@Au NPs (31 nm), PMA@Au NPs (54 nm), PMA@Au NPs (94 nm).

2.4.3. Flower uptake to different size NPs study by ICP-MS

In order to investigate the Au NPs, KI and iohexol distribution in daisy flower, the ICP-MS was chosen as the analysis method. Briefly, each flower after incubation was divided into 6 parts as shown in Figure 2-4. From stem to petal respectively is stem 1, stem 2, stem 3, stem 4, blossom and petal. Each stem length is around 1 cm and each part was weighed by balance. Then they were put into the glass tube and the heating gun was used to burn them at 650 $^{\circ}\text{C}$ for 30 second (stem and petal) and 3 min (blossom). After burning, aqua regia (200 μL , $V_{\text{HNO}_3}/V_{\text{HCl}} = 1/3$) was added into the glass tube for 2 d. Then 1.8 mL HCl (2 %) was added and mixed well. In order to remove the solid suspension, 220 nm filter was used to filtrate for

measurement by ICP-MS.

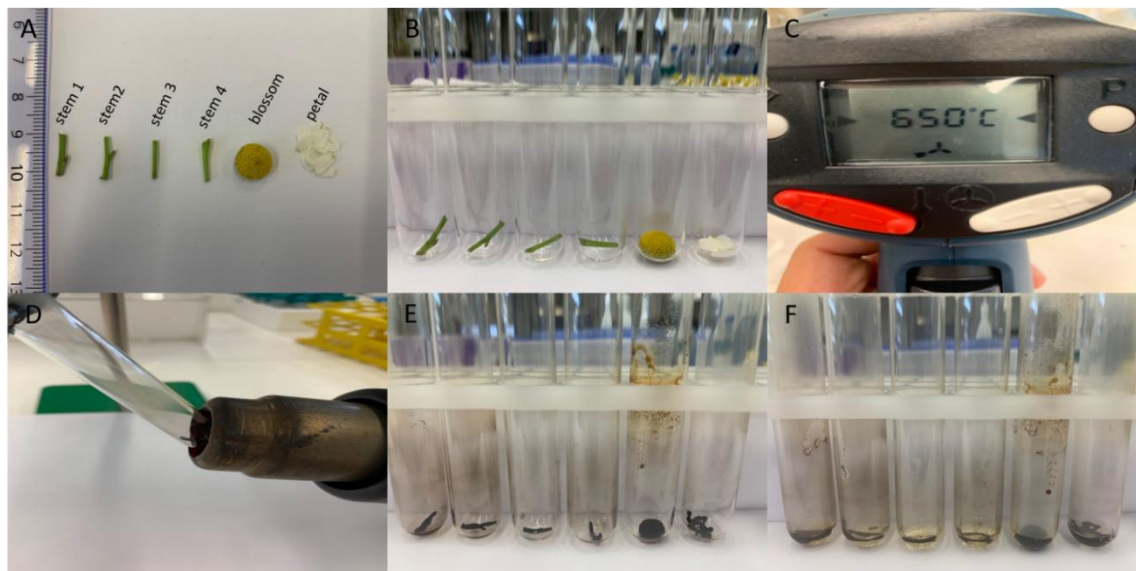


Figure 2-4. (A) Each flower is divided into 6 parts. (B) The flower parts are put in separate glass tubes. (C, D) A heating gun was used for burning the flower parts at 650 °C. (E) Picture of the different flower parts after burning. (F) The burned flower parts are digested in 200 μ L aqua regia for 48 h.

2.4.4 In vivo synchrotron-based XFI of different size NPs in flower

In order to investigate the distribution of different size Au NPs in flower *in vivo*, synchrotron-based X-ray fluorescence imaging (XFI) was used to image *in vivo* as shown in Figure 2-5. ACC@Au NPs (1.6 nm), PMA@Au NPs (5 nm), PMA@Au NPs (31 nm) and PMA@Au NPs (54 nm) were selected to incubate one flower for XFI. XFI work was finished by Prof. Dr Florian Grüner group in University of Hamburg (UHH) and Center for Free-Electron Laser Science (CFEL).

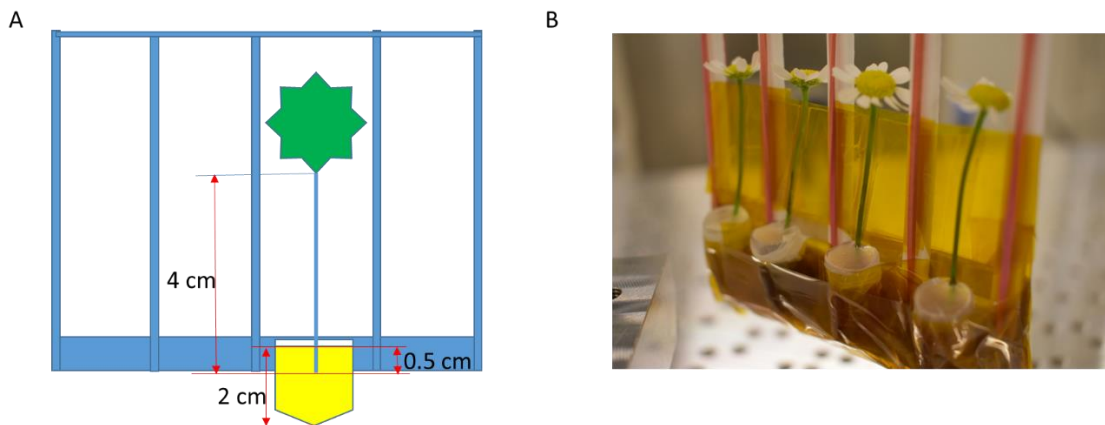


Figure 2-5. (A) Sketch of the flower incubation for XFI. (B) Image of 4 flowers in 4 different incubation solutions for XFI. The image was from Prof. Dr Florian Grüner group in University of Hamburg (UHH) and Center for Free-Electron Laser Science (CFEL).

2.5. Results and discussion

2.5.1. Characterization of Au NPs

In our study, a library of water-soluble Au NPs from 1.5 nm to 100 nm was synthesized according to previously reported literature⁷²⁻⁷⁶. Au nanoclusters either ATT or ACC as surface, Au NPs with BSA as surface, and Au NPs with diameters from around 5 - 100 nm with PMA as outer layer were synthesized. TEM images of Au NPs demonstrate that they were in well dispersed as shown in Figure 2-6. TEM images were processed by ImageJ software to analyze to get the Au NPs core diameters d_c as shown in Figure 2-7 and table 2-2. Based on TEM NPs core diameters d_c , they were named as ATT@Au NPs (1.4 nm), ACC@Au NPs (1.6 nm), PMA@Au NPs (5 nm), BSA@Au NPs (10 nm), PMA@Au NPs (14 nm), PMA@Au NPs (31 nm), PMA@Au NPs (54 nm), PMA@Au NPs (94 nm) respectively. UV/vis absorption spectra of the NPs were recorded as shown in Figure 2-8. Different NPs show different absorption. Au NPs 5, 14, 31, 54 and 94 nm showed characteristic absorption peak and the characteristic absorption peak wavelength was increase with their core size increasing. Number hydrodynamic diameter N (d_h) and intensity hydrodynamic diameter I (d_h) of the NPs were measured by DLS as shown in Figure 2-9 and 2-10. The mean values ($d_{h,N}$) \pm SD and ($d_{h,I}$) \pm SD as derived from these histograms are displayed in Table 2-2. The intensity hydrodynamic distribution of

ATT@Au NPs and ACC@Au NPs was obviously different compared with number hydrodynamic. It was because ATT@Au NPs (1.4 nm) and ACC@Au NPs (1.6 nm) were very small and the scattering intensities were small, thus the determined hydrodynamic diameters $d_{h,l}$ are unreliable when measuring by DLS. For the bigger size NPs, it showed good distribution. Zeta potentials (ζ) was determined with laser Doppler anemometry (LDA) and the mean values \pm SD as derived from these histograms are displayed Figure 2-11 and Table 2-2. The result showed all NPs with negative zeta potential. In order to have a reference to the kinetics, molecular iodine-based contrast agent iohexol or KI, both contain iodine was optionally supplemented in water at an elemental iodine concentration of $C_I = 100 \mu\text{g/mL}$.

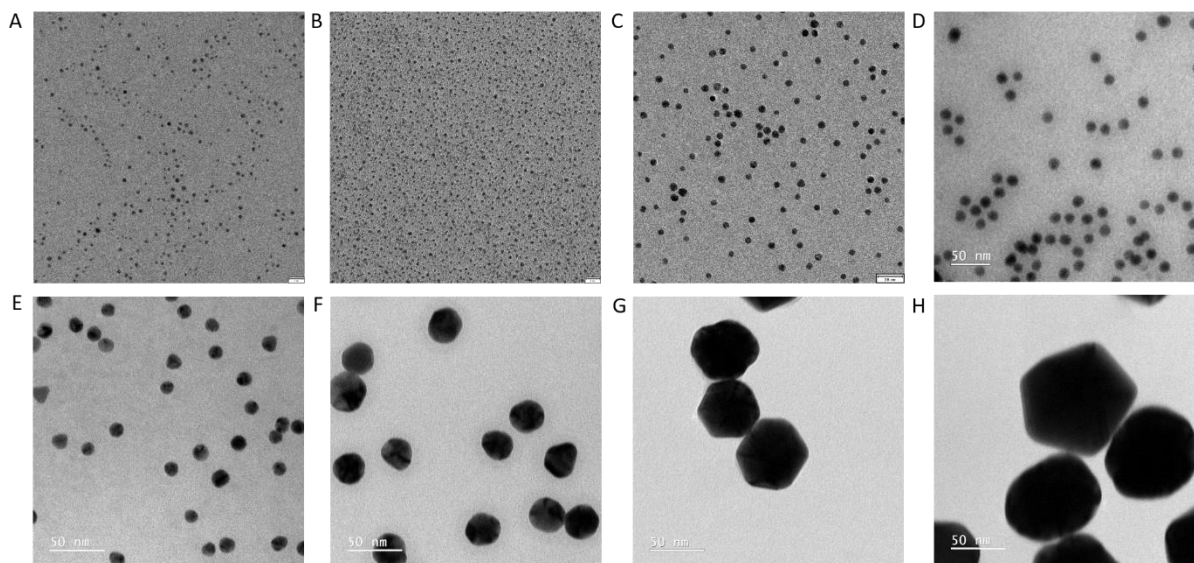


Figure 2-6. TEM images of (A) ATT@Au NPs (1.4 nm) (scale bar: 9 nm), (B) ACC@Au NPs (1.6 nm) (scale bar: 7 nm), (C) PMA@Au NPs 5 nm (scale bar: 20 nm), (D) BSA@Au NPs (10 nm) (scale bar: 50 nm), (E) PMA@Au NPs (14 nm) (scale bar: 50 nm), (F) PMA@Au NPs (31 nm) (scale bar: 50 nm), (G) PMA@Au NPs (54 nm) (scale bar: 50 nm) and (H) PMA@Au NPs (94 nm) (scale bar: 50 nm). The histograms of the size distributions are shown in Figure 2-7.

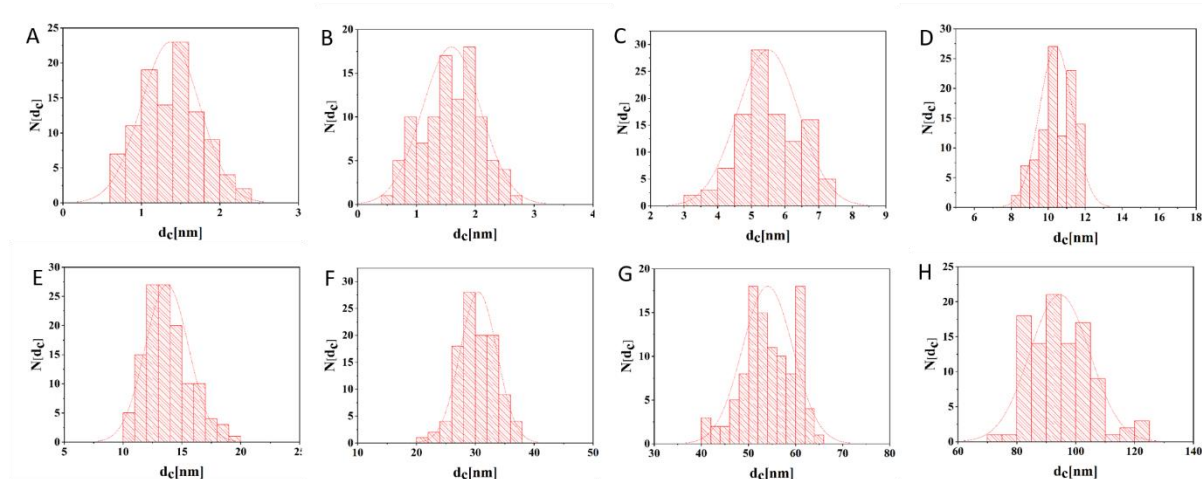


Figure 2-7. Size distribution histograms $N(d_c)$ of the inorganic core diameters d_c . The mean values \pm standard deviation (SD) as derived from these histograms are displayed in Table SI-II.1. (A) ATT@Au NPs (1.4 nm), (B) ACC@Au NPs (1.6 nm), (C) PMA@Au NPs (5 nm), (D) BSA@Au NPs (10 nm), (E) PMA@Au NPs (14 nm), (F) PMA@Au NPs (31 nm), (G) PMA@Au NPs (54 nm) and (H) PMA@Au NPs (94 nm).

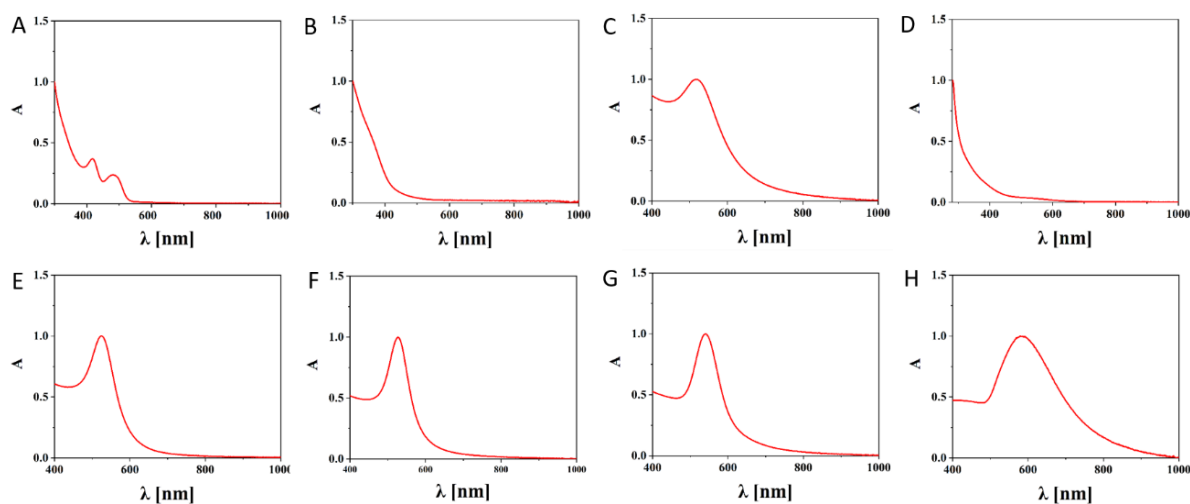


Figure 2-8. Normalized UV/vis absorption spectra $A(\lambda)$ of diluted NP solutions in water. (A) ATT@Au NPs (1.4 nm), (B) ACC@Au NPs (1.6 nm), (C) PMA@Au NPs (5 nm), (D) BSA@Au NPs (10 nm), (E) PMA@Au NPs (14 nm), (F) PMA@Au NPs (31 nm), (G) PMA@Au NPs (54 nm), and (H) PMA@Au NPs (94 nm).

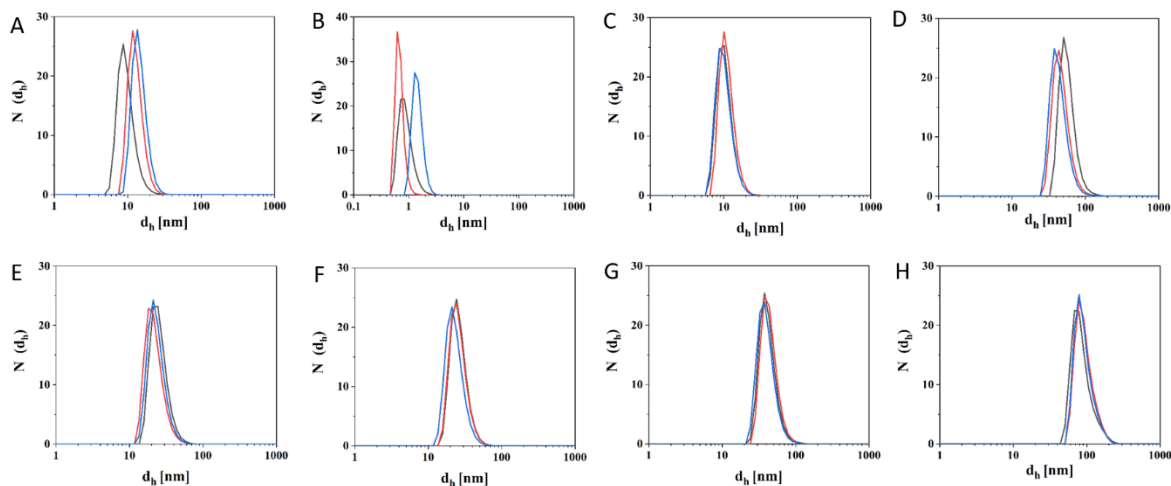


Figure 2-9. Number-weighted distribution $N(d_h)$ of the hydrodynamic diameter d_h as determined in water with DLS (3 measurements are shown). The mean values $(d_{h,N}) \pm SD$ as derived from these histograms are displayed in Table SI-II.1. (A) ATT@Au NPs (1.4 nm), (B) ACC@Au NPs (1.6 nm), (C) PMA@Au NPs (5 nm), (D) BSA@Au NPs (10 nm), (E) PMA@Au NPs (14 nm), (F) PMA@Au NPs (31 nm), (G) PMA@Au NPs (54 nm) and (G) PMA@Au NPs (94 nm).

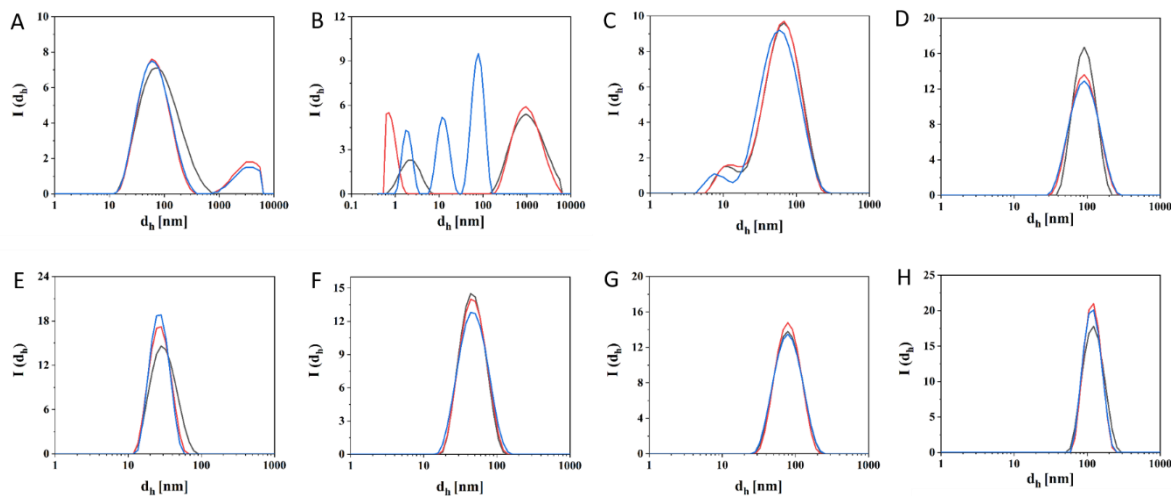


Figure 2-10. Intensity-weighted distribution $I(d_h)$ of the hydrodynamic diameter d_h as determined in water with DLS (3 measurements are shown). The mean values $(d_{h,I}) \pm SD$ as derived from these histograms are displayed in Table SI-II.1. (A) ATT@Au NPs (1.4 nm), (B) ACC@Au NPs (1.6 nm), (C) PMA@Au NPs (5 nm), (D) BSA@Au NPs (10 nm), (E) PMA@Au NPs (14 nm), (F) PMA@Au NPs (31 nm), (G) PMA@Au NPs (54 nm) and (G) PMA@Au NPs (94 nm). In case of the very small ATT@Au NPs (1.4 nm), (B) ACC@Au NPs (1.6 nm) the scattering

intensities were small and thus the determined hydrodynamic diameters are unreliable.

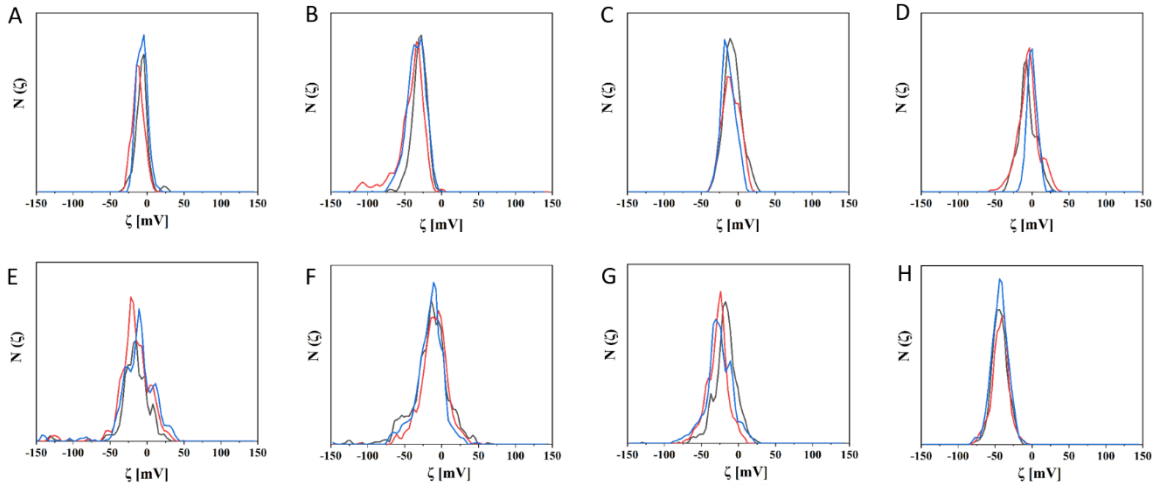


Figure 2-11. Zetapotential distribution $N(\zeta)$ as determined in water with LDA. The mean values \pm SD as derived from these histograms are displayed in Table SI-II.1. (A) ATT@Au NPs (1.4 nm), (B) ACC@Au NPs (1.6 nm), (C) PMA@Au NPs (5 nm), (D) BSA@Au NPs (10 nm), (E) PMA@Au NPs (14 nm), (F) PMA@Au NPs (31 nm), (G) PMA@Au NPs (54 nm) and (G) PMA@Au NPs (94 nm).

Table 2-2. The mean core diameters d_c , hydrodynamic diameters $d_{h,N}$ and $d_{h,I}$, and the zeta potentials ζ of the different NPs samples with the corresponding standard deviations. For the Au^{3+} ions (dissolved $HAuCl_4$) the core diameter d_c was assumed as atomic Au diameter.⁷⁷ For the I ions (dissolved KI) the core diameter d_c was assumed as atomic I diameter.⁷⁷ For iohexol a core diameter was estimated as maximum extension based on the structural formula.⁷⁸ The iohexol size was approximated as benzene ring length plus two longer branch extension chemical bond lengths ($d_c \approx 2*L_{O-H} + 4*L_{C-N} + 2*L_{O-C} + 6*L_{C-C} + L_{benzene\ ring}$). In case of the very small ATT@Au NPs (1.4 nm) and ACC@Au NPs (1.6 nm) the scattering intensities were small and thus the $d_{h,I}$ are unreliable.

sample	d_c [nm]	$d_{h,N}$ [nm]	$d_{h,I}$ [nm]	ζ [mV]
HAuCl ₄	13.72	-	-	-
ATT@Au NPs (1.4 nm)	1.37 ± 0.37	19.91 ± 0.58	387.77 ± 243.29	-9.6 ± 0.4

ACC@Au NPs (1.6 nm)	1.56 ± 0.52	1.02± 0.4	703.83± 574.77	-34.4 ± 4.1
BSA@Au NPs (10 nm)	10.42± 0.90	49.89± 6.93	97.36± 1.30	-19.3 ± 0.7
PMA@Au NPs (5 nm)	5.49 ± 0.91	7.29± 1.22	66.14± 2.14	-26.1 ± 1.9
PMA@Au NPs (14 nm)	13.72 ± 1.83	18.12± 0.33	29.38± 2.49	-21.3 ± 4.1
PMA@Au NPs (31 nm)	30.52 ± 3.12	25.29±1.63	50.40± 0.92	-34.4 ± 4.1
PMA@Au NPs (54 nm)	53.90 ± 5.33	42.40± 2.04	84.88± 0.71	-29.7 ± 1.5
PMA@Au NPs (94 nm)	94.48 ± 10.20	91.05± 3.64	123.13± 2.86	-41.2 ± 0.2
KI	0.266	-	-	-
iohexol	2.1128	-	-	-

2.5.2. Distribution study of different size Au NPs in daisy flower by ICP-MS

In order to study the distribution of different size Au NPs in the whole flower, ICP-MS was employed to evaluate. Briefly, daisy flower was chosen as the model plant as shown in Figure 2-1. They were incubated in different size Au NPs with KI or iohexol as inner reference to study the kinetic. Flower also was incubated in only H_{Au}Cl₄ salt, KI or iohexol respectively as the control experiment. The incubation solution concentration was shown in Table 2-1. As shown in Figure 2-2 and Figure 2-3, the flowers were incubated in mixed solution of gold element concentration (100 µg/mL) and iodine element concentration (100 µg/mL). The flower was cut with stem length around 4 cm. Three flowers were incubated per Eppendorf (2 mL) with 1 mL incubation solution as shown in Table 2-1. The stem was soaped in the solution around 0.5 cm. For the 50 and 100 nm Au NPs, due to the gravity, the NPs will precipitate to the tube bottom. The Eppendorf tube was shaken around every 3 h to make sure the flower can always touch the Au NPs to get rid of gravity factor.

After desired incubation time, flower was divided into 6 parts as shown in Figure 2-4 and weighed. The detailed ICP sample preparation procedure was shown in section 2.4.3. Au element amount of each part and I element of each part was evaluated by ICP-MS. The amounts of Au and of I per mass of the plant part X = stem 1, stem 2, stem 3, stem 4, blossom, and petals, $m_{Au}(X)/m_{flower}(X)$ and $m_I(X)/m_{flower}(X)$ respectively, are plotted in dependence of

the incubation time and the core diameter of the applied Au NPs. Meanwhile, the proportion ($m_{Au(X)}/m_{Au(tot)}$ or $m_I(X)/m_I(tot)$) of Au ($m_{Au(X)}$) or I ($m_I(X)$) amount of each flower part to Au ($m_{Au(tot)}$) or I ($m_I(tot)$) amount of the whole flower respectively, are also plotted in dependence of the incubation time and the core diameter of the applied Au NPs. For each data point were analyzed from 3-9 different flowers (apart from very few conditions where only 2 flowers were analyzed, as the standard deviations of the mean values were small). Some outliers were removed.

2.5.2.1. ICP-MS result of control experiment

$H AuCl_4$ salt was used to incubate the flower as a reference. As shown in Figure 2-12A, Au can be detected in the stem and majorly located in stem 1 and amount decreased along the stem to blossom. No Au was detected in petal. With incubation time going on, the uptake was also increasing. The proportion of Au of each part to the whole flower also was calculated as shown in Figure 2-12B. More than 80 % Au located in the stem 1 and the proportion of Au decreased along the stem to blossom. And the Au proportion of each part was not significantly different with incubation time going on. The whole flower to Au uptake was increased with incubation time going on as shown in Figure 2-12C.

Small molecule iohexol and KI salt distribution in flower were also individually studied as the inner reference. As shown in Figures 2-13 and 2-14, the iodine can be detected in the whole flower. Along the stem, no significant difference of iodine amount was observed and relative lower amount in blossom. The iodine amount also increased with incubation time increasing. Compared with KI and iohexol data, $H AuCl_4$ showed the obvious different result. Au majorly located in the stem 1 may be because the exudate from flower incision reduced $H AuCl_4$ leading to sediment in xylem and the xylem was partly stuck to influence material transportation. When $H AuCl_4$ was transported in the xylem, sap was also possible to reduce $H AuCl_4$ ⁷⁹.

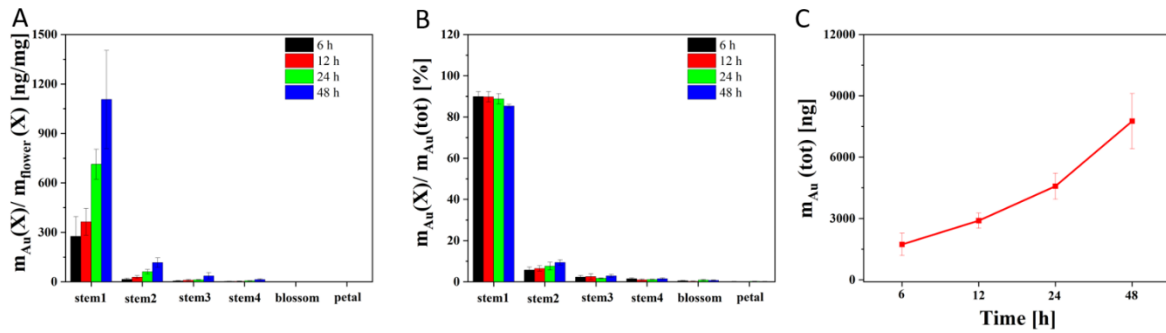


Figure 2-12. (A) Amount of Au found in the respective flower parts, normalized to the mass of the flower parts, (B) Proportion of Au found in the respective flower parts, normalized to the total mass of Au found in the whole flower, plotted versus the position of the flower parts along the stem (X =stem 1, stem 2, stem 3, stem 4, blossom and petal). (C) Total amount of Au found in one whole flower, plotted versus the incubation time.

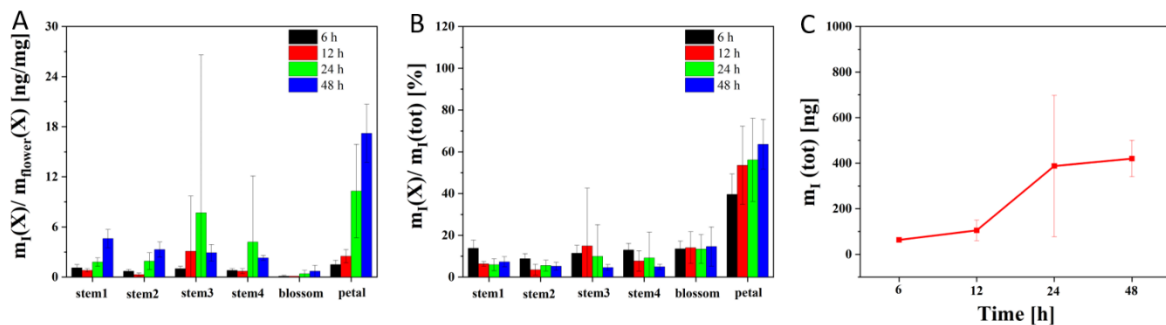


Figure 2-13. Iohexol uptake by flower after different time incubation (A) Amount of I found in the respective flower parts, normalized to the mass of the flower parts, (B) Proportion of I found in the respective flower parts, normalized to the total mass of I found in the whole flower, plotted versus the position of the flower parts along the stem (X =stem 1, stem 2, stem 3, stem 4, blossom and petal). (C) Total amount of I found in one whole flower, plotted versus the incubation time.

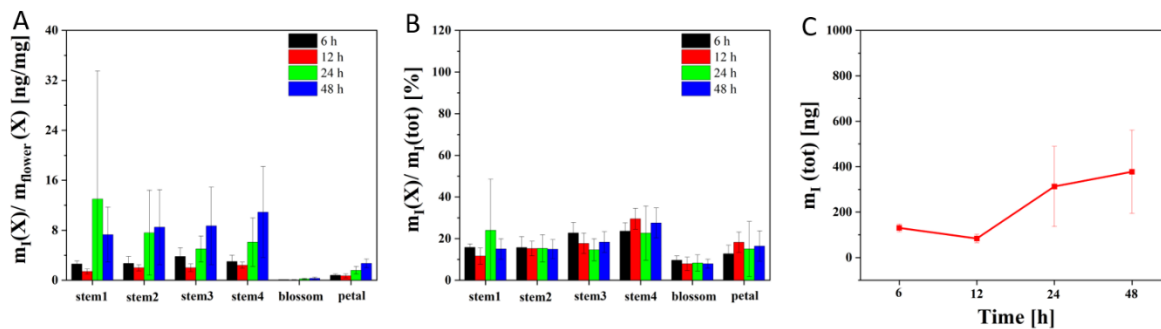


Figure 2-14. KI uptake by flower after different time incubation. (A) Amount of I found in the respective flower parts, normalized to the mass of the flower parts, (B) Proportion of I found in the respective flower parts, normalized to the total mass of I found in the whole flower, plotted versus the position of the flower parts along the stem (X =stem 1, stem 2, stem 3, stem 4, blossom and petal). (C) Total amount of I found in one whole flower, plotted versus the incubation time

2.5.2.2. ICP-MS result by NPs with iohexol as inner reference

In this section, ICP-MS data of flower incubated by different size NPs with iohexol as inner reference was shown and discussed. Amount of Au or I found in the respective flower parts normalized by mass of the flower parts was shown in Figure 2-15. Almost all Au amount was decreased along the flower from stem to petal except for ACC@Au NPs 1.4 nm can be delivered to petal. And different size NPs showed different amount of Au in each flower part. Iohexol, as inner reference, also can be delivered to petal. With incubation time increasing, the Au and I amount also was increased. But the proportion of Au or I in each flower part cannot be concluded. Thus Proportion of Au or I found in the respective flower parts, normalized to the total mass of Au or I found in the whole flower was processed as shown in Figure 2-16. Au majorly located in the stem 1 and the proportion of Au decreased along the stem to petal except for ACC@Au NPs 1.4 nm which majorly located in petal. Moreover, the Au proportion of each part was not significantly different with incubation time increasing. Obvious comparison of the uptake amount and proportion in each flower part each size NPs were shown in Figures 2-17 and 2-18. With incubation time increasing, Au amount was also increased in each flower part. With the NPs size increasing, the Au cannot obviously be

detected in blossom and petal. The proportion of Au in each flower part did not significantly change with incubation time increasing. Figure 2-19 showed the total Au amount in the whole flower. It indicated Au amount in each flower was incubation time-dependent and no obvious size-dependent result.

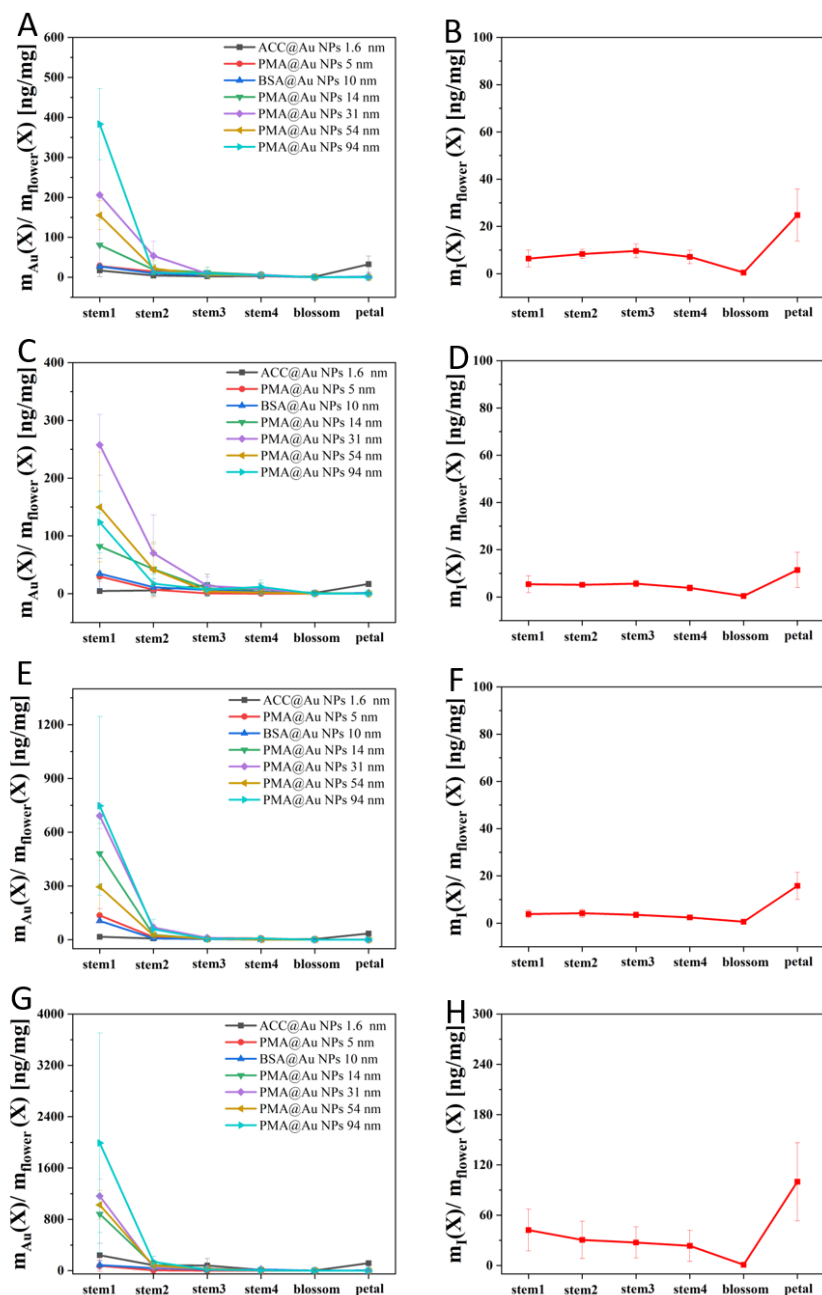


Figure 2-15. Amount of Au or I found in the respective flower parts, normalized to the mass of the flower parts, plotted versus the position of the flower parts along the stem (X=stem 1, stem

2, stem 3, stem 4, blossom and petal). (A), (C), (E) and (G) corresponded for Au at 6, 12, 24 and 48 h respectively. (B), (D), (F) and (H) corresponded for I at 6, 12, 24 and 48 h respectively.

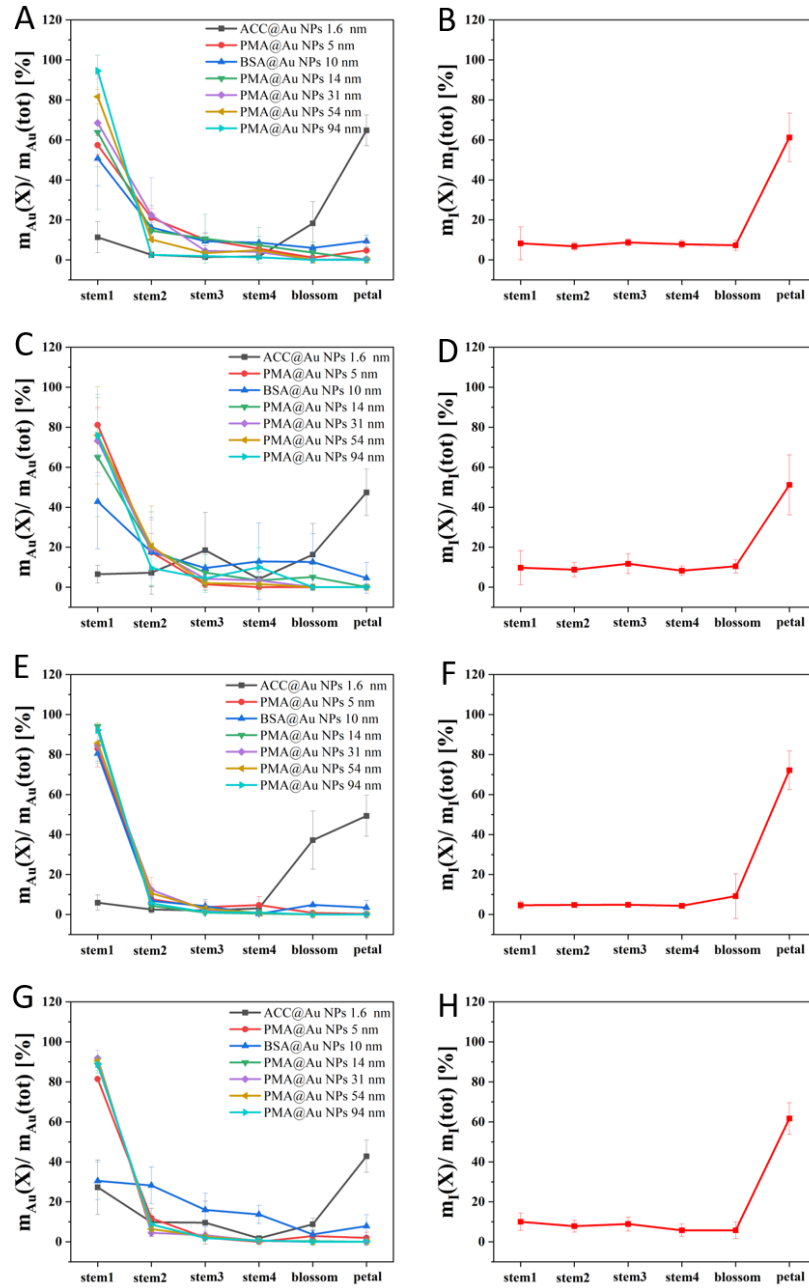


Figure 2-16. Proportion of Au or I found in the respective flower parts, normalized to the total mass of Au or I found in the whole flower, plotted versus the position of the flower parts along the stem(X =stem 1, stem 2, stem 3, stem 4, blossom and petal). (A), (C), (E) and (G) corresponded for Au at 6, 12, 24 and 48 h respectively. (B), (D), (F) and (H) corresponded for I at 6, 12, 24 and 48 h respectively.

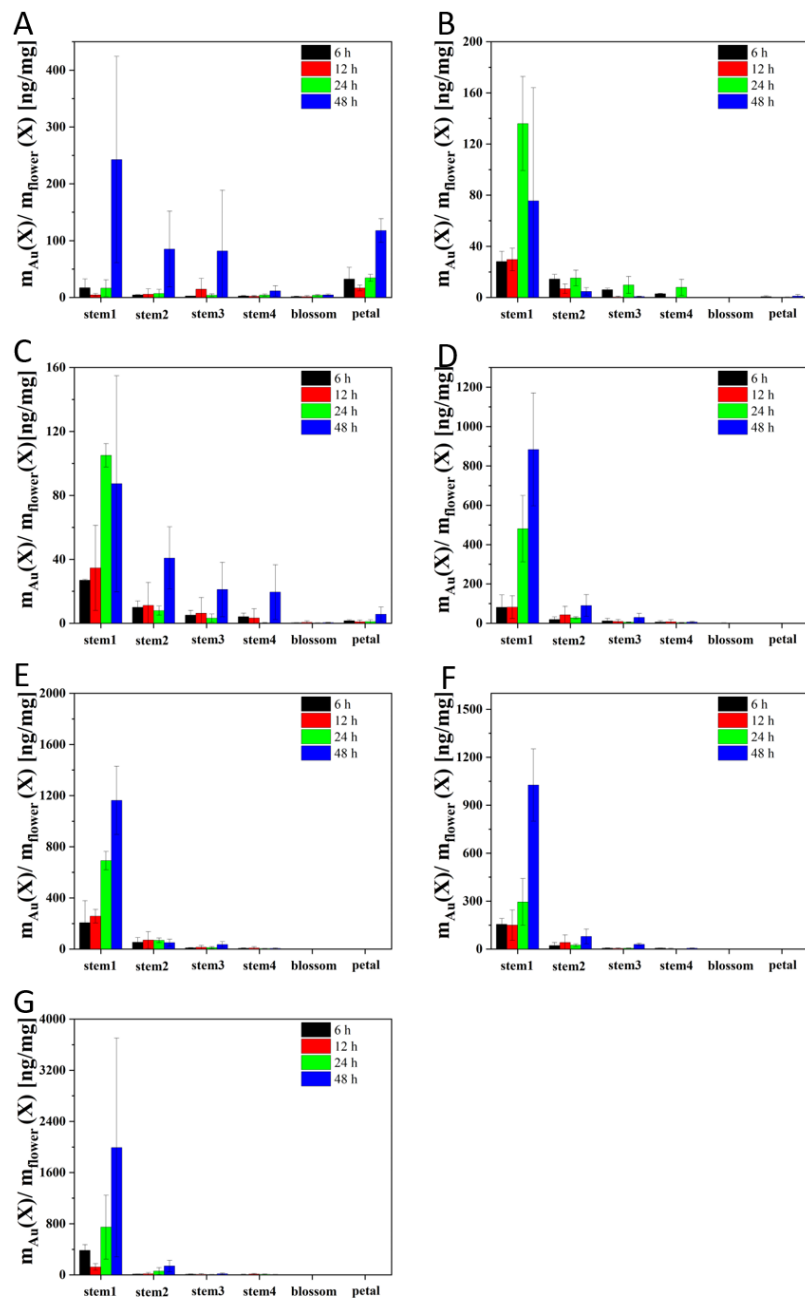


Figure 2-17. Amount of Au found in the respective flower parts, normalized to the mass of the flower parts, plotted versus the position of the flower parts along the stem (X =stem 1, stem 2, stem 3, stem 4, blossom and petal). (A), (B), (C), (D), (E), (F) and (G) corresponded for ACC@Au NPs (1.6 nm), PMA@Au NPs (5 nm), BSA@Au NPs (10 nm), PMA@Au NPs (14 nm), PMA@Au NPs (31 nm), PMA@Au NPs (54 nm), PMA@Au NPs (94 nm) respectively.

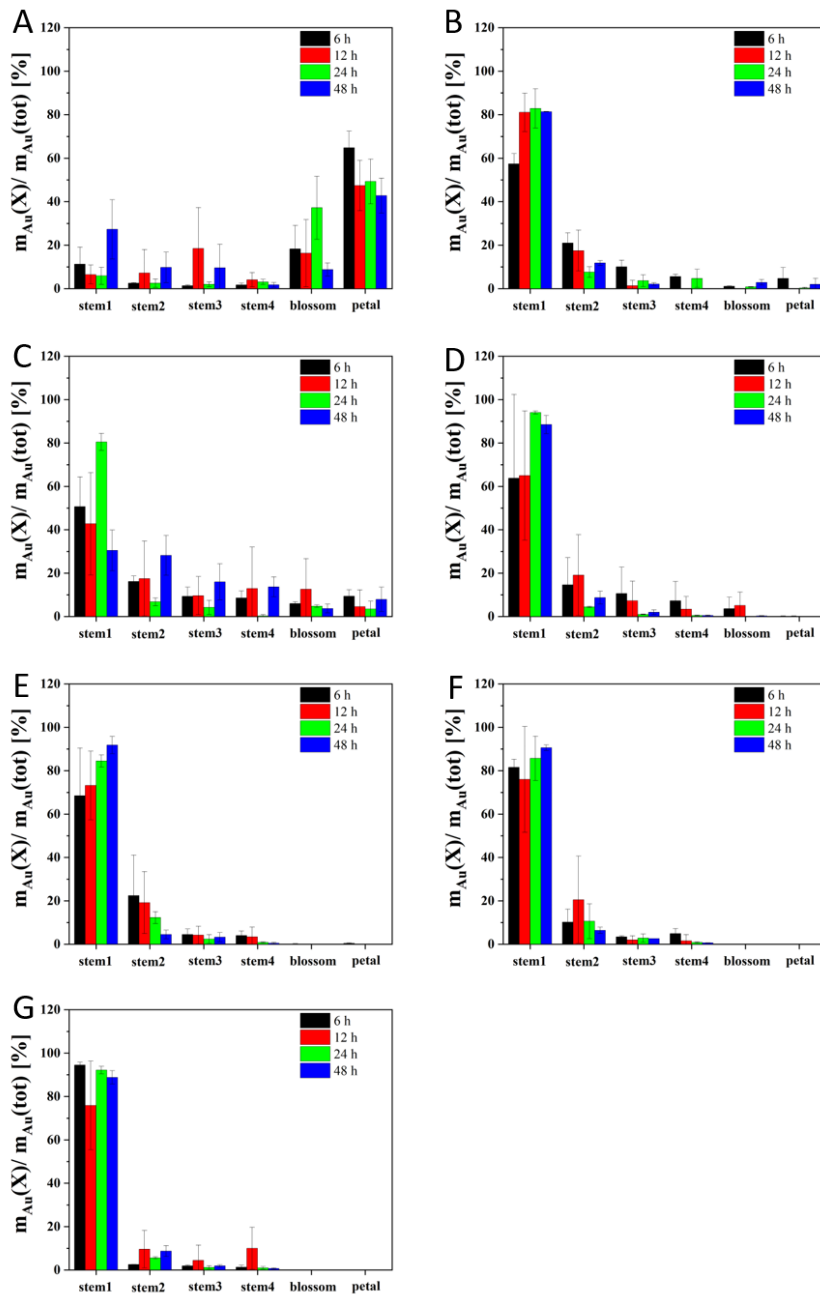


Figure 2-18. Proportion of Au found in the respective flower parts, normalized to the total mass of Au found in the whole flower, plotted versus the position of the flower parts along the stem ($X = \text{stem 1, stem 2, stem 3, stem 4, blossom and petal}$). (A), (B), (C), (D), (E), (F) and (G) corresponded for ACC@Au NPs (1.6 nm), PMA@Au NPs (5 nm), BSA@Au NPs (10 nm), PMA@Au NPs (14 nm), PMA@Au NPs (31 nm), PMA@Au NPs (54 nm), PMA@Au NPs (94 nm) respectively.

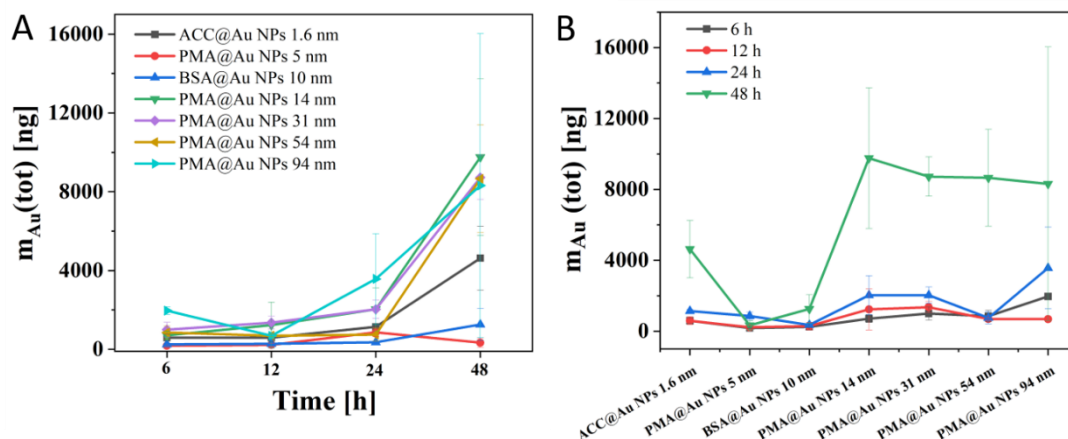


Figure 2-19. (A) Total amount of Au found in one whole flower, plotted versus the incubation time. (B) Total amount of Au found in one whole flower, plotted versus the core diameter of the different size NPs.

2.5.2.3. ICP-MS result by NPs with KI as inner reference

This section showed ICP-MS data of flower incubated by different size NPs with KI as inner reference. In this part, ATT@Au NPs 1.4 nm was included to study. Amount of Au or I found in the respective flower parts, normalized to the mass of the flower parts was shown in Figure 2- 20. Almost all Au amount was decreased along the flower from stem to petal except for ACC@Au NPs 1.6 nm can be delivered to petal. Interestingly, ATT@Au NPs 1.4 nm was closed to ACC@Au NPs 1.6 nm. But it cannot be detected in petal. KI, as inner reference, also can be delivered to petal. With incubation time increasing, the Au and I amount also was increased. Proportion of Au or I found in the respective flower parts, normalized to the total mass of Au or I found in the whole flower was processed as shown in Figure 2-16. Au still majorly located in the stem 1 and the proportion of Au decreased along the stem to petal for the bigger NPs. ACC@Au NPs 1.4 nm majorly located in petal. Moreover, the Au proportion of each part was not significantly different with incubation time increasing. Obvious comparison of the uptake amount and proportion in each flower part each size NPs was shown in Figures 2-22 and 2-23. With incubation time increasing, Au amount was also increased in each flower part. With the NPs size increasing, Au cannot obviously be detected in blossom and petal for

bigger size NPs. Figure 2-24 showed the total Au amount in the whole flower. It also indicated Au amount in each flower was incubation time-dependent and no obvious size-dependent result.

Based on these two set of ICP-MS result of flower incubated by different size NPs with iohexol and KI, we can conclude that iohexol and KI were selected as the inner reference to cross-check whether the flower was stuck leading to breaking the material transportation. Based on ICP-MS result, the iohexol and KI can be detected along the flower from stem to blossom to petal. These two sets of Au result have no obvious difference, and it means Au NPs were not affected by iohexol and KI when incubation with them. No obvious side-dependent distribution of different size Au NPs was observed in flower.

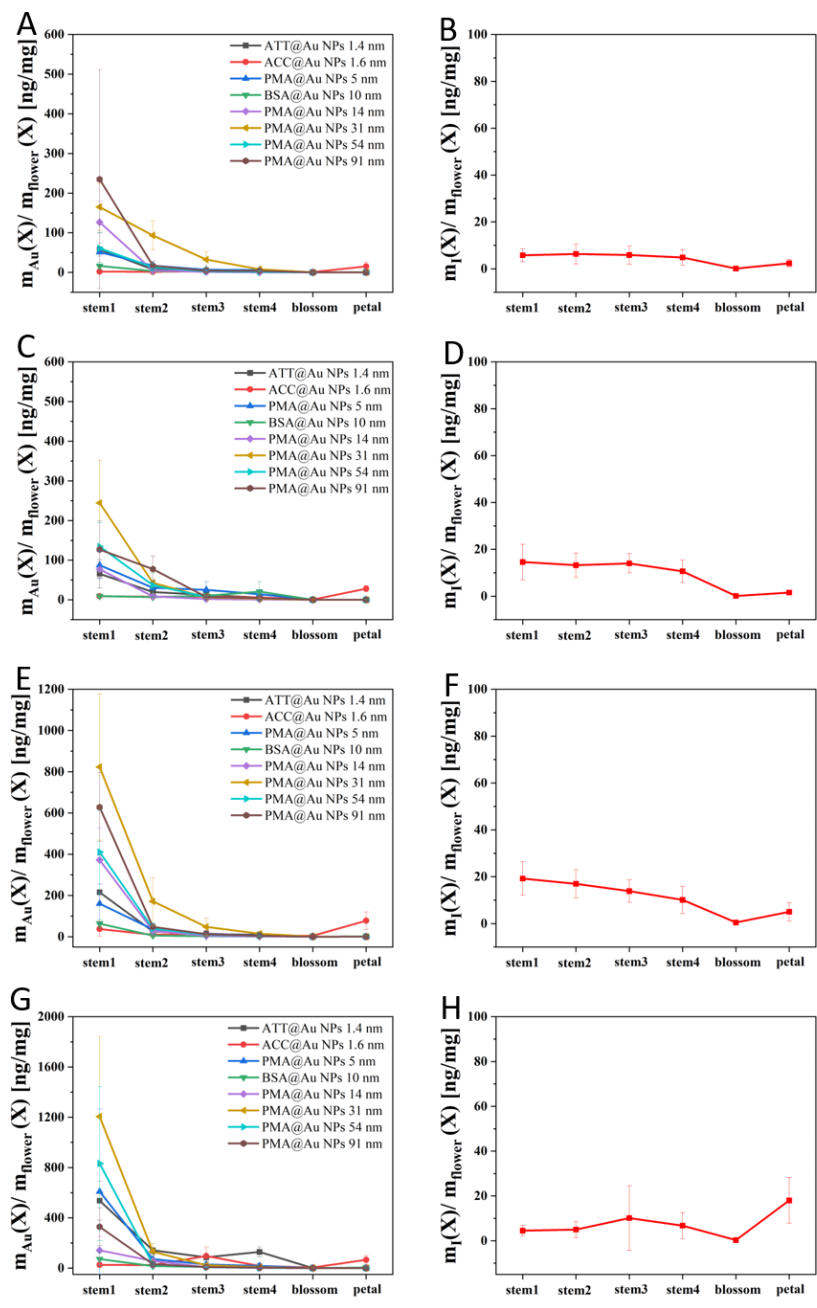


Figure 2-20. Amount of Au or I found in the respective flower parts, normalized to the mass of the flower parts, plotted versus the position of the flower parts along the stem (X =stem 1, stem 2, stem 3, stem 4, blossom and petal). (A), (C), (E) and (G) corresponded for Au at 6, 12, 24 and 48 h respectively. (B), (D), (F) and (H) corresponded for I at 6, 12, 24 and 48 h respectively.

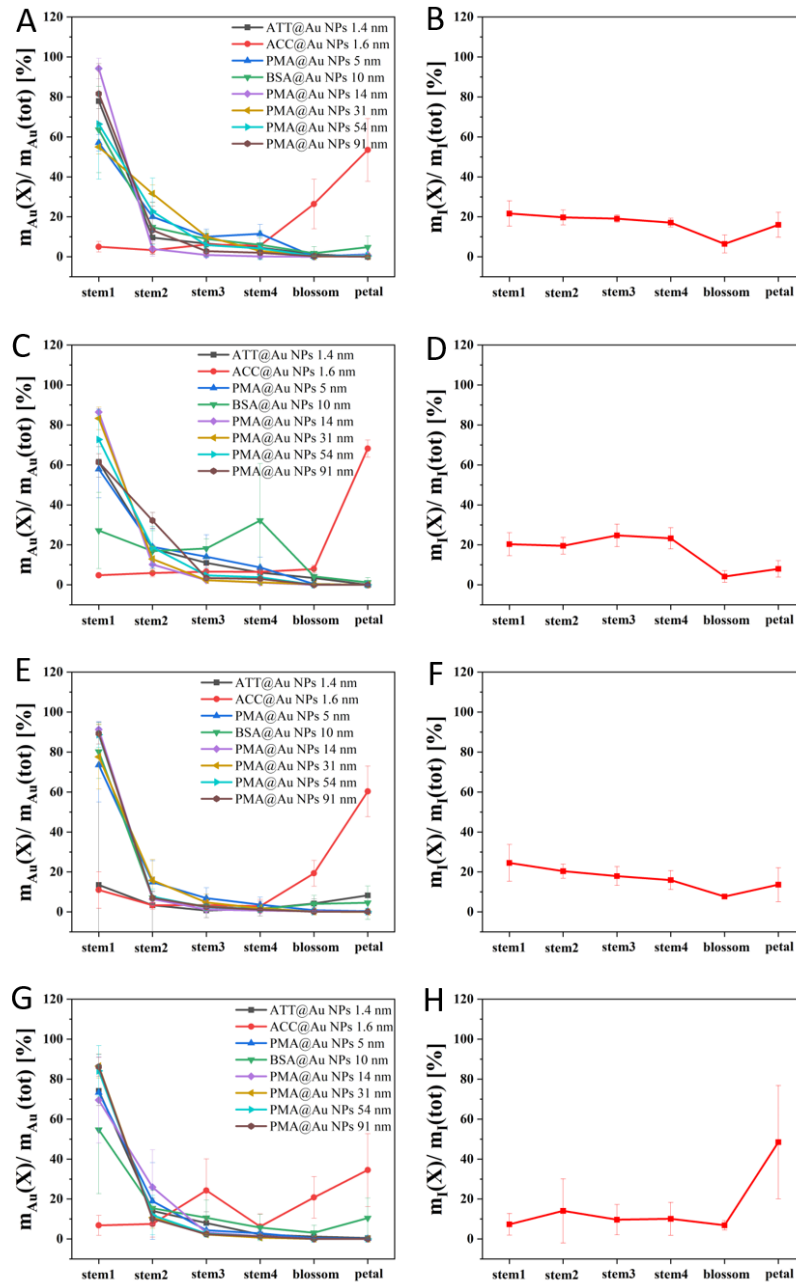


Figure 2-21. Proportion of Au or I found in the respective flower parts, normalized to the total mass of Au or I found in the whole flower, plotted versus the position of the flower parts along the stem ($X = \text{stem 1, stem 2, stem 3, stem 4, blossom and petal}$). (A), (C), (E) and (G) corresponded for Au at 6, 12, 24 and 48 h respectively. (B), (D), (F) and (H) corresponded for I at 6, 12, 24 and 48 h respectively.

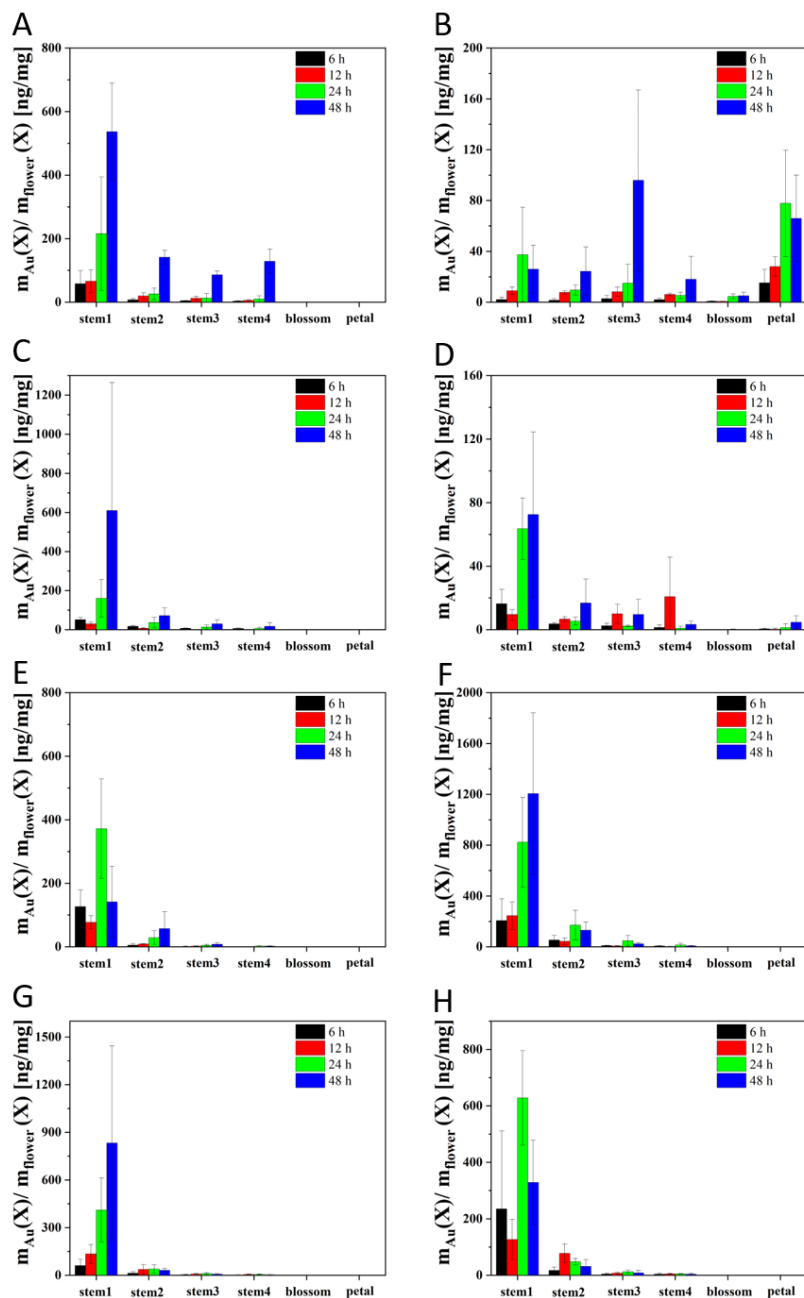


Figure 2-22. Amount of Au found in the respective flower parts, normalized to the mass of the flower parts, plotted versus the position of the flower parts along the stem (X=stem 1, stem 2, stem 3, stem 4, blossom and petal). (A), (B), (C), (D), (E), (F), (G) and (H) corresponded for ATT@Au NPs (1.4 nm), ACC@Au NPs (1.6 nm), PMA@Au NPs (5 nm), BSA@Au NPs (10 nm), PMA@Au NPs (14 nm), PMA@Au NPs (31 nm), PMA@Au NPs (54 nm), PMA@Au NPs (94 nm) respectively.

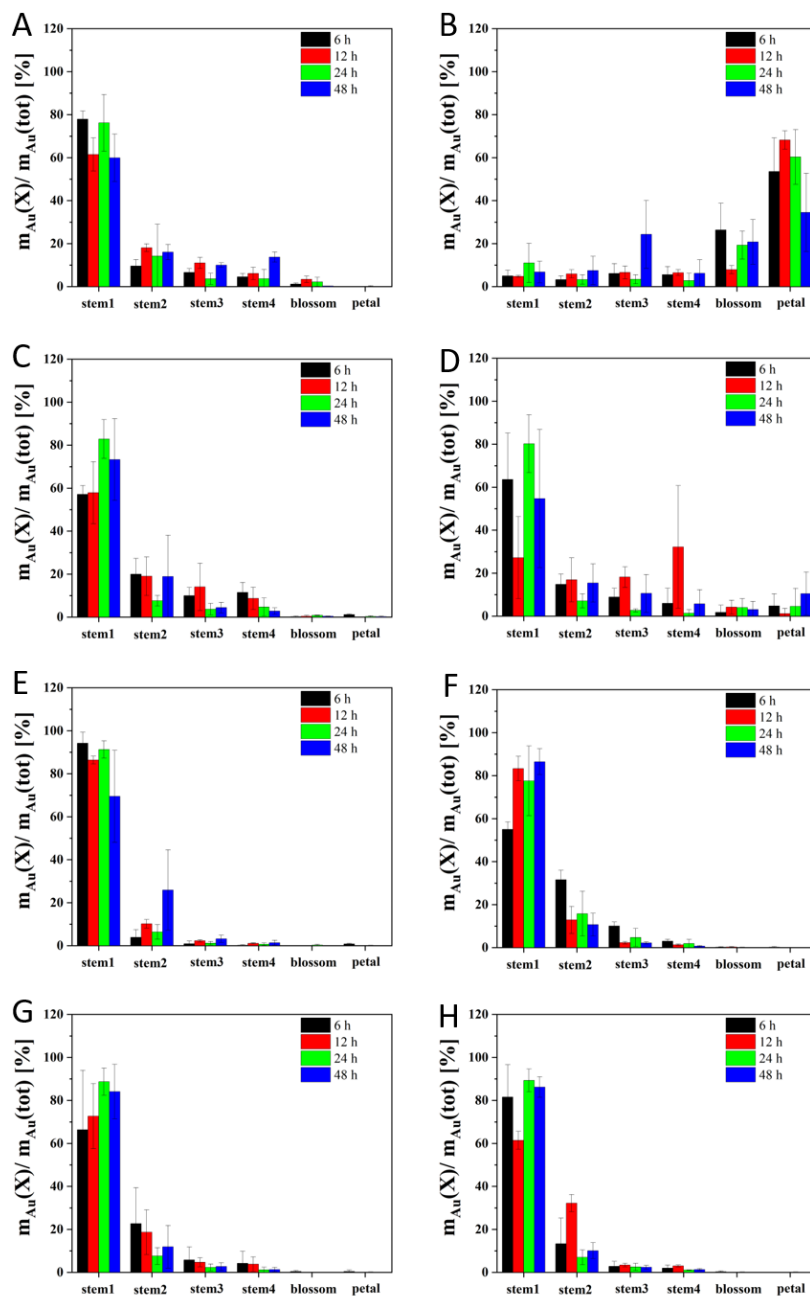


Figure 2-23. Proportion of Au found in the respective flower parts, normalized to the total mass of Au found in the whole flower, plotted versus the position of the flower parts along the stem(X =stem 1, stem 2, stem 3, stem 4, blossom and petal). (A), (B), (C), (D), (E), (F), (G) and (H) corresponded for ATT@Au NPs (1.4 nm), ACC@Au NPs (1.6 nm), PMA@Au NPs (5 nm), BSA@Au NPs (10 nm), PMA@Au NPs (14 nm), PMA@Au NPs (31 nm), PMA@Au NPs (54 nm), PMA@Au NPs (94 nm) respectively.

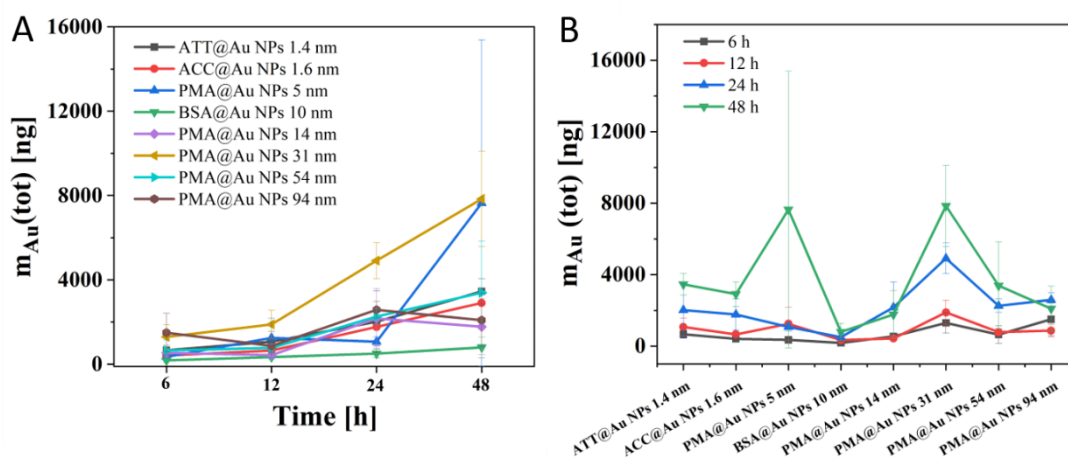


Figure 2-24. (A) Total amount of Au found in one whole flower, plotted versus the incubation time. (B) Total amount of Au found in one whole flower, plotted versus the core diameter of the different size NPs.

2.5.3. In vivo distribution study of NPs in flower by XFI

ICP-MS results cannot directly reveal different size NPs transportation in flower and it is hard to see the real dynamics of NP distribution in flower. Thus, synchrotron based X-ray fluorescence imaging was employed to record. For this, flowers were incubated in ACC@Au NPs (1.6 nm), PMA@Au NPs (5 nm), PMA@Au NPs (31 nm) and PMA@Au NPs (54 nm) with iohexol as same as for ICP-MS measurements. As shown in Figure 2-25, as the full XFI spectral range was recorded, data analysis allowed for the determination of the fluorescence of different elements, as here in particular Au and I. It is important to point out that each time series was recorded *in situ* on one individual flower, in contrast to the ICP-MS measurements, for which each time point was recorded with different flowers, as ICP-MS involves destruction of the sample (*i.e.*, burning and dissolution).

As evident from the data shown in Figure 2-25, *in situ* measurements are possible and the flowers were kept alive during imaging. The data are compatible with the ICP-MS result. High-resolution images allow to account for the details of individual flowers. The Au and I fluorescence were gradually increasing with incubation time increasing. Meanwhile, compared Figure 2-25C, D, E and F, it showed the size-dependent in stem with NPs size

increasing. The whole stem was shown Au fluorescence for ACC@Au NPs 1.6 nm. Au fluorescence also can be seen in the whole stem for PMA@Au NPs 5 nm relatively weak than ACC@Au NPs 1.6 nm. With the NPs size increasing, the Au fluorescence is decreasing. In addition, some accumulation of Au NPs within a certain part the stem can be seen. This might reflect the actual point where the NPs stuck in the stem. The fluorescence of I also showed similar distribution.

Meanwhile, time series of XFI data of individual flowers incubated in PMA@Au NPs 5 nm and KI was recorded by XFI as shown in Figure 2-26. It showed obviously stronger Au fluorescence and more homogenous signal compared with Figure 2-25D. Thus, it was clear that there was variety to be expected within flowers with the same incubation conditions, which was also reflected in the larger error bars in the ICP-MS measurements.

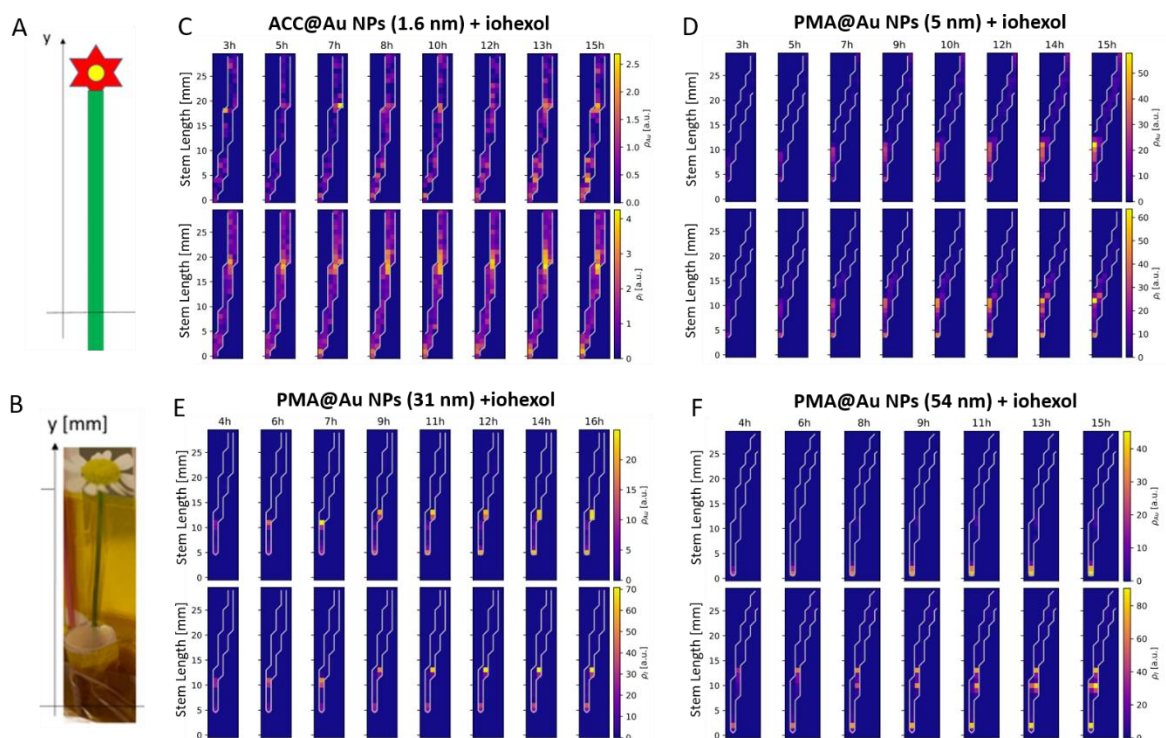


Figure 2-25. Time series of XFI data of individual flowers incubated in different solutions of Au NPs and iohexol. (A) The sketch of flower and (B) Image of flower in incubation solution for XFI. (C), (D), (E) and (F) corresponded to ACC@Au NPs (1.6 nm), PMA@Au NPs (5 nm), PMA@Au

NPs (31 nm) and PMA@Au NPs (54 nm) respectively. Au channel in up and I channel in down. The color bar from purple to yellow indicates gradually increase signal. The XFI images were from Christian Körnig of Prof. Dr Florian Grüner group in University of Hamburg (UHH) and Center for Free-Electron Laser Science (CFEL).

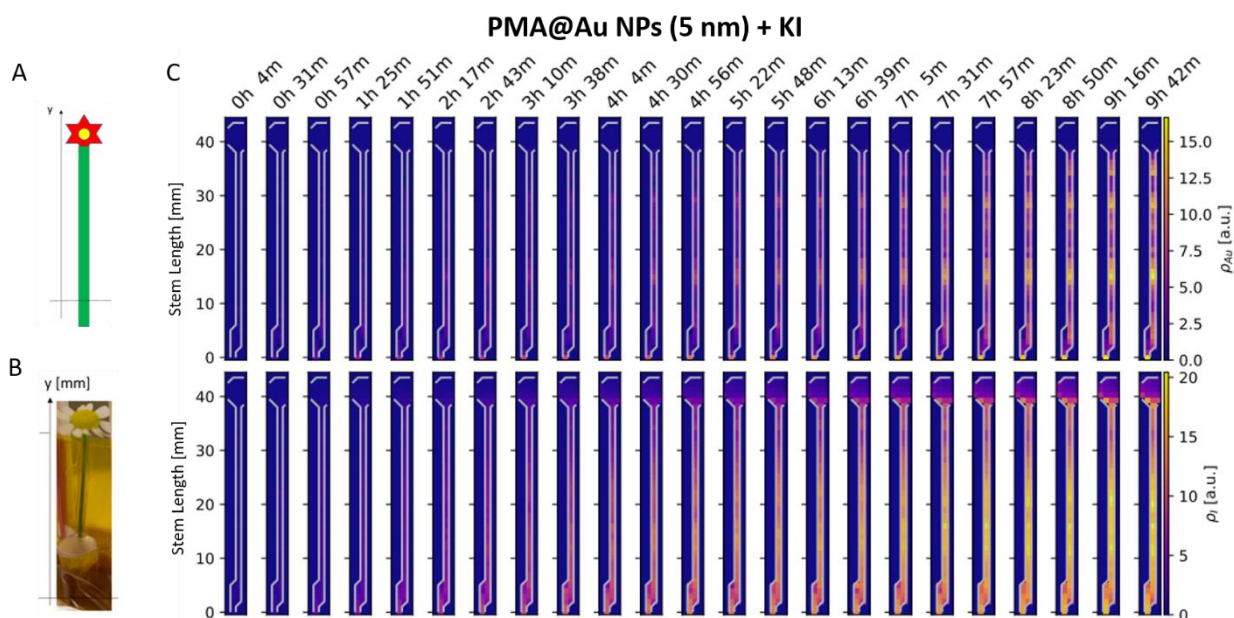


Figure 2-26 (A) The sketch of flower and (B) Image of flower in incubation solution for XFI. (C) Time series of XFI data of individual flowers incubated in different solutions of PMA@Au NPs (5 nm) and KI. Au channel in up and I channel in down. The color bar from purple to yellow indicates gradually increase signal. The XFI images were from Christian Körnig of Prof. Dr Florian Grüner group in University of Hamburg (UHH) and Center for Free-Electron Laser Science (CFEL).

2.5.4. Conclusion

In our study, a library of 1-100 nm water-soluble Au NPs were successfully synthesized. TEM images, UV/vis absorption spectra, core diameters d_c as determined from the TEM images, hydrodynamic diameters d_h as determined from DLS, and zeta potentials ζ as determined with LDA showed the series NPs with good quality. Meanwhile, ICP-MS was employed to study the NPs distribution in flower with incubation time and NPs size. ICP-MS result indicated obvious time-dependent uptake of flower to NPs namely higher uptake of flower to NPs with

incubation time increasing. But no obvious NPs size dependent for the NPs distribution in flower. Further *in vivo* distribution study of NPs in flower by XFI *in situ* revealed that the obvious size-dependent transportation in flower that is smaller size NPs can be transported along flower stem to petal. Simultaneously, it reflected the existed actual point where the NPs stuck in the stem to and there was variety to be expected within flowers with the same incubation conditions. In general, ICP-MS need to entirely destroy the sample to measure and it need huge time to prepare the sample when met the huge sample amount. Compared with ICP-MS, XFI possessed effectively nondestructive imaging, allowing potentially for recording in-situ/in-vivo biodistributions.

3. Cell labeled by Iohexol, Pd NPs, QDs and Ag NPs for *in vitro* XFI

3.1. Introduction

Cell therapy has shown potential optimistic result to treat disease⁸⁰⁻⁸¹. Preclinical application of cell therapy is with great promises^{61, 82-84}. However, some key questions influence their application. It is necessary to understand the cell how to migrate and distribute in the whole body⁸⁵. Therefore, cell tracing is imperative in their working process. Noninvasive imaging is a useful method to qualitatively and quantitatively monitor cell inside the host⁸⁶. Meanwhile, this method need the cell labeled by contrast agent^{5, 86-90}. XFI is a promising detection method and received widely spread attention due to it enable trace different element at the same time and low detection limitation^{28, 60, 91-93}. In our study, we labeled the macrophage (MHS) and T cell (CTLL-2) by palladium NPs, quantum dot, silver NPs and iohexol (a commercial small molecule iodine contrast agent) and systematically study the interaction of NPs with cells. Finally, XFI was employed for imaging in mouse to evaluate iohexol and palladium NPs imaging effect.

3.2. Major reagents

Name	Purity	Company	Function
RPMI 1640 medium		Sigma Aldrich	For cell culture
Sodium pyruvate solution		Sigma Aldrich	For cell culture
β -mercaptoethanol	99 %	Sigma Aldrich	For cell culture
Fetal bovine serum		Biochrom	For cell culture
Penicillin/streptomycin		Gibco Invitrogen Corporation	For cell culture
Phosphate buffered saline		Invitrogen	For cell culture
0.05 % trypsin/EDTA		Thermofisher	For cell culture
Resazurin	80 %	Sigma Aldrich	For cytotoxicity
Fluorescein Diacetate		TCI	For cell live/dead

Ethidium Homo Dimer 1		Biotium	staining study For cell live/dead staining study
Oleylamine	>70 %	Sigma Aldrich	For Pd NPs synthesis
Oleic acid	90 %	Sigma Aldrich	For Pd NPs synthesis
1-Octadecene	90 %	Sigma Aldrich	For Pd NPs synthesis
Borane-morpholine	95 %	Sigma Aldrich	For Pd NPs synthesis
Palladium acetylacetonate	99 %	Sigma Aldrich	For Pd NPs synthesis
Silver nitrate	99 %	Sigma Aldrich	For Ag NPs synthesis
Trisodium citrate	99 %	Alfa Aesar	For Ag NPs synthesis
Tannic acid	99 %	Sigma Aldrich	For Ag NPs synthesis

3.3. Key instrument

Name	Model	Company	Function
Dynamic light scattering (DLS)	NANO ZS	Malvern	NPs characterization
UV–Vis absorption spectrophotometer	Agilent 8453	Agilent technologies	Absorption spectra measurement
Inductively coupled plasma mass	7700 Series studies	Agilent	For daisy flower uptake
Transmission electron microscopy (TEM)	JEM- 1400PLUS	JEOL	For NPs morphology visualization
Confocal microscopy	LSM510	Carl Zeiss Microscopy GmbH	For cellular live/dead staining study

3.4. Experiments and methods

3.4.1. Synthesis of NPs

3.4.1.1. Synthesis of Pd NPs

The Pd NPs were synthesized as previously reported⁹⁴. Briefly, Palladium acetylacetonate (0.1 g, 0.328 mmol) was added into the mixture of 1-octadecene (8 mL) and oleylamine (10 mL).

Then the mixture was heated to 100 °C till it forms into solution by N₂ protection. Subsequently, the solution with borane-morpholine (0.2 g) dissolved in oleylamine (2 mL) was injected the last step mixture. Then it was heated to 130 °C at the rate of 4-5 °C per min and kept under N₂ protection for 20 min. Ethanol (20 mL) was added to separate the NPs and collect the NPs by centrifuge. Finally, the NPs were washed twice by ethanol (20 mL) and dispersed in 10 mL hexane for PMA coating.

3.4.1.2. Synthesis of Ag NPs

The Ag NPs was synthesized as previously synthesized⁹⁵. For that, the sodium citrate (5 mM) and tannic acid (0.25 mM) in 100 mL Milli-Q water were prepared and heated to boil with condenser to get rid of the evaporation in three neck flask for 15 min. After boiling, AgNO₃ (25 mM, 1mL) was added and the solution become light yellow immediately to form the 15 nm Ag NPs seed. Then 19.5 mL of sample was extracted and adding 16.5 mL Milli-Q water. The temperature of solution was decreased to 90 °C. Subsequently, sodium citrate (25 mM, 500 µL) and tannic acid (2.5 mM, 1.5 mL) were added. After 1 min, the AgNO₃ (25 mM, 1mL) was injected and keep reacting for 20-30 min. Then repeat the above step till the Ag NPs to 50 nm under the UV checking.

3.4.1.3. QDs and iohexol

The QDs with core/shell/shell of CdSe/CdS/ZnS was from Fraunhofer-Zentrum für Angewandte Nanotechnologie CAN. Iohexol was commercial from GE Healthcare Buchler GmbH & Co. KG.

3.4.1.4. PMA coating of NPs

3.4.1.4.1. PMA coating of Pd NPs

In order to stabilize the Pd NPs, the PMA was used to coat on Pd NPs surface referred to a similar method reported⁷⁵. Briefly, 4 mL Pd NPs (section 3.4.1.1) and 1 mL PMA (0.5 M) were dispersed in 100 mL chloroform in flask and evaporate by rotary evaporation. This evaporation was repeated 3 times. The SSB buffer (pH = 12) was added into the dry flask till dissolved all NPs from flask wall. Finally, the Pd NPs were washed twice by 10 mL Milli-Q water and

centrifuged at 137,000 rcf for 30 min. Finally, the Pd NPs were dispersed in Milli-Q water for future use.

3.4.1.4.2. PMA coating of Ag NPs

In order to stabilize the Ag NPs, ligand exchange and PMA coating were carried out⁷⁵. Briefly, PEG2000 with sulfhydryl was added into the Ag NPs solution (3.4.1.2) in the ratio ($C_{PEG}/C_{NP} = 20 \times 10^4$) overnight. Then the DDA was dissolved in chloroform and added into the Ag NPs after PEGylation in the ratio (C_{DDA}/C_{NP}) of 20×10^6 overnight. Then the organic phase was collected by separation funnel. To remove the free DDA, the organic phase was centrifuged and the precipitation was collected. Then the precipitation was dispersed in 20 mL chloroform to wash twice at 6500 rpm for 10 min. The resulting DDA capped Ag NPs was further coated by polymer⁷⁵. PMA was added in the ratio (C_{PMA}/C_{NP}) of 100. The PMA and Ag NPs were mixed in 100 mL chloroform in flask and evaporate by rotary evaporation. This evaporation was repeated for 3 times. The SSB buffer (pH = 12) was added into the dry flask till dissolved all NPs from flask wall. Finally, Ag NPs were washed by 10 mL Milli-Q water and centrifuged twice. Finally, the Ag NPs was dispersed in Milli-Q water for future use.

3.4.1.4.3. PMA coating of QDs

In order to stabilize the QDs and incubate the cell by QDs, the PMA coating was carried out⁷⁵. Briefly, the QDs and PMA were added into the 100 mL chloroform in flask. The PMA was added in the ratio (C_{PMA}/C_{NP}) of 100. This evaporation was repeated for 3 times. The SSB buffer (pH = 12) was added into the dry flask till dissolved all NPs from flask wall. Finally, QDs were washed twice by 10 mL Milli-Q water and centrifuged at 137,000 rcf for 30 min. Finally, the QDs were dispersed in Milli-Q water for future use.

3.4.2. Colloidal stability of NPs

Pd NPs, QDs and Ag NPs were dispersed in Milli-Q water and completed cell medium to respectively form their solution. Their number hydrodynamic distribution was recorded by DLS at 0 h and 24 h.

3.4.3. Cell culture

3.4.3.1. MHS cell culture

The mouse macrophage alveolar cell line MHS was obtained from American Type Culture Collection (ATCC) (Manassas, VA, USA). RPMI 1640 medium with heat inactivated 10 % FBS, 1 mM Na-pyruvate, 100 U/mL penicillin, and 100 µg/mL streptomycin (Gibco Invitrogen Corporation) and β-mercaptoethanol (0.05 mM) was used to culture the cell at 37 °C in 5 % CO₂.

3.4.3.2. CTLL-2 cell culture

The mouse lymphocyte cytotoxic T lymphocyte was obtained from American Type Culture Collection (ATCC) (Manassas, VA, USA). RPMI 1640 medium with heat inactivated 10 % FBS, 10 % T-STIM with Con A, 1 mM Na-pyruvate, 100 U/mL penicillin, and 100 µg/mL streptomycin (Gibco Invitrogen Corporation) was used to culture the cell at 37 °C in 5 % CO₂.

3.4.4. Cell cytotoxicity study by Resazurin experiment

3.4.4.1. MHS cell cytotoxicity

In order to investigate the cell viability of MHS macrophages exposed to different NPs and iohexol, the Resazurin assay was conducted to evaluate as previously reported. Briefly, 3.3×10^4 cell in 100 µL medium was seeded in the 96 well plate for overnight. The different concentration iohexol and NPs was added and incubated for 24 h. After that, cell was washed by phosphate buffer saline (100 µL) for once. Subsequently, the Alamar Blue solution (Thermal Fisher scientific) was added into the well and incubate for another 4 h at 37 °C. Then the fluorolog-3 was used to measure the fluorescence from 580 nm to 590 nm. The higher fluorescence intensity, the better cell viability. Thus, the cell viability is proportional to the fluorescence intensity. The results were normalized by the fluorescence of control cell without treatment.

3.4.4.2. CTLL-2 cell cytotoxicity

The cell viability of CTLL-2 cell was evaluated in the same method as MHS cell. Due to the CTLL-2 is suspension, thus the 24 well plate was used to incubate. For that, 20×10^4 was exposed in

different concentration of iohexol and NPs in 24 well plate for 24 h at 37 °C. Then the cell was centrifuged and washed once by PBS. Subsequently, the Alamar blue solution was added and seed in 96 well plate in the cell number 3.3×10^4 for 8 h at 37 °C. Then the fluorolog-3 was used to measure the fluorescence from 580 nm to 590 nm. The higher fluorescence intensity, the better cell viability. Thus, the cell viability is proportional to the fluorescence intensity. Finally, the result was normalized by the fluorescence of control cell without treatment.

3.4.5. Cell viability study by cell live/dead staining experiment

3.4.5.1. MHS cell live/dead staining

The cell live/dead staining assay was conducted to visually demonstrate the iohexol and NPs cytotoxicity to MHS. Briefly, 3.3×10^4 cell in $V_{\text{medium}} = 100 \mu\text{L}$ was seeded in the 96 well plate for overnight. The different concentration iohexol and NPs was added and incubated for 24 h. After that, cell was washed by phosphate buffer saline (100 μL) for once. Meanwhile, no iohexol or NPs treated cell as negative control and killed cell by ethanol as positive control. Subsequently, the Fluorescein diacetate (4 μM) and Ethidium homo dimer 1 (2 μM) in PBS was added into the 96 well plate in 100 μL each well for 30 min. After that, the confocal scanning laser microscopy was used to image.

3.4.5.2. CTLL-2 cell live/dead staining

The cell live/dead staining assay also was used to demonstrate the iohexol and NPs cytotoxicity to CTLL-2. Briefly, 20×10^4 was exposed in different concentration of iohexol and NPs in 24 well plate for 24 h at 37 °C. Then the cell was centrifuged and washed once by PBS. Meanwhile, no iohexol or NPs treated cell as negative control and killed cell by ethanol as positive control. After that, the cell was dispersed in the PBS with Fluorescein diacetate (4 μM) and Ethidium homo dimer 1 (2 μM) for 30 min. Then the confocal scanning laser microscopy was used to image.

3.4.6. Cell uptake study

3.4.6.1. MHS cell uptake study

The labelling efficiency of MHS macrophages to iohexol and NPs was evaluated by ICP-MS as

previously reported. Briefly, 10^6 cell in 2 mL medium was seeded in the 6 well plate overnight at 37 °C and 5 % CO₂. The next d, the medium was changed with different iohexol or NPs concentration medium and incubate for 6 h and 24 h. After incubation, the supernatant was discarded and wash each well three times by PBS. Then the 100 μL trypsin ethylenediaminetetraacetic acid (EDTA) (0.01 % trypsin–EDTA, Thermo Fisher Scientific) was added into each well for 1 min to detach the cells. 1 mL cell medium was added to collect all cells and centrifuge at 300 rcf for 5 min. Then 1 mL PBS was added to count the cell number. Finally, the supernatant was discarded and collect the cell pellet for ICP-MS measurement.

3.4.6.2. CTLL-2 cell uptake study

The labeling efficiency of CTLL-2 cell to iohexol and Pd NPs was also evaluated by ICP-MS. Briefly, due to CTLL-2 is suspension cell, 10^6 cells were exposed in different iohexol and NPs concentrations and was seed in 6 well plate at 37 °C and 5 % CO₂ for 6 h and 24 h. Then the cell was collected by centrifuge at 300 rcf for 5 min and the supernatant was discarded. The cell pellet was washed by 1 mL PBS for 3 times. Then count the cell number and collect the cell pellet for ICP-MS measurement.

3.4.7. Cell proliferation study

3.4.7.1. MHS cell proliferation study

In order to study whether the cell proliferation was influenced after labeled by iohexol and NPs, the cell proliferation experiment was carried out. 3.3×10^4 cell in V_{medium} 100 μL was seeded in the 96 well plate for overnight. Then the medium was replaced by different concentration of iohexol and NPs to incubate for another 24 h at 37 °C and 5 % CO₂. The colchicine (5 μM) was added to suppress cell proliferation as positive control. Then the medium was replaced by medium which contained EdU (5 μM) to incubate 6 h. After incubation, the medium was removed and add the 3.7 % formaldehyde 100 μL in each well to incubate 15 min at room temperature. After that, the fixative was removed and 3 % BSA in PBS (100 μL) was used to wash for twice. Then 100 μL of 0.5 % Triton X-100 in PBS was added in each well and incubate for 20 min at room temperature. Remove the permeabilization buffer and wash twice by 3 % BSA in PBS (100 μL) to label the Alexa Fluor azide 488. Namely,

the reaction solution with Tris buffer at pH = 8.5, 100 mM CuSO₄, Alexa Fluor azide and ascorbic acid was prepared as the Invitrogen Click-iT EdU Imaging Kits procedure. Then 50 µL reaction solution was added to each well and incubate for 30 min protected from light. After that, remove the reaction solution and wash once by 3 % BSA in PBS (100 µL). 100 µL PBS was added to wash once and add 50 µL Hoechst (5 µg/mL) in PBS to stain the nuclei for 30 min at room temperature. Wash each well twice by 100 µL PBS. Finally, 100 µL PBS was added in each well to image by confocal microscopy.

3.4.7.2. CTLL-2 cell proliferation study

The cell proliferation experiment was carried out in the same method with MHS macrophages. Briefly, 10⁶ cells were exposed by iohexol and NPs in different concentration in 2 mL cell medium and incubated in 6 well plate for 24 h at 37 °C and 5 % CO₂. After that, the cell medium was replaced by medium with EdU (5 µM) by centrifuge at 300 rcf for 5 min to incubate 6 h in 1.5 mL Eppendorf tube. The cells were collected by centrifuge and discard the supernatant. 3.7 % formaldehyde 200 µL was added to incubate 15 min at room temperature. Then the fixative was removed by centrifuge and the 3 % BSA in PBS (200 µL) was used to wash for twice. Then 200 µL of 0.5 % Triton X-100 in PBS was added in tube and incubate for 20 min at room temperature. Remove the permeabilization buffer and wash twice by 3 % BSA in PBS (200 µL) to label the Alexa Fluor azide 488. Namely, the reaction solution with Tris buffer at pH = 8.5, 100 mM CuSO₄, Alexa Fluor azide and ascorbic acid was prepared as the Invitrogen Click-iT EdU Imaging Kits procedure. Then 100 µL reaction solution was added to each well and incubate for 30 min protected from light. After that, remove the reaction solution and wash once by 3 % BSA in PBS (200 µL). 200 µL PBS was added to wash once more and add 100 µL Hoechst (5 µg/mL) in PBS to stain the nuclei for 30 min at room temperature. Wash twice by 100 µL PBS. Finally, add 1000 µL PBS to count the cell number and reseed in 96 well plate in 3.3*10⁴ cell in 100 µL PBS per well to image by confocal microscopy. Note, all step which need to change the medium and wash was operated by centrifuge at 300 rcf for 5 min.

Imaging was performed by confocal laser scanning microscopy. In order to image the EdU-Alexa Fluor 488, $\lambda_{exc} = 488$ nm and beam splitter at 505 nm were used to collect in green channel.

Meanwhile, the Hoechst fluorescence was collected by $\lambda_{exc} = 405$ nm and beam splitter at 460 nm in blue channel. Then the cell profiler was used to process the image. The nuclei with blue fluorescence and proliferating cell with green fluorescence were counted respectively. Cell number with green fluorescence was divided by cell number with blue fluorescence and multiply 100 % to get the cell proliferation. The cell proliferation was got in each image and average each concentration. The data was get from three individual experiment.

3.4.8. Cell migration study

3.4.8.1. MHS cell migration

In order to study whether the migration ability of cells labeled by iohexol and NPs was influenced, the cell migration experiment was conducted. Briefly, 10^6 MHS cells were seeded in 6 well plate overnight. Then the cell medium was replace by cell medium with different concentration iohexol and NPs to incubate for 24 h at 37 °C and 5 % CO₂. The cells were detached by trypsin-EDTA and transferred the cells into free FBS cell medium. The migration chamber was put in 24 well plate. 100 μ L serum-free medium was added into the chamber firstly. Then 200 μ L cell solution (3×10^4 cell inside) prepared in last step was placed in to the chamber and 800 μ L completed cell medium was placed in each well to incubate for 16 h at 37 °C and 5 % CO₂. Then remove the medium from the chamber and washed by PBS twice. The 3.7 % formaldehyde in PBS was used to fix the cell for 10 min at room temperature. Then the cells were washed by PBS twice and the inner side cell of chamber was wiped away by swab to remove the cell not migrated. Finally, the chamber was placed on the microscopy plate to image by confocal laser scanning microscopy. The cell image was analyzed by Image J software to count cell number. The migration cell number was divided by seed cell number multiply 100 % to get the cell migration percent.

3.4.8.2. CTLL-2 cell migration study

For the CTLL-2 cell, the same method was used. 10^6 CTLL-2 cells were exposed in different concentration iohexol and NPs and incubated for 24 h at 37 °C and 5 % CO₂. Then the cells were collected by centrifuge and redispersed in free-serum medium. The migration chamber was put in 24 well plate. 100 μ L serum-free medium was added into the chamber firstly. Then

200 μL cell solution (3×10^4 cell inside) prepared in last step was placed into the chamber and 800 μL completed cell medium was placed in each well to incubate for 16 h at 37 $^{\circ}\text{C}$ and 5 % CO_2 . Then remove the medium from the chamber and washed by PBS twice. The 3.7 % formaldehyde in PBS was used to fix the cell for 10 min at room temperature. Then the cells were washed by PBS twice and the inner side cell of chamber was wiped away by swab to remove the cell not migrated. Finally, the chamber was placed on the microscopy plate to image by confocal laser scanning microscopy. The cell image was analyzed by Image J. to count cell number. The migration cell number was divided by seed cell number multiply 100 % to get the cell migration percent.

3.4.9. Cell exocytosis study

3.4.9.1. MHS cell exocytosis study

In order to study the labeling efficiency (the retention of iohexol or NPs in cells), the cell exocytosis experiment was carried out to evaluate. Briefly, the 10^6 MHS cells in 2 mL cell medium were seeded in 6 well plate overnight at 37 $^{\circ}\text{C}$ and 5 % CO_2 . Then the medium was replaced by 2 mL cell medium with different concentration iohexol or NPs to expose 24 h. After that, the medium was removed and washed by PBS for 3 times to remove the non-internalization NPs or iohexol. Subsequently, the 2 mL new cell medium was added in each well and incubated for 0, 6, and 24 h. After the desired incubation time, the cell was collected and ready for ICP measurement.

3.4.9.2. CTLL-2 cell exocytosis study

The same method was used to study the CTLL-2 cell exocytosis. Briefly, 10^6 CTLL-2 cells were exposed by different concentrations iohexol or NPs in 2 mL in 6 well plate and incubate for 24 h at 37 $^{\circ}\text{C}$ and 5 % CO_2 . Then the cells were collected by centrifuge and washed by PBS for 3 time to remove the non-internalization iohexol or NPs. Then the 2 mL new medium was added to incubate 0, 6 and 24 h. After desired incubation time, the cells were collected and were ready for ICP measurement.

3.4.10. Cell growth

To determine the cell growth, for instance, to see the cells number increases upon the proliferation, 10^6 cells in 2 mL cell medium were seeded 6 well plate and incubate the cell in 24 h, 48 h and 72 h. After desired time, the cell number was counted. The data was got from 3 times experiments.

3.4.11. Cell area

To determine the cell area, 4×10^4 MHS cells with 200 μ L were seeded in Ibidi plate to incubate overnight at 37 °C and 5 % CO₂. CTLL-2 is suspension cell, so no need to seed in advance. The next the d, the medium was discarded and wash 3 times by 200 μ L PBS. Then 200 μ L 3.7 % formaldehyde was added to fix the cell for 15 min at room temperature. Subsequently, 200 μ L PBS was used to wash the cells for 3 times and 0.7 % Triton X-100 was added to permeabilize 10 min at room temperature. Then, the cells were washed with 200 μ L PBS and blocked by 3 % BSA in PBS for 30 min to avoid non-specific absorption. The cytoskeleton was stained by phalloidin-TRITC (50 μ g/mL) in 200 μ L PBS for 45 min and the nuclei was stained by Hoechst (5 μ g/mL) in 200 μ L PBS for 10 min. Finally, the cells were washed by PBS for 3 times to image by confocal laser scanning microscopy. The skeleton was shown in red channel and nuclei was shown in blue channel. Image J. was used to analyze the cell area and more than 200 cells was analyzed for the final data. Note, for the CTLL-2 cell, all washing step need to be finished by centrifuge in 1.5 mL Eppendorf tube.

3.4.12. *In vitro* synchrotron-based XFI by mouse

CTLL-2 and MHS were incubated at the concentration as shown in Table 3-1. CTLL-2 was incubated by iohexol and Pd NPs respectively. MHS was also incubated by iohexol and Pd NPs respectively. In order to decrease the imaging mouse number, cell labeled by iohexol and Pd NPs was mixed to inject on sacrificed mouse back. Wild type mouse from Prof. Dr. med. Samuel Huber group in University Medical Center Hamburg-Eppendorf. The same row MHS or CTLL-2 was mixed injection on the mouse back. Ten injection sites (a-j) for MHS and seven

injection sites (k-q) for CTLL-2. Injection cell number is 2.4 Million per site including iohexol labeled (1.2 Million) and Pd NPs labeled (1.2 Million). Then synchrotron-based X-ray fluorescence imaging was carried out by Prof. Dr Florian Grüner group in University of Hamburg (UHH) and Center for Free-Electron Laser Science (CFEL).

Table 3-1. Concentration of I and Pd element used iohexol and Pd NPs were exhibited as mass concentration as well as the injection site marked by a - q.

Site	Cell lineage	Iohexol c_i (mg/mL)	Pd NPs C_{Pd} ($\mu\text{g/mL}$)	Site	Cell lineage	Iohexol c_i (mg/mL)	Pd NPs C_{Pd} ($\mu\text{g/mL}$)
a	MHS	32	100	k	CTLL-2	32	40
b	MHS	16	80	l	CTLL-2	16	20
c	MHS	8	40	m	CTLL-2	8	10
d	MHS	4	20	n	CTLL-2	4	5
e	MHS	2	10	o	CTLL-2	2	2.5
f	MHS	1	5	p	CTLL-2	1	1.25
g	MHS	0.5	2.5	q	CTLL-2	0.5	0.62
h	MHS	0.25	1.25	-	-	-	-
i	MHS	0.12	0.62	-	-	-	-
j	MHS	0.06	0.31	-	-	-	-

3.5. Result and discussion

3.5.1. NPs synthesis and characterization

In our study, Pd NPs, QDs and Ag NPs were synthesized and coated by PMA on their surface to form water soluble NP according to previously reported literature^{75, 94-95}. After that, the Pd NPs, QDs and Ag NPs were fully characterized by TEM images, core diameters d_c as determined from the TEM images, hydrodynamic diameters d_h as determined from DLS, and zeta potentials ζ as determined with LDA. As shown in Figure 3-1 and Table 3-2, Pd NPs morphology is uniform from TEM image. The core diameter size is around 5.05 ± 0.85 nm based on TEM by ImageJ. The hydrodynamic diameter was 16.89 ± 2.22 nm by DLS and negative zeta potential is -43.63 ± 1.85 mV. For QDs, as shown in Figure 3-2 and Table 3-2, the TEM shows uniform shape. The core diameter size is around 5.05 ± 0.85 nm based on TEM by ImageJ. The hydrodynamic diameter was 9.18 ± 0.50 nm by DLS and zeta potential is -27.00 ± 2.95 mV. For

Ag NPs, as shown in Figure 3-3 and Table 3-2, the TEM shows uniform shape. The core diameter size is around 5.05 ± 0.85 nm based on TEM by ImageJ. The hydrodynamic diameter was 9.18 ± 0.50 nm by DLS and zeta potential is -27.00 ± 2.95 mV. Meanwhile, commercial molecular iodine-based contrast agent iohexol (5-[N-(2,3-Dihydroxypropyl)acetamido]-2,4,6-triiodo-N,N'-bis(2,3-dihydroxypropyl) isophthalamide) was used in our study.

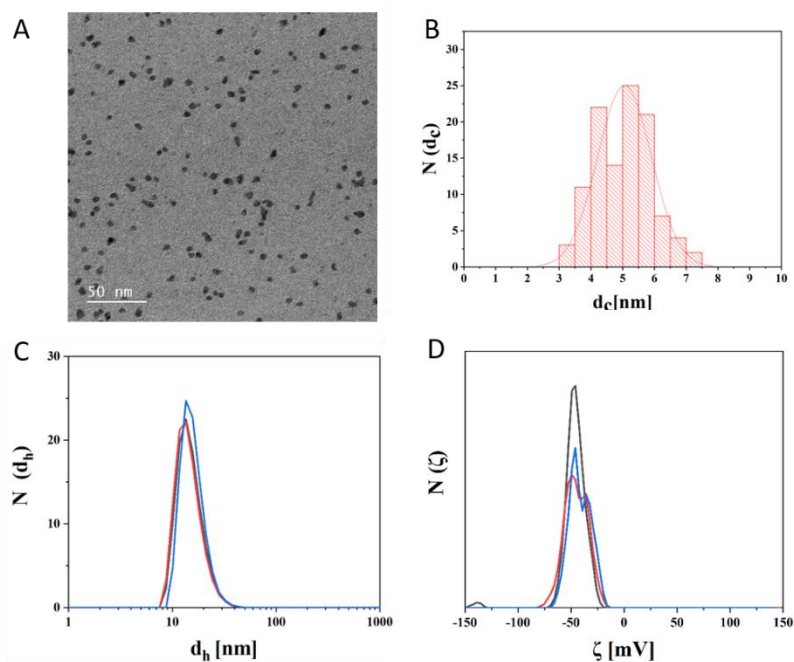


Figure 3-1. (A) The TEM of Pd NPs with PMA coating in water. (B) The respective size distribution histogram $N(d_c)$ of the Pd NPs core diameter d_c . The mean values \pm standard deviation (SD) is $d_c = 5.05 \pm 0.85$ nm. (C) Number hydrodynamic distribution $N(d_h)$ of the hydrodynamic diameter d_h in water. (D) ζ -potential distribution $N(\zeta)$ of the Pd NPs in water.

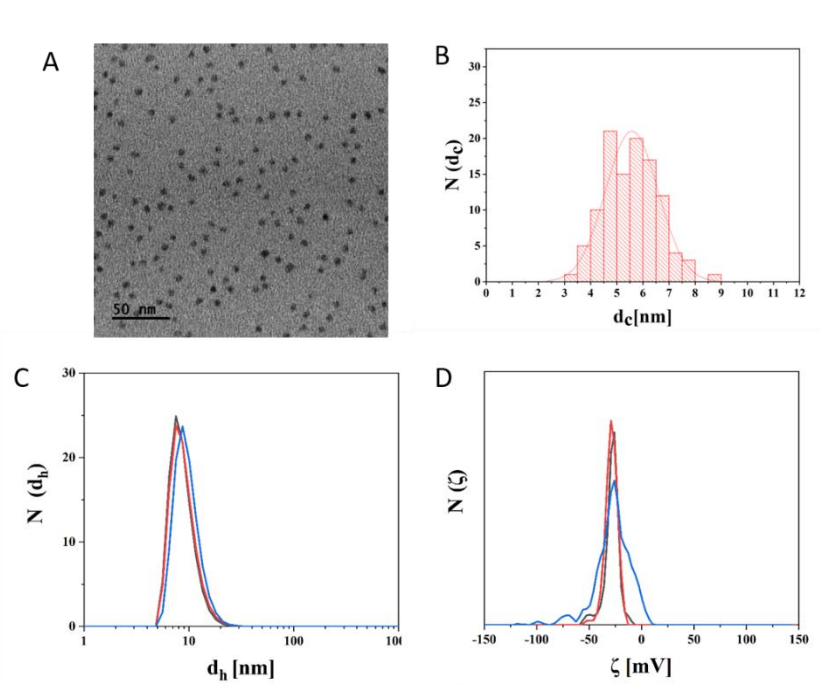


Figure 3-2. (A) The TEM of QDs with PMA coating in water. (B) The respective size distribution histogram $N(d_c)$ of the QDs core diameter d_c . The mean values \pm standard deviation (SD) is $d_c = 5.57 \pm 1.01$ nm. (C) Number hydrodynamic distribution $N(d_h)$ of the hydrodynamic diameter d_h in water. (D) ζ -potential distribution $N(\zeta)$ of the QDs in water.

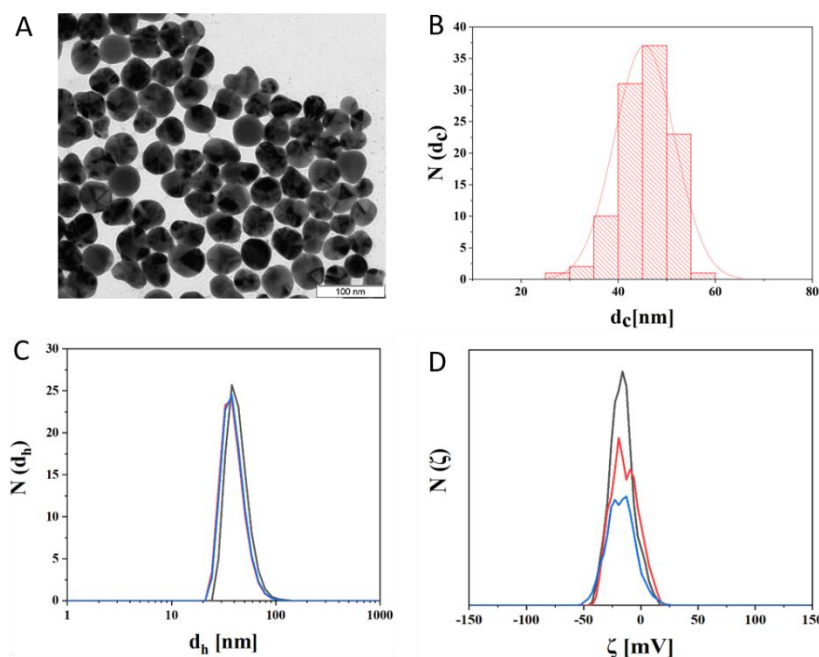


Figure 3-3. (A) The TEM of Ag NPs with PMA coating in water. (B) The respective size distribution histogram $N(d_c)$ of the Ag NPs core diameter d_c . The mean values \pm standard deviation (SD) is $d_c = 45.41 \pm 6.20$ nm. (C) Number hydrodynamic distribution $N(d_h)$ of the hydrodynamic diameter d_h in water. (D) ζ -potential distribution $N(\zeta)$ of the Ag NPs in water.

Table 3-2. The mean core diameters d_c , hydrodynamic diameters $d_{h, N}$, and zeta potentials ζ of the different NPs samples with the corresponding standard deviations.

Sample	d_c [nm]	$d_{h, N}$ [nm]	ζ [mV]
Pd NPs	5.05 ± 0.85	16.89 ± 2.22	-43.63 ± 1.85
QDs	5.57 ± 1.01	9.18 ± 0.50	-27.00 ± 2.95
Ag NPs	45.41 ± 6.20	41.99 ± 3.33	-15.73 ± 2.18

3.5.2 Colloidal stability of Pd NPs, QDs and Ag NPs

Considering the following cell experiment, the NPs stability is necessary to be investigated. It was well known that NPs agglomeration will influence experiment result. Thus, NPs stability is essential and was tested in Milli-Q water and completed cell medium by DLS as shown in Figures 3-4, 3-5 and 3-6. Briefly, Pd NPs, QDs and Ag NPs were dispersed in Milli-Q water and completed cell medium at room temperature. The number hydrodynamic diameters

distribution was recorded at 0 h and 24 h by DLS respectively. As shown in Figure 3-4, the number hydrodynamic distribution $N(d_h)$ of Pd NPs showed negligible change in Milli-Q water at 0 h and 24 h at room temperature. It also showed negligible change in completed cell medium at 0 h and 24 h at room temperature. These results indicated Pd NPs with high stability in Milli-Q water and completed cell medium. Meanwhile, the number hydrodynamic distribution of QDs and Ag NPs also showed negligible change as shown in Figures 3-5 and 3-6, indicating high stability in Milli-Q water and completed cell medium.

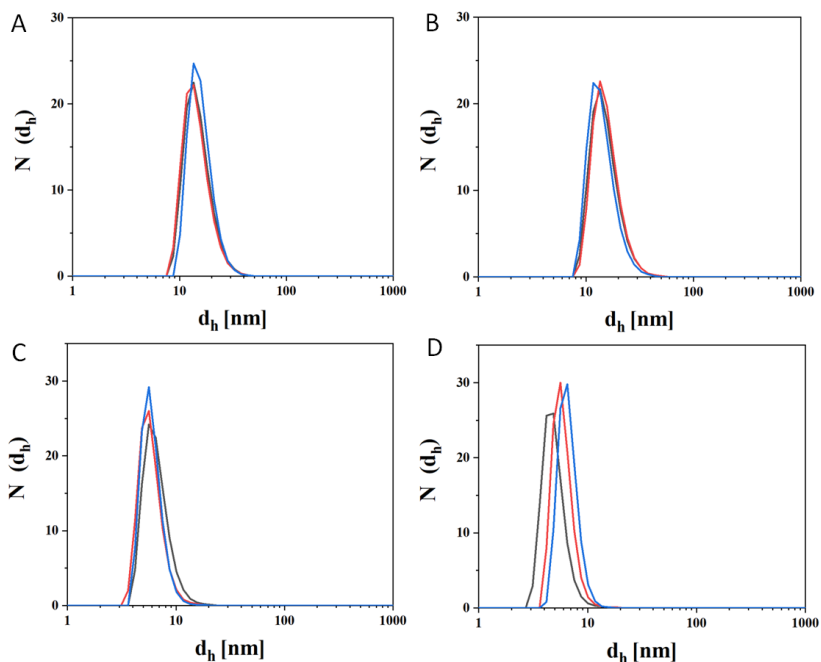


Figure 3-4. Number hydrodynamic diameter $N(d_h)$ of Pd NPs by DLS in water 0 h (A) and 24 h (B) as well as in completed medium 0 h (C) and 24 h (D).

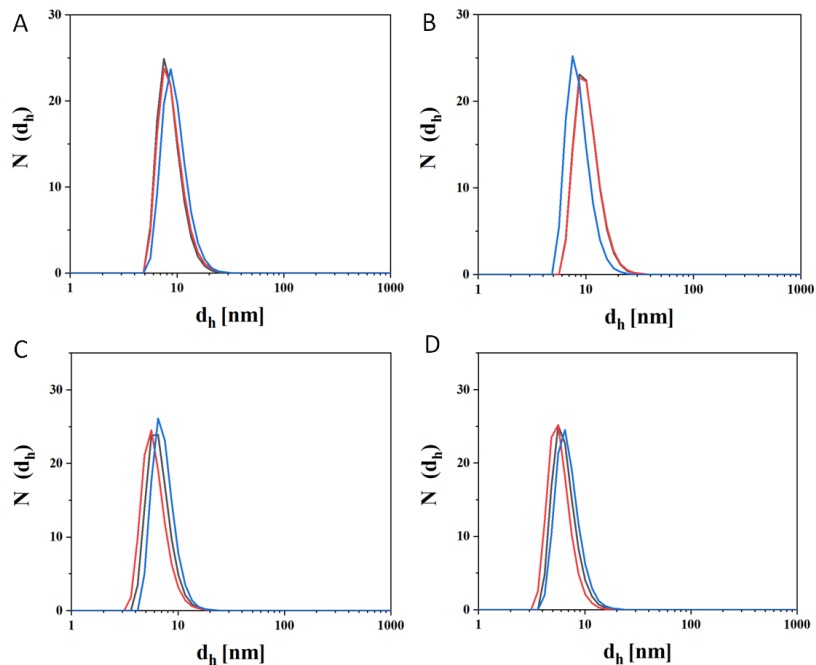


Figure 3-5. Number hydrodynamic diameter $N(d_h)$ of QDs by DLS in water 0 h (A) and 24 h (B) as well as in completed medium 0 h (C) and 24 h (D).

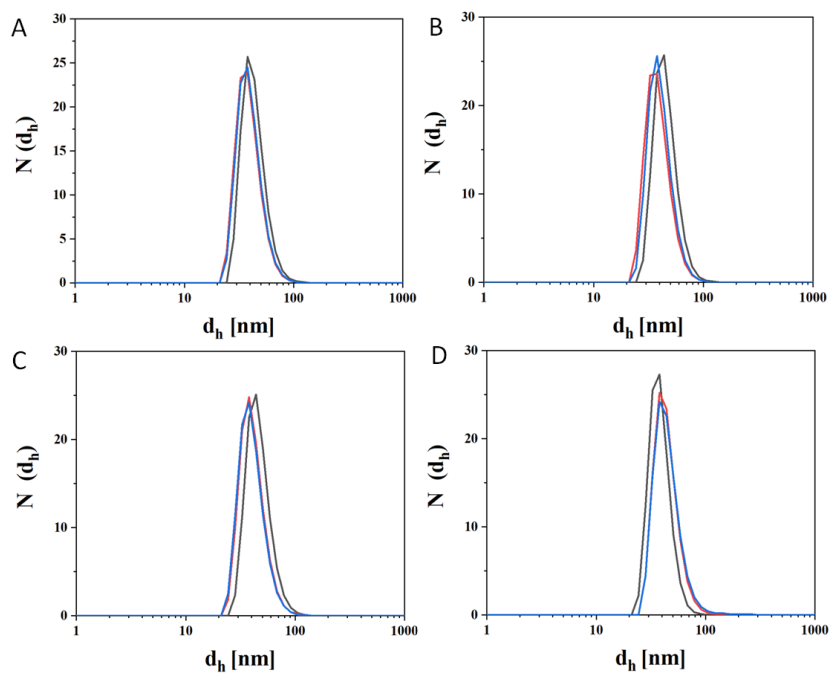


Figure 3-6. Number hydrodynamic diameter $N(d_h)$ of Ag NPs by DLS in water 0 h (A) and 24 h (B) as well as in completed medium 0 h (C) and 24 h (D).

3.5.3. Cell viability of iohexol, Pd NPs, QDs and Ag NPs

To investigate the compatibility of iohexol, Pd NPs, QDs and Ag NPs to cell *in vitro*, the cytotoxicity of iohexol, Pd NPs, QDs and Ag NPs was evaluated in CTLL-2 and MHS cells by resazurin. CTLL-2 (Figure 3-7) and MHS (Figure 3-8) cells were incubated by iohexol, Pd NPs, QDs and Ag NPs with different concentrations for 24 h at 37 °C. As shown in Figures 3-7A and 8A, the cell viability of CTLL-2 and MHS to iohexol for was not affected. It indicated that iohexol was nontoxic to CTLL-2 and MHS cells even though up to 32 mg/mL after 24 h in cell culture medium. Pd NPs cell viability was shown in Figure 3-7B and 3-8B. It showed that the cell viability was strongly affected. It means Pd NPs was toxic to CTLL-2 and MHS in high concentration. At relatively lower concentration, it was entirely safe. For QDs (Figures 3-7C and 3-8C) and Ag NPs (Figures 3-7D and 3-8D) data also showed they were toxic to CTLL-2 and MHS in high concentration and entirely safe at relatively lower concentration. Cell toxicity results showed that iohexol possessed significantly good biocompatibility. As for Pd NPs, QDs and Ag NPs, they were toxic in higher concentration and entirely safe in lower concentration.

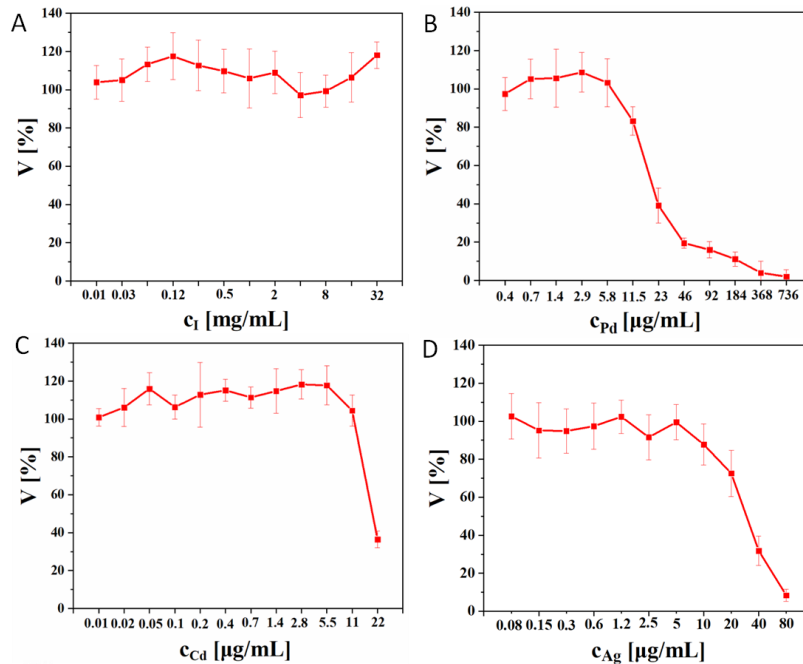


Figure 3-7. Cell viability V of CTLL-2 exposed to iohexol (A), Pd NPs (B), QDs (C) and Ag NPs (D) at different I, Pd, Cd and Ag element concentrations after 24 h by resazurin assay. Results are presented from three individual experiment.

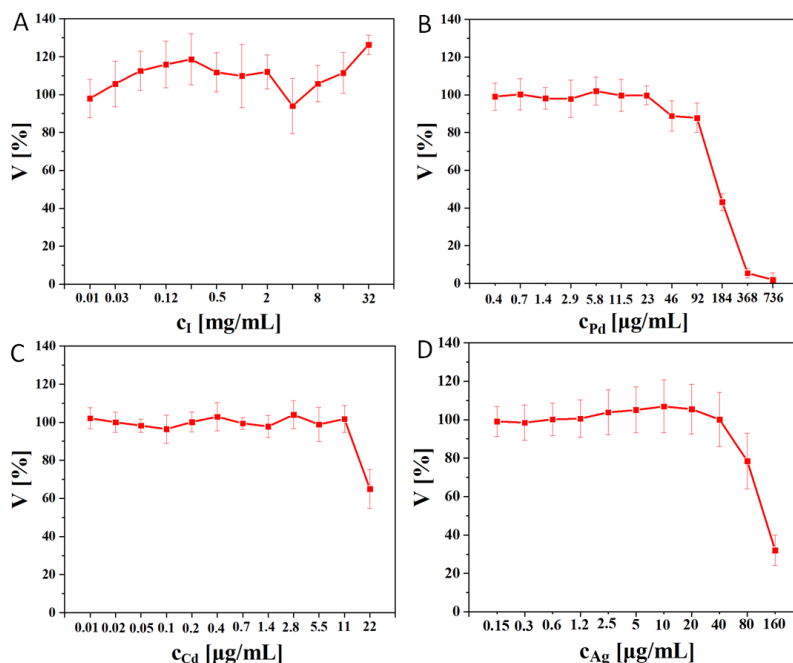


Figure 3-8. Cell viability V of MHS exposed to iohexol (A), Pd NPs (B), QDs (C) and Ag NPs (D) at different I, Pd, Cd and Ag element concentrations after 24 h by resazurin assay. Results are presented from three individual experiment.

3.5.4. Cellular live/dead staining experiment

To further study the biocompatibility of iohexol, Pd NPs, QDs and Ag NPs to cell *in vitro*, the cytotoxicity of iohexol, Pd NPs, QDs and Ag NPs was evaluated in CTLL-2 and MHS cells by live/dead staining experiment by confocal laser scanning image (CLSM). The green fluorescence indicates the live cell and the red fluorescence indicate the dead cell. As shown in Figures 3-9 and 3-11, negative control means cells were not treated by iohexol, Pd NPs, QDs and Ag NPs. Positive control means cells were killed by ethanol. Nearly all cells showed green fluorescence indicating nearly all cells alive in negative control and all cells showed red fluorescence indicating all cells dead. Meanwhile, in order to quantify analyze live cell ratio, the CLSM images were analyzed by cell profile. Then live cell number with green and dead cell number with red were gotten. According to the live and dead cell number to calculate the cell viability as shown in Figures 3-10 and 3-12.

CTLL-2 cell live/dead staining images were shown in Figure 3-9, compared with negative

control, for the iohexol, almost all cells were alive up to 16 mg/mL. At 32 mg/mL, the dead cell number slightly increased. For Pd NPs, QDs and Ag NPs, nearly all cells were alive at lower incubation concentration. With Pd NPs, QDs and Ag NPs incubation concentration increasing, the dead cell number was increased and nearly all cells dead in high incubation concentration. Quantitative cell viability based on live/dead staining image was shown in Figure 3-10. The data was closed to cell viability result (3.5.3).

MHS cell live/dead staining images were shown in Figure 3-11, compared with negative control, for the iohexol, almost all cells were alive up to 32 mg/mL. For Pd NPs, almost all cells were alive up to 140 $\mu\text{g/mL}$. For QDs and Ag NPs, with incubation concentration increasing, the dead cell also increased. Quantitative cell viability based on live/dead staining image was shown in Figure 3-12. The data was closed to cell viability result (3.5.3) except for the Pd NPs. The live/dead staining experiment showed the Pd NPs safe concentration was 140 $\mu\text{g/mL}$.

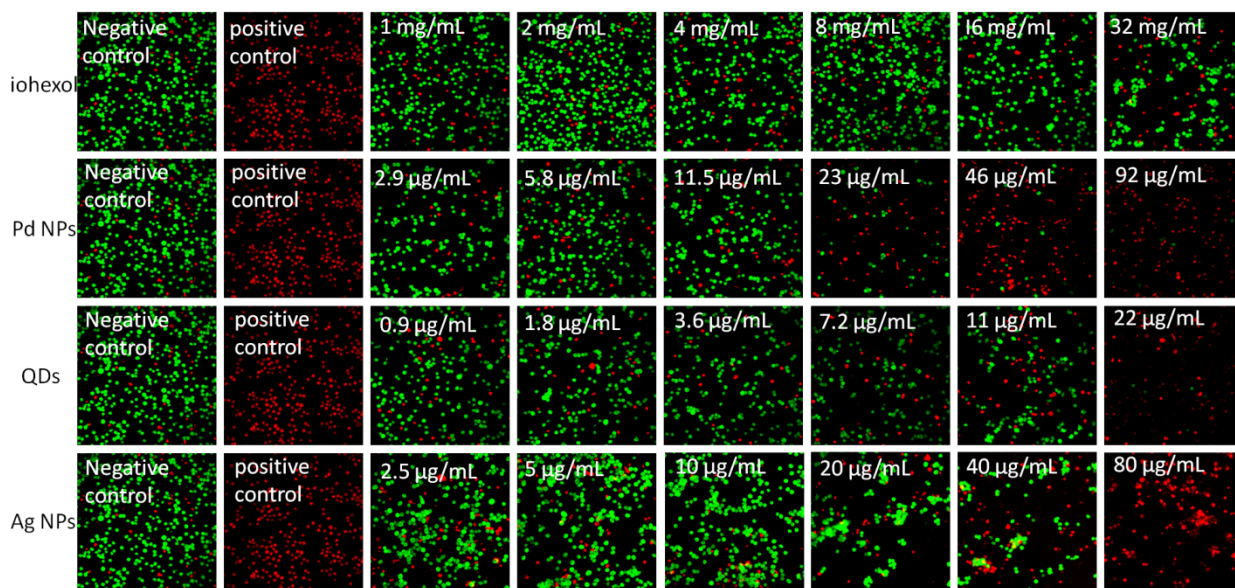


Figure 3-9. The CTLL-2 cell CLSM image exposed to iohexol, Pd NPs, QDs and Ag NPs at different I, Pd, Cd and Ag element concentrations after 24 h by live/dead staining experiment. From top to bottom is iohexol, Pd NPs, QDs and Ag NPs respectively.

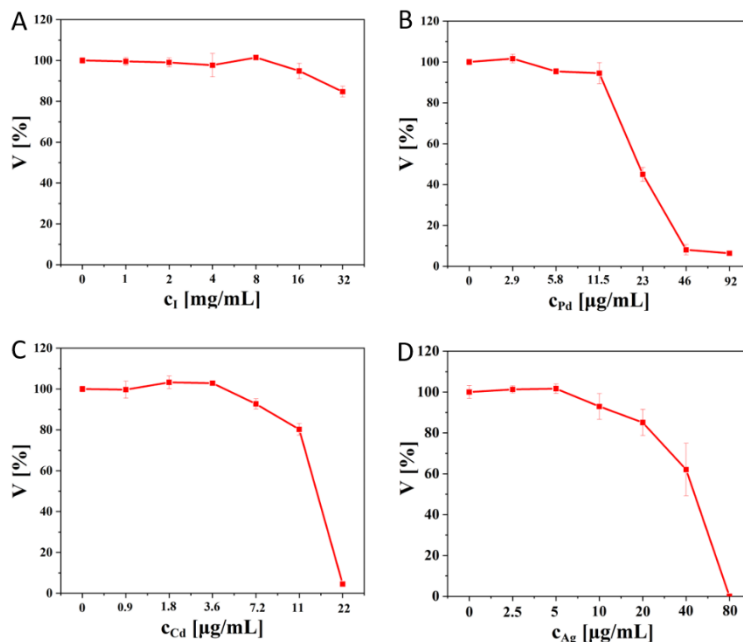


Figure 3-10. Cell viability V of CTLL-2 exposed to iohexol (A), Pd NPs (B), QDs (C) and Ag NPs (D) at different I, Pd, Ca and Ag element concentrations by cell live/dead staining assay after 24 h. Results are presented from three individual experiment.

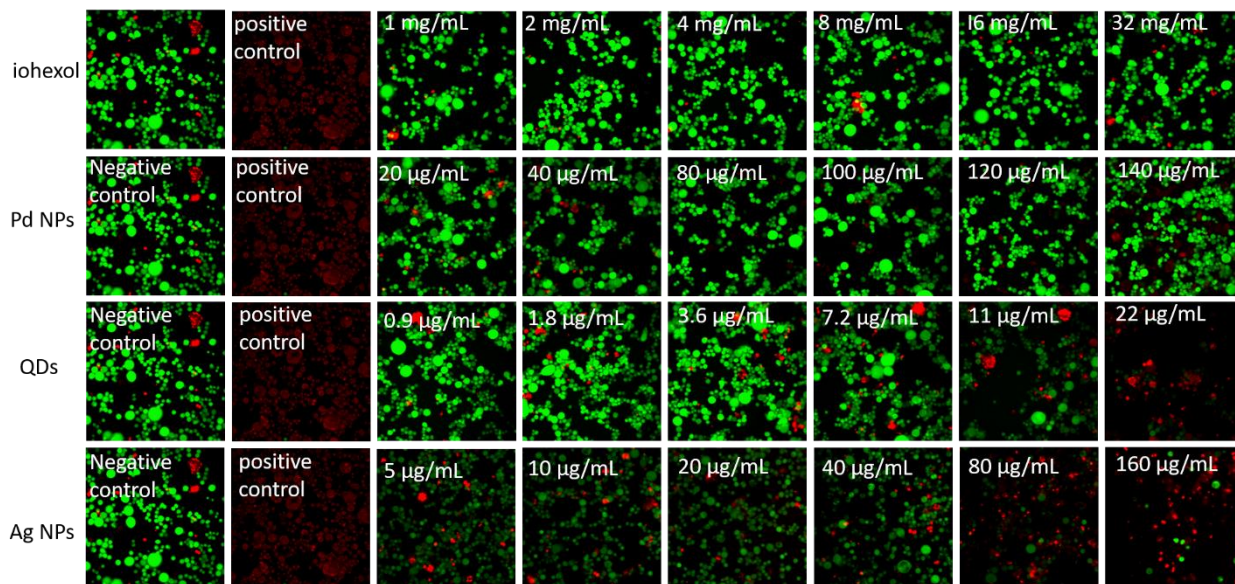


Figure 3-11. The MHS cell CLSM image exposed to iohexol, Pd NPs, QDs and Ag NPs at different I, Pd, Cd and Ag element concentrations after 24 h by live/dead staining experiment. From top to bottom is iohexol, Pd NPs, QDs and Ag NPs respectively.

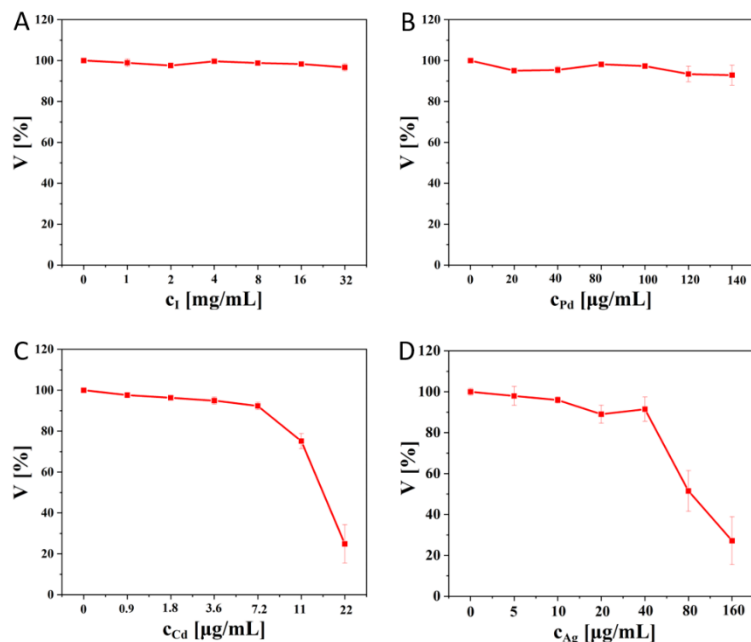


Figure 3-12. Cell viability V of MHS after 24 h exposed to iohexol (A), Pd NPs (B), QDs (C) and Ag NPs (D) at different I, Pd, Cd and Ag element concentrations by cell live/dead staining assay. Results are presented from three individual experiment.

3.5.5. Cellular uptake studied by ICP-MS

The labeling amount of cell by iohexol, Pd NPs, QDs and Pd NPs is essential for their application. Labeling amount should be as much as possible based on entirely safe incubation concentration from results (3.5.3 and 3.5.4) for synchronon based XFI. In order to probe the labeling efficacy of CTLL-2 and MHS to iohexol, Pd NPs, QDs and Ag NPs, cell uptake study was conducted and evaluated by ICP-MS. The amount of I, Pd, Cd and Ag found per cell (m_I/cell , m_{Pd}/cell , m_{Cd}/cell and m_{Ag}/cell) after exposing CTLL-2 and MHS to different concentration of I, Pd, Cd and Ag element for 6 h and 24 h as shown in Figures 3-13 and 3-14. In all cases, the cell uptake amount was concentration-dependent with incubation concentration increasing. The cell uptake amount of I was obviously higher than Pd NPs, QDs and Ag NPs. It was because incubation concentration of I much higher than other 3 element at entirely safe incubation concentration base on results (3.5.3 and 3.5.4). For CTLL-2, the cell uptake amount to NPs is similar even though their different size (Pd NPs and QDs core diameter is around 5 nm and Ag

NPs is around 45 nm). For MHS, cell uptake amount to Ag NPs is much higher than Pd NPs and QDs. Base on previously reported⁷⁶, the cell uptake amount to 50 nm NPs was also higher than 5 nm NPs for adherent cell. Comparing CTLL-2 uptake data with MHS, the CTLL-2 cell uptake amount to iohexol and NPs is lower 5-10 times than MHS at the same incubation concentration. This obvious difference of cell uptake amount can attribute to that their inherent nature difference. CTLL-2 is T cell that majorly played important role in cell-mediated immunity. However, MHS is macrophage cell which possessed the ability of ingest and process foreign materials⁸⁶. Thus the uptake study showed MHS with better uptake to iohexol and NPs.

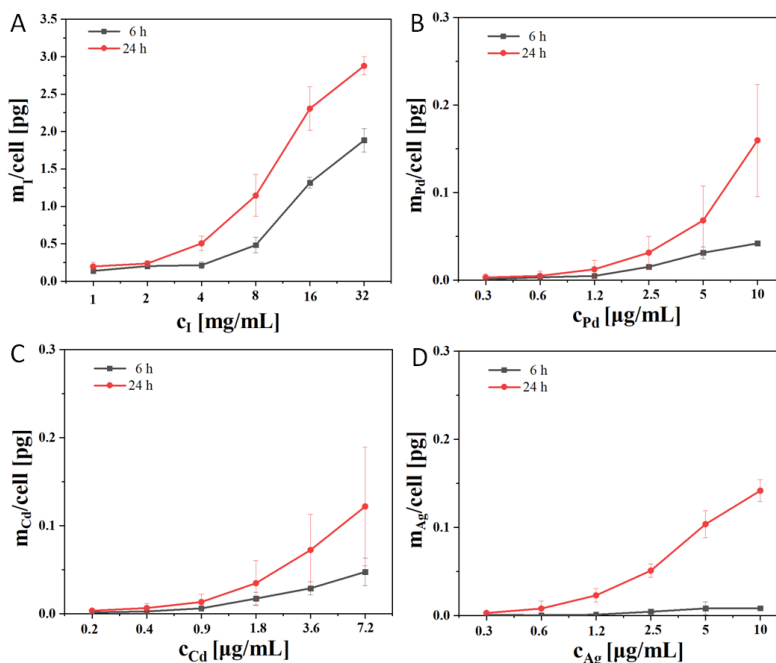


Figure 3-13. Amount of elemental found per cell in CTLL-2 exposed to iohexol (A), Pd NPs (B), QDs (C) and Ag NPs (D) at different I, Pd, Cd and Ag element concentrations after 6 and 24 h by ICP-MS. Results are presented from three individual experiment.

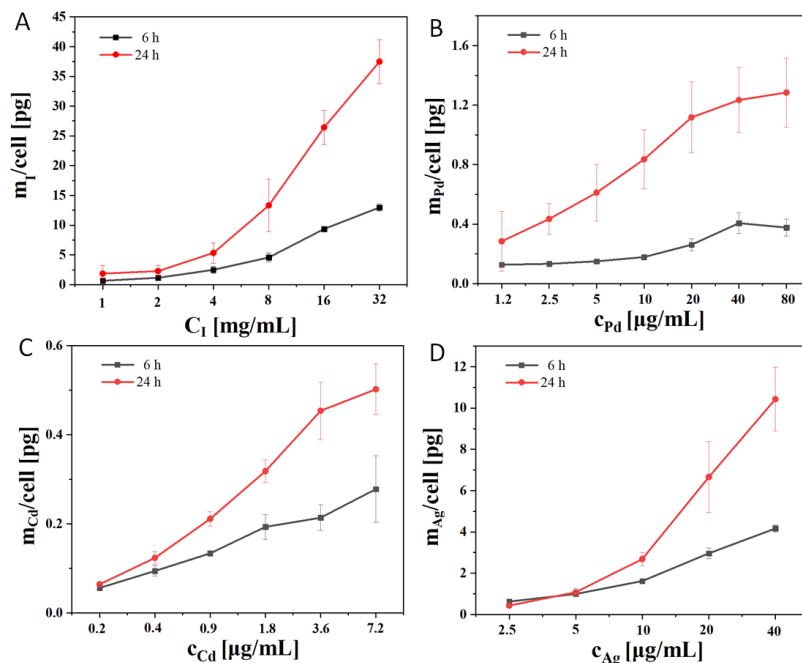


Figure 3-14. Amount of elemental found per cell in CTLL-2 exposed to iodhexol (A), Pd NPs (B), QDs (C) and Ag NPs (D) at different I, Pd, Cd and Ag element concentrations after 6 and 24 h by ICP-MS. Results are presented from three individual experiment.

3.5.6. Cellular proliferation study

As one factor influencing the cell labeling efficiency, cell division will dilute the internal iodhexol and NPs amount. It will further influence its application. Thus, cellular proliferation of CTLL-2 and MHS to iodhexol, Pd NPs, QDs and Ag NPs for 24 h was studied as shown in Figures 3-15 and 3-16. Compared with negative control (NC), the proliferation of CTLL-2 and MHS incubated with iodhexol for 24 h was not affected even though in high concentration. After incubated by Pd NPs, QDs and Ag NPs, the proliferation was not influenced at lower concentration and was obviously decreased with concentration increasing.

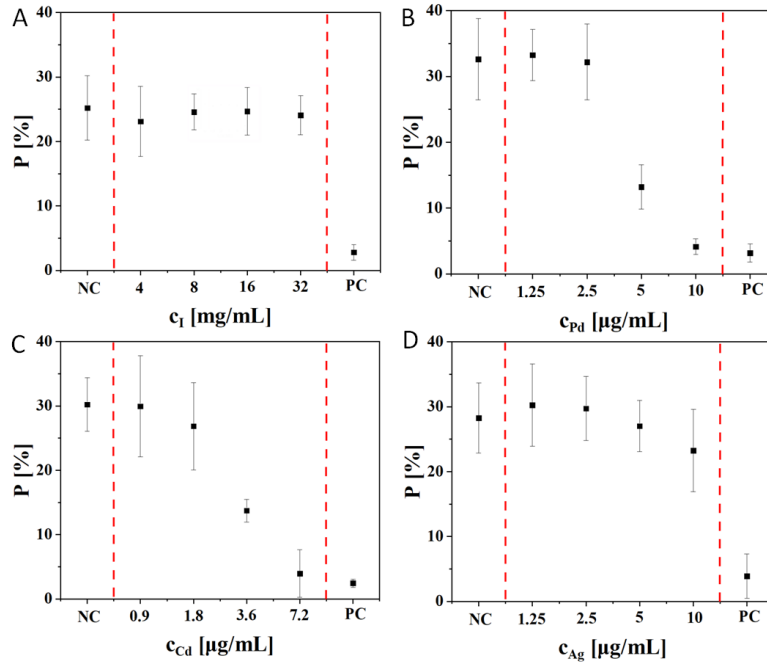


Figure 3-15. Cell proliferation P of CTLL-2 cell after 24 h exposure to (A) iohexol, (B) Pd NPs, (C) QDs and (D) Ag NPs at different I, Pd, Cd and Ag element concentrations. The colchicine was chosen as positive control (PC) and only exposed by medium as negative control (NC). Results are presented as percent proliferation P [%] (mean) from three individual experiment.

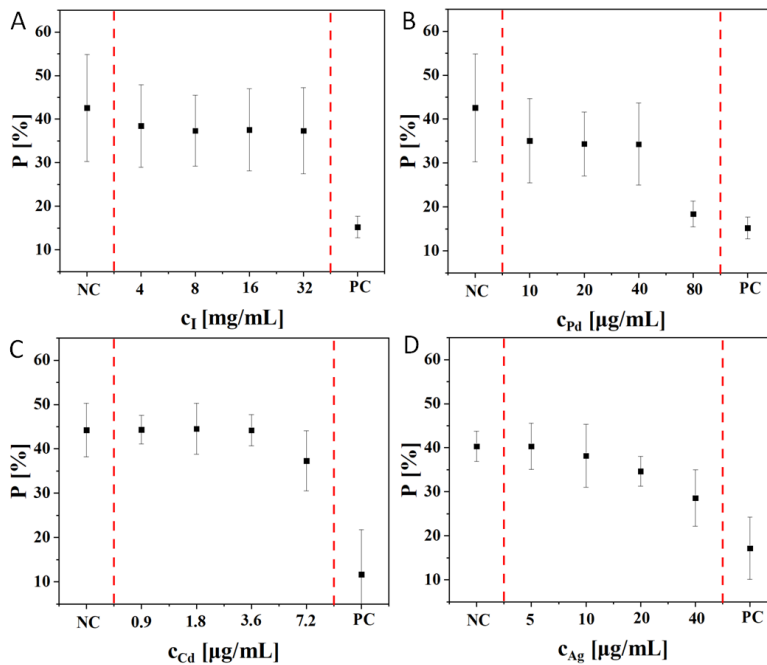


Figure 3-16. Cell proliferation P of MHS cell after 24 h exposure to (A) iohexol, (B) Pd NPs, (C)

QDs and (D) Ag NPs at different I, Pd, Cd and Ag element concentrations. The colchicine was chosen as positive control (PC) and only exposed by medium as negative control (NC). Results are presented as percent proliferation P [%] (mean) from three individual experiment.

3.5.7. Cell exocytosis study

Exocytosis as another cell process will also dilute the internalized iohexol, Pd NPs, QDs and Ag NPs. Thus, retention studies are significant to be evaluated. In this part, MHS was selected to study the exocytosis of iohexol, Pd NPs, QDs and Ag NPs. MHS was incubated iohexol, Pd NPs, QDs and Ag NPs for 24 h. Then the incubation medium was replaced by fresh new completed medium and incubate another 6 h and 24 h. As shown in Figure 3-17, it showed the retention amount of different element per cell after incubation medium replaced by fresh cell medium. With incubation time going on, the m_I/cell was strongly decreased after 24 h. The m_{Pd}/cell , m_{Cd}/cell and m_{Ag}/cell were slightly decrease after 24 h. In order to directly observe the exocytosis ratio, the exocytosis ratio was calculated based on Figure 3-17 data. As shown in Figure 3-18, the exocytosis ratio is around 40 % after 6 h and more than 90 % after 24 h for incubation by iohexol. For Pd NPs, QDs and Ag NPs, the exocytosis ratio is around 20 % after 24 h. All these data indicated that the exocytosis of iohexol was much higher than NPs. As for the exocytosis of 5 nm Pd NPs, 5 nm QDs and 45 nm Ag NPs, no obvious difference was observed.

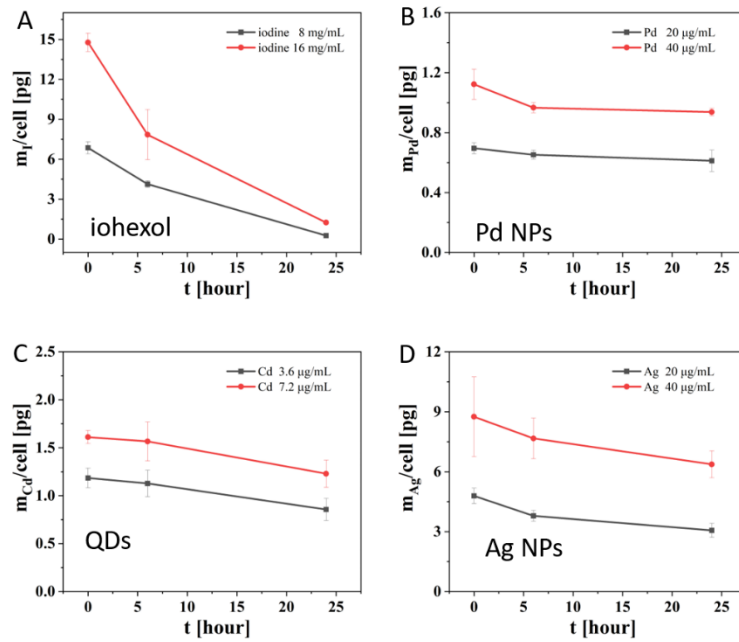


Figure 3-17. (A) Amount of I per cell m_I/cell of labeled by iohexol after incubation in cell medium for another 0, 6 and 24 h. (B) Amount of Pd per cell m_{Pd}/cell of labeled by iohexol after incubation another 0, 6 and 24 h. (C) Amount of Cd per cell m_{Cd}/cell of labeled by QDs after incubation another 0, 6 and 24 h. (D) Amount of Ag per cell m_{Ag}/cell of labeled by Ag NPs after incubation another 0, 6 and 24 h. The data was from three experiments.

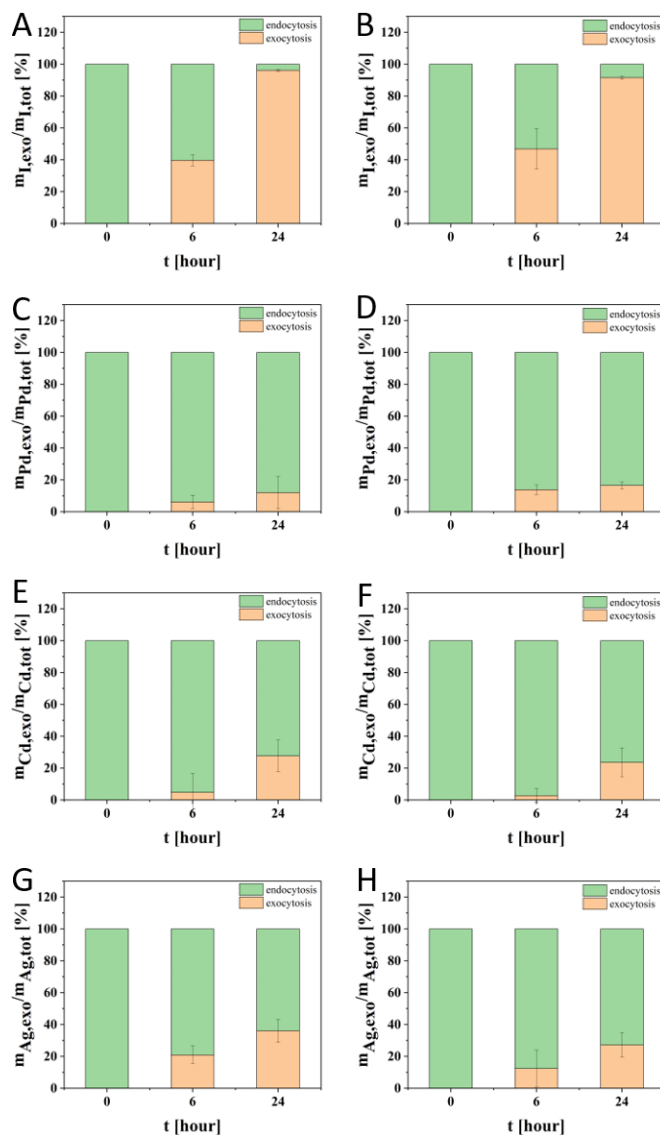


Figure 3-18. Exocytosis ratio of iohexol, Pd NPs, QDs and Ag NPs by MHS. MHS were exposed to iohexol at I concentration 8 mg/mL (A) and 16 mg/mL (B), Pd NPs at Pd concentration 20 μ g/mL (C) and 40 μ g/mL (D), QDs at Cd 20 μ g/mL (E) and 40 μ g/mL (F), Ag NPs at Ag concentration 20 μ g/mL (G) and 40 μ g/mL (H) for 24 h. Then washing away residual NPs from the medium and the outer cell membrane and continue culturing in fresh growth medium for another 0, 6 and 24 h. The data was from three experiments.

3.5.8. Cell growth and area

The cell cross-section area A_{cell} and cell division $T_{1/2,\text{cell}}$ were also possible to affect labeling amount. As shown in Figure 3-19 and Table 3-2, A_{cell} and $T_{1/2,\text{cell}}$ were experimentally determined for CTLL-2 and MHS. Results showed that the MHS A_{cell} was around 1.7 times bigger than CTLL-2. Based on cell uptake result from 3.5.5, MHS uptake to iohexol, Pd NPs, QDs and Ag NPs was higher than CTLL-2. Cell cross-section area was also one possible reason attributed to higher uptake.

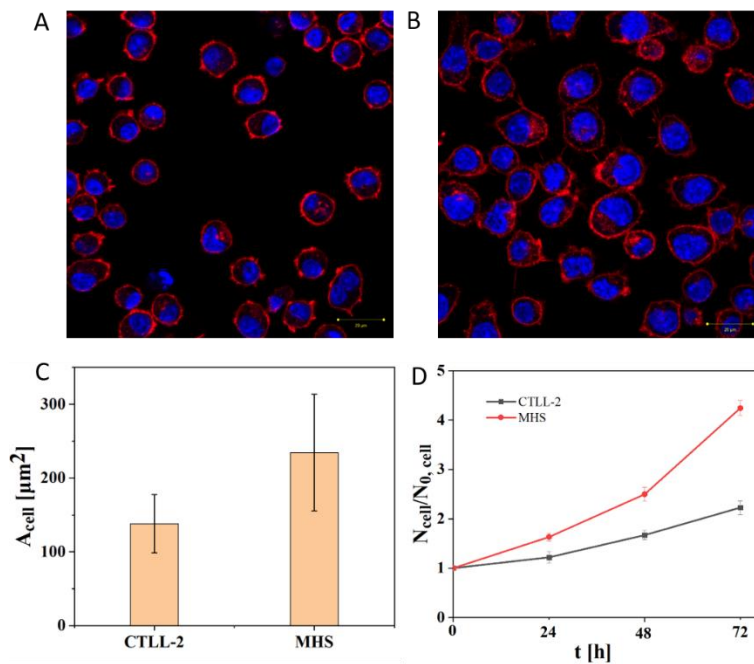


Figure 3-19. Sketch of morphology of CTLL-2 (A) and MHS (B) cells with fluorescence image which stained by cytoskeleton and nuclei. Scale bar: 20 μM . (C) Cross-section area of CTLL-2 and MHS cells (A_{cell}) which was calculated more than 200 cells by Image J. (D) Cell division as described by the time-dependent number of cells in culture N_{cell} versus the initial amount of seeded cells $N_{0,\text{cell}}$ ($N_{\text{cell}}/N_{0,\text{cell}}$).

Table 3-3. Basic characteristics of the investigated cell types comprising the cross-section area A_{cell} and the average time to cell division $T_{1/2, cell}$

	CTLL-2	MHS
$A_{cell} [\mu\text{m}^2]$	138 ± 40	234 ± 79
$T_{1/2, cell} [\text{h}]$	58 ± 5	28 ± 2

3.5.9. Transwell migration study

In order to study whether the cell migration is influenced after labeled iohexol, Pd NPs, QDs and Ag NPs, transwell migration assay was carried out. The cell migration of CTLL-2 and MHS cells incubated with iohexol, Pd NPs, QDs and Ag NPs for 24 h was investigated by porous membrane as shown in Figure 3-20 and 3-21. For CTLL-2, compared with control, cell migration was not obviously affected after labeled by iohexol and Pd NPs. Cell migration labeled by QDs and Ag NPs was slightly decreased. For MHS, in all cases, cell migration was not obviously affected after labeled by iohexol, Pd NPs, QDs and Ag NPs compared with control. Based on these data, all incubation concentration in study was tolerable for CTLL-2 and MHS.

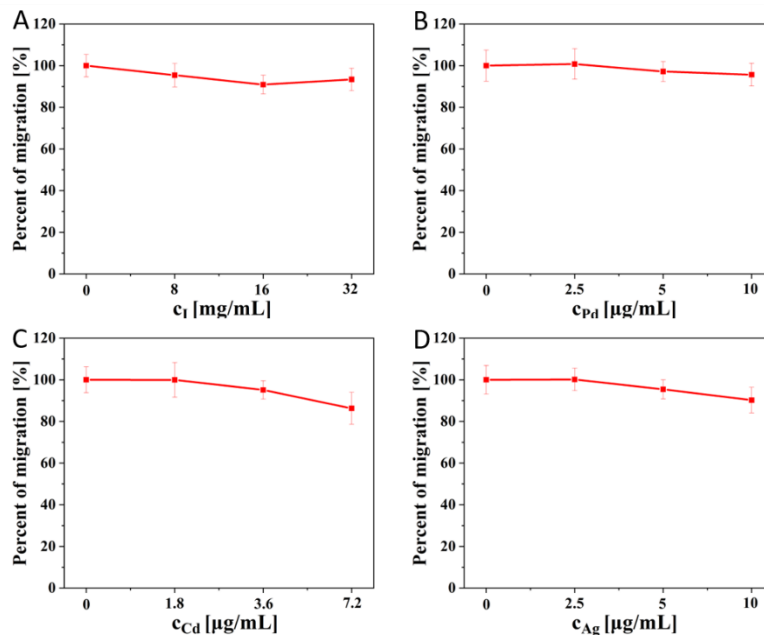


Figure 3-20. Cell migration percent of CTLL-2 cell after 24 h exposure to (A) iohexol, (B) Pd NPs, (C) QDs and (D) Ag NPs at different I, Pd, Cd and Ag element concentrations. Results are

presented as percent of migration [%] (mean) from three individual experiment.

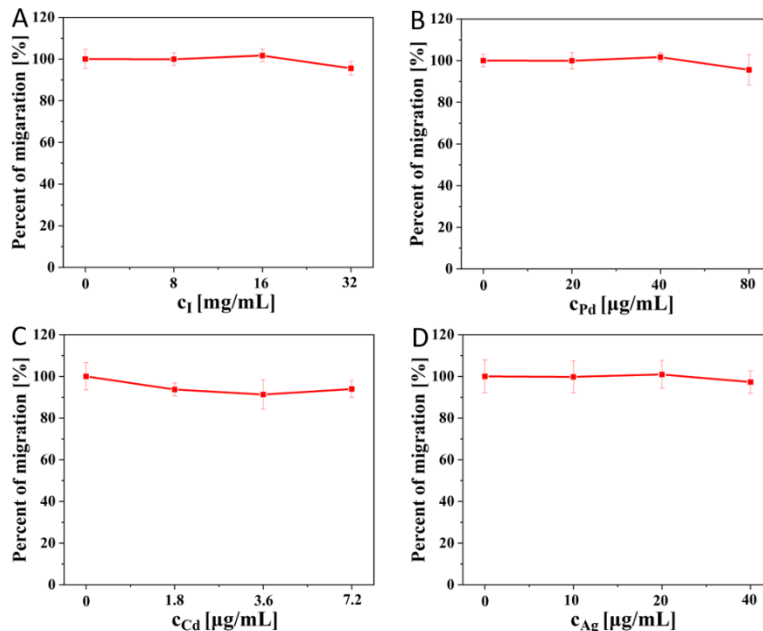


Figure 3-21. Cell migration percent of MHS cell after 24 h exposure to (A) iohexol, (B) Pd NPs, (C) QDs and (D) Ag NPs at different I, Pd, Cd and Ag element concentrations. Results are presented as percent of migration [%] (mean) from three individual experiment.

3.5.10. *In vitro* synchrotron-based XFI

Finally, synchrotron-based XFI potential of CTLL-2 and MHS labeled by iohexol and Pd NPs was explored as shown in Figure 3-22 and 3-23. For CTLL-2, no fluorescence was detected in three injection sites (o, p and q) which was CTLL-2 with lower concentration labeled by iohexol and Pd NPs. Four injection sites (k, l, m and n) signal of I (Figure 3-22A) and Pd (Figure 3-22C) was detected. And the tendency detected signal per cell by XFI was concentration dependent (Figures 3-22B and 3-22D) corresponding to ICP-MS data. But the I and Pd amount per cell from XFI was slightly higher than ICP-MS data. For MHS, 2 injection site (i and j) which cannot be detected were MHS with lower concentration labeled by iohexol and Pd NPs. 8 injection sites (a-h) signal of I (Figure 3-22A) and Pd (Figure 3-22C) were detected. And the tendency detected signal per cell by XFI was concentration dependent (Figure 3-22B and 3-22D) corresponding to ICP-MS data. I and Pd amount per cell from XFI was also corresponded with ICP-MS data very well.

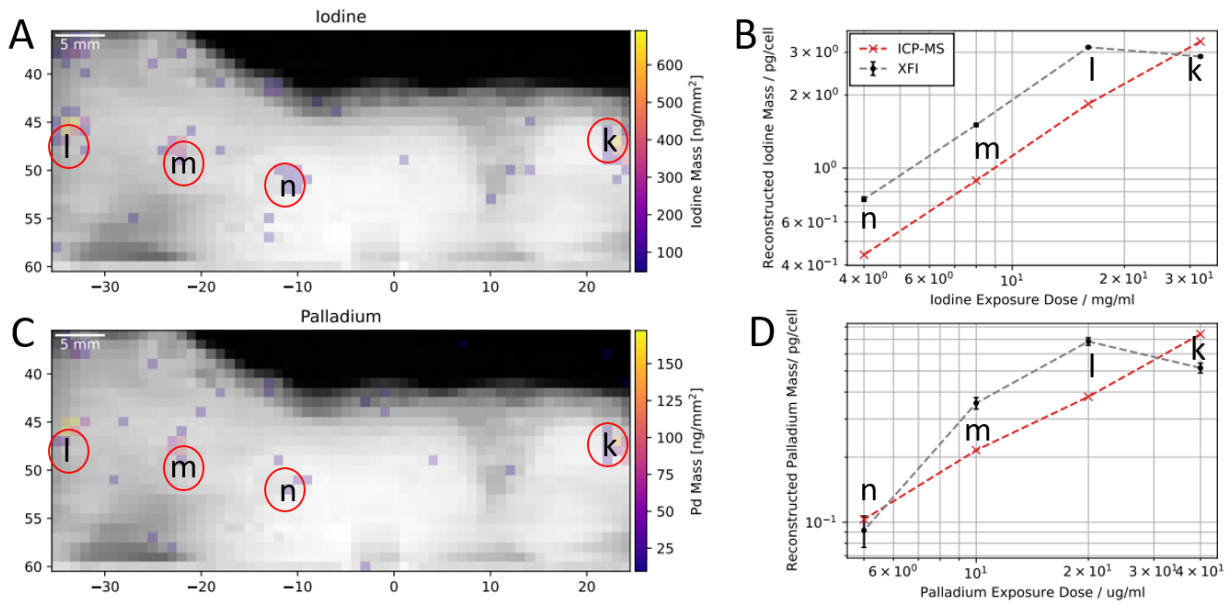


Figure 3-22. Synchrotron-based XFI image I element channel (A) and Pd element channel (C) after injection on mouse back by CTLL-2 labeled by iohexol and Pd NPs. The color bar from purple to yellow indicates gradually increase signal. (B) Amount of I per cell determined by ICP-MS and XFI. (D) Amount of Pd per cell determined by ICP-MS and XFI. Red color indicates ICP-MS data and gray color indicates XFI data. The Figure and XFI data were from Christian Körnig of Prof. Dr Florian Grüner group in University of Hamburg (UHH) and Center for Free-Electron Laser Science (CFEL).

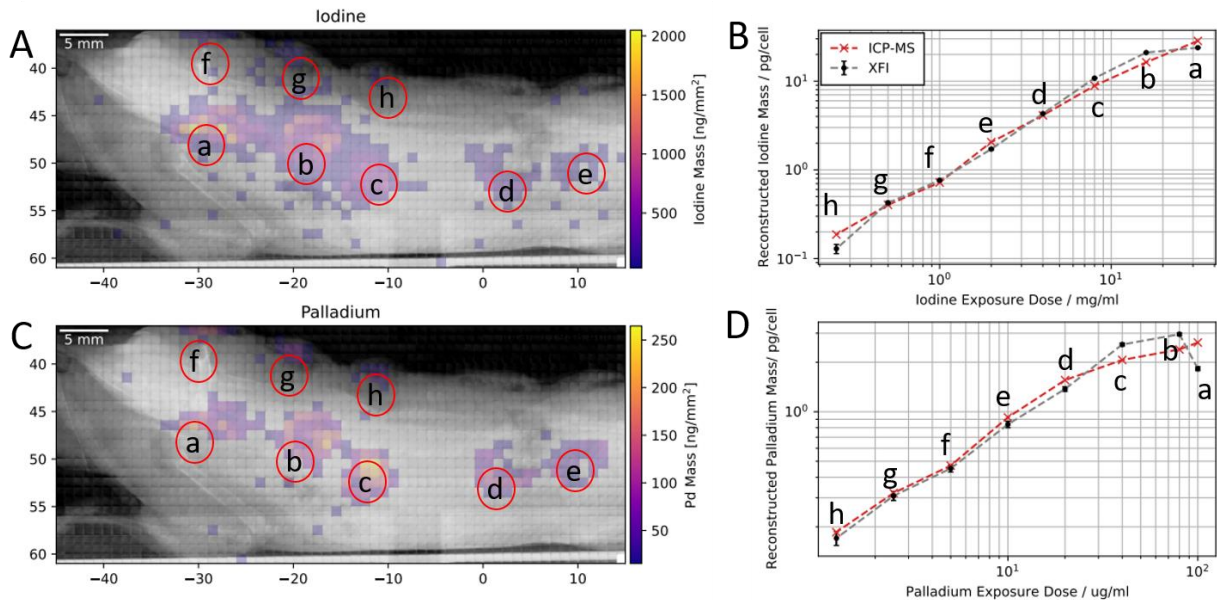


Figure 3-23. Synchrotron-based XFI image I element channel (A) and Pd element channel (C) after injection on mouse back by MHS labeled by iohexol and Pd NPs. The color bar from purple to yellow indicates gradually increase signal. (B) Amount of I per cell determined by ICP-MS and XFI. (D) Amount of Pd per cell determined by ICP-MS and XFI. Red color indicates ICP-MS data and gray color indicates XFI data. The figure and XFI data were from Christian Körnig of Prof. Dr Florian Grüner group in University of Hamburg (UHH) and Center for Free-Electron Laser Science (CFEL).

3.6. Conclusion

Considering the importance of immune cell as carrier and contrast agent in bioimaging, immune cell labeled by contrast agent was achieved and used *in vitro* XFI imaging in the present study. In our study, CTLL-2 and MHS cell were chosen as carrier. Small molecular iohexol and three NPs including Pd NPs, QDs, Ag NPs were selected as contrast agent. Preliminary study consisted of colloidal stability, cell viability, live/dead staining and cell uptake for CTLL-2 and MHS to iohexol and NPs were carried out. Results showed satisfied colloidal stability in cell medium. CTLL-2 and MHS could be effectively labeled by iohexol, Pd NPs, QDs and Ag NPs by ICP-MS measurement. Compared with CTLL-2, result indicated MHS possessed higher endocytosis to iohexol and NPs maybe due to its inherent ability of ingest. Further study including cellular proliferation and exocytosis were used to investigate cell label

efficiency to iohexol and NPs. Results indicated proliferation of CTLL-2 and MHS was not affected by iohexol but the NPs showed influence to proliferation in higher incubation concentration. Exocytosis results showed cell treated by iohexol with obvious exocytosis in short time and NPs with better retention ability in cell in long time. Finally, *in vitro* XFI results indicated CTLL-2 and MHS labeled by iohexol and Pd NPs can be successfully detected and MHS with stronger signal. In summary, MHS was more usable carrier due to it with better endocytosis to iohexol and NPs. Small molecular iohexol was suitable for short time imaging and NPs were suitable for long time imaging.

References

1. Rudramurthy, G. R.; Swamy, M. K., Potential applications of engineered nanoparticles in medicine and biology: an update. *J Biol Inorg Chem* **2018**, *23* (8), 1185-1204.
2. Shang, Y.; Hasan, M. K.; Ahammed, G. J., et al., Applications of Nanotechnology in Plant Growth and Crop Protection: A Review. *Molecules* **2019**, *24* (14).
3. Maji, S. K.; Sreejith, S.; Joseph, J., et al., Upconversion nanoparticles as a contrast agent for photoacoustic imaging in live mice. *Adv Mater* **2014**, *26* (32), 5633-8.
4. Zhou, Z.; Huang, D.; Bao, J., et al., A synergistically enhanced T(1) -T(2) dual-modal contrast agent. *Adv Mater* **2012**, *24* (46), 6223-8.
5. Hsu, J. C.; Nieves, L. M.; Betzer, O., et al., Nanoparticle contrast agents for X-ray imaging applications. *Wiley Interdiscip Rev Nanomed Nanobiotechnol* **2020**, *12* (6), e1642.
6. Kim, D.; Park, S.; Lee, J. H., et al., Antibiofouling Polymer-Coated Gold Nanoparticles as a Contrast Agent for *in vivo* X-ray Computed Tomography Imaging. *Journal of the American Chemical Society* **2007**, *129* (24), 7661-7665.
7. Park, Y. I.; Kim, J. H.; Lee, K. T., et al., Nonblinking and Nonbleaching Upconverting Nanoparticles as an Optical Imaging Nanoprobe and T1 Magnetic Resonance Imaging Contrast Agent. *Advanced Materials* **2009**, *21* (44), 4467-4471.
8. Kim, J.; Lee, Y. M.; Kang, Y., et al., Tumor-Homing, Size-Tunable Clustered Nanoparticles for Anticancer Therapeutics. *ACS Nano* **2014**, *8* (9), 9358-9367.
9. Li, Y.; Humphries, B.; Yang, C., et al., Nanoparticle-Mediated Therapeutic Agent Delivery for Treating Metastatic Breast Cancer-Challenges and Opportunities. *Nanomaterials (Basel)* **2018**, *8* (6).
10. Du, X.; Li, X.; Xiong, L., et al., Mesoporous silica nanoparticles with organo-bridged silsesquioxane framework as innovative platforms for bioimaging and therapeutic agent delivery. *Biomaterials* **2016**, *91*, 90-127.
11. Aghebati-Maleki, A.; Dolati, S.; Ahmadi, M., et al., Nanoparticles and cancer therapy: Perspectives for application of nanoparticles in the treatment of cancers. *Journal of Cellular Physiology* **2020**, *235* (3), 1962-1972.
12. Chen, L.; Liang, J., An overview of functional nanoparticles as novel emerging antiviral therapeutic agents. *Materials Science and Engineering: C* **2020**, *112*, 110924.
13. Lin, L.; Nufer, K.; Tomihara, S., et al., Non-Invasive Nanoparticle Imaging Technologies for Cosmetic and Skin Care Products. *Cosmetics* **2015**, *2* (3), 196-210.
14. Mousavi, S. Z.; Nafisi, S.; Maibach, H. I., Fullerene nanoparticle in dermatological and cosmetic applications. *Nanomedicine* **2017**, *13* (3), 1071-1087.
15. Singh, R.; Lillard, J. W., Jr., Nanoparticle-based targeted drug delivery. *Exp Mol Pathol* **2009**, *86* (3), 215-23.
16. Chen, X.; Tong, R.; Shi, Z., et al., MOF Nanoparticles with Encapsulated Autophagy Inhibitor in Controlled Drug Delivery System for Antitumor. *ACS Appl Mater Interfaces* **2018**, *10* (3), 2328-2337.
17. Yu, X.; Trase, I.; Ren, M., et al., Design of Nanoparticle-Based Carriers for Targeted Drug Delivery. *J Nanomater* **2016**, 2016.
18. Liu, R.; Lal, R., Synthetic apatite nanoparticles as a phosphorus fertilizer for soybean (Glycine max). *Sci Rep* **2014**, *4*, 5686.
19. Abdelsalam, N. R.; Kandil, E. E.; Al-Msari, M. A. F., et al., Effect of foliar application of NPK nanoparticle fertilization on yield and genotoxicity in wheat (*Triticum aestivum* L.). *Science of The Total Environment* **2019**, *653*, 1128-1139.
20. Lv, Z.; Jiang, R.; Chen, J., et al., Nanoparticle-mediated gene transformation strategies for plant genetic engineering. *Plant J* **2020**, *104* (4), 880-891.
21. Cunningham, F. J.; Goh, N. S.; Demirer, G. S., et al., Nanoparticle-Mediated Delivery towards

Advancing Plant Genetic Engineering. *Trends in Biotechnology* **2018**, *36* (9), 882-897.

22. Torney, F.; Trewyn, B. G.; Lin, V. S., et al., Mesoporous silica nanoparticles deliver DNA and chemicals into plants. *Nat Nanotechnol* **2007**, *2* (5), 295-300.
23. Sarlak, N.; Taherifar, A.; Salehi, F., Synthesis of nanopesticides by encapsulating pesticide nanoparticles using functionalized carbon nanotubes and application of new nanocomposite for plant disease treatment. *J Agric Food Chem* **2014**, *62* (21), 4833-8.
24. Pho, Q. H.; Losic, D.; Ostrikov, K., et al., Perspectives on plasma-assisted synthesis of N-doped nanoparticles as nanopesticides for pest control in crops. *Reaction Chemistry & Engineering* **2020**, *5* (8), 1374-1396.
25. Anjum, N. A.; Rodrigo, M. A. M.; Moulick, A., et al., Transport phenomena of nanoparticles in plants and animals/humans. *Environ Res* **2016**, *151*, 233-243.
26. Rajput, V.; Minkina, T.; Mazarji, M., et al., Accumulation of nanoparticles in the soil-plant systems and their effects on human health. *Annals of Agricultural Sciences* **2020**, *65* (2), 137-143.
27. Ma, X.; Yan, J., Plant uptake and accumulation of engineered metallic nanoparticles from lab to field conditions. *Current Opinion in Environmental Science & Health* **2018**, *6*, 16-20.
28. Sanchez-Cano, C.; Alvarez-Puebla, R. A.; Abendroth, J. M., et al., X-ray-Based Techniques to Study the Nano-Bio Interface. *ACS Nano* **2021**, *15* (3), 3754-3807.
29. Wang, W.-N.; Tarafdar, J. C.; Biswas, P., Nanoparticle synthesis and delivery by an aerosol route for watermelon plant foliar uptake. *Journal of Nanoparticle Research* **2013**, *15* (1), 1417.
30. Loeschner, K.; Hadrup, N.; Qvortrup, K., et al., Distribution of silver in rats following 28 d of repeated oral exposure to silver nanoparticles or silver acetate. *Particle and Fibre Toxicology* **2011**, *8* (1), 18.
31. Kreyling, W. G.; Abdelmonem, A. M.; Ali, Z., et al., *In vivo* integrity of polymer-coated gold nanoparticles. *Nature Nanotechnology* **2015**, *10* (7), 619-623.
32. Liu, Z.; Escudero, A.; Carrillo-Carrion, C., et al., Biodegradation of Bi-Labeled Polymer-Coated Rare-Earth Nanoparticles in Adherent Cell Cultures. *Chemistry of Materials* **2020**, *32* (1), 245-254.
33. Talamini, L.; Violatto, M. B.; Cai, Q., et al., Influence of Size and Shape on the Anatomical Distribution of Endotoxin-Free Gold Nanoparticles. *ACS Nano* **2017**, *11* (6), 5519-5529.
34. Judy, J. D.; Unrine, J. M.; Bertsch, P. M., Evidence for Biomagnification of Gold Nanoparticles within a Terrestrial Food Chain. *Environmental Science & Technology* **2011**, *45* (2), 776-781.
35. Nold, P.; Hartmann, R.; Feliu, N., et al., Optimizing conditions for labeling of mesenchymal stromal cells (MSCs) with gold nanoparticles: a prerequisite for *in vivo* tracking of MSCs. *J Nanobiotechnology* **2017**, *15* (1), 24.
36. Kahl, H.; Stauffer, T.; Körnig, C., et al., Feasibility of Monitoring Tumor Response by Tracking Nanoparticle-Labelled T Cells Using X-ray Fluorescence Imaging—A Numerical Study. *International Journal of Molecular Sciences* **2021**, *22* (16), 8736.
37. Li, Y.; Shaker, K.; Larsson, J. C., et al., A Library of Potential Nanoparticle Contrast Agents for X-Ray Fluorescence Tomography Bioimaging. *Contrast Media & Molecular Imaging* **2018**, *2018*, 8174820.
38. Hernandez-Viezcas, J. A.; Castillo-Michel, H.; Andrews, J. C., et al., *In situ* Synchrotron X-ray Fluorescence Mapping and Speciation of CeO₂ and ZnO Nanoparticles in Soil Cultivated Soybean (Glycine max). *ACS Nano* **2013**, *7* (2), 1415-1423.
39. Manohar, N.; Reynoso, F.; Jayarathna, S., et al., High-sensitivity imaging and quantification of intratumoral distributions of gold nanoparticles using a benchtop x-ray fluorescence imaging system. *Opt Lett* **2019**, *44* (21), 5314-5317.
40. Lv, J.; Zhang, S.; Luo, L., et al., Accumulation, speciation and uptake pathway of ZnO nanoparticles in maize. *Environmental Science: Nano* **2015**, *2* (1), 68-77.
41. Veronesi, G.; Moros, M.; Castillo-Michel, H., et al., *In vivo* Biotransformations of Indium Phosphide Quantum Dots Revealed by X-Ray Microspectroscopy. *ACS Appl Mater Interfaces* **2019**, *11* (39), 35630-

35640.

42. Lv, J.; Christie, P.; Zhang, S., Uptake, translocation, and transformation of metal-based nanoparticles in plants: recent advances and methodological challenges. *Environmental Science: Nano* **2019**, *6* (1), 41-59.
43. Chertok, B.; Moffat, B. A.; David, A. E., et al., Iron oxide nanoparticles as a drug delivery vehicle for MRI monitored magnetic targeting of brain tumors. *Biomaterials* **2008**, *29* (4), 487-96.
44. Shibu, E. S.; Ono, K.; Sugino, S., et al., Photocaging Nanoparticles for MRI and Fluorescence Imaging *in vitro* and *in vivo*. *ACS Nano* **2013**, *7* (11), 9851-9859.
45. Shin, T. H.; Kim, P. K.; Kang, S., et al., High-resolution T1 MRI via renally clearable dextran nanoparticles with an iron oxide shell. *Nat Biomed Eng* **2021**, *5* (3), 252-263.
46. Xie, J.; Chen, K.; Huang, J., et al., PET/NIRF/MRI triple functional iron oxide nanoparticles. *Biomaterials* **2010**, *31* (11), 3016-22.
47. Beik, J.; Asadi, M.; Khoei, S., et al., Simulation-guided photothermal therapy using MRI-traceable iron oxide-gold nanoparticle. *Journal of Photochemistry and Photobiology B: Biology* **2019**, *199*, 111599.
48. Hsu, J. C.; Naha, P. C.; Lau, K. C., et al., An all-in-one nanoparticle (AION) contrast agent for breast cancer screening with DEM-CT-MRI-NIRF imaging. *Nanoscale* **2018**, *10* (36), 17236-17248.
49. Betzer, O.; Shwartz, A.; Motiei, M., et al., Nanoparticle-Based CT Imaging Technique for Longitudinal and Quantitative Stem Cell Tracking within the Brain: Application in Neuropsychiatric Disorders. *ACS Nano* **2014**, *8* (9), 9274-9285.
50. Kim, D.; Jeong, Y. Y.; Jon, S., A Drug-Loaded Aptamer-Gold Nanoparticle Bioconjugate for Combined CT Imaging and Therapy of Prostate Cancer. *ACS Nano* **2010**, *4* (7), 3689-3696.
51. Kim, J.; Chh, P.; Hsu, J., et al., Use of Nanoparticle Contrast Agents for Cell Tracking with Computed Tomography. *Bioconjug Chem* **2017**, *28* (6), 1581-1597.
52. Lee, J. H.; Jun, Y. W.; Yeon, S. I., et al., Dual-mode nanoparticle probes for high-performance magnetic resonance and fluorescence imaging of neuroblastoma. *Angew Chem Int Ed Engl* **2006**, *45* (48), 8160-2.
53. Popovic, Z.; Liu, W.; Chauhan, V. P., et al., A nanoparticle size series for *in vivo* fluorescence imaging. *Angew Chem Int Ed Engl* **2010**, *49* (46), 8649-52.
54. Li, X.; Wang, C.; Tan, H., et al., Gold nanoparticles-based SPECT/CT imaging probe targeting for vulnerable atherosclerosis plaques. *Biomaterials* **2016**, *108*, 71-80.
55. Sandiford, L.; Phinikaridou, A.; Protti, A., et al., Bisphosphonate-Anchored PEGylation and Radiolabeling of Superparamagnetic Iron Oxide: Long-Circulating Nanoparticles for *in vivo* Multimodal (T1 MRI-SPECT) Imaging. *ACS Nano* **2013**, *7* (1), 500-512.
56. Zhao, L.; Li, Y.; Zhu, J., et al., Chlorotoxin peptide-functionalized polyethylenimine-entrapped gold nanoparticles for glioma SPECT/CT imaging and radionuclide therapy. *J Nanobiotechnology* **2019**, *17* (1), 30.
57. Decelle, J.; Veronesi, G.; Gallet, B., et al., Subcellular Chemical Imaging: New Avenues in Cell Biology. *Trends in Cell Biology* **2020**, *30* (3), 173-188.
58. Martínez-Criado, G.; Segura-Ruiz, J.; Alén, B., et al., Exploring Single Semiconductor Nanowires with a Multimodal Hard X-ray Nanoprobe. *Advanced Materials* **2014**, *26* (46), 7873-7879.
59. Pushie, M. J.; Pickering, I. J.; Korbas, M., et al., Elemental and Chemically Specific X-ray Fluorescence Imaging of Biological Systems. *Chemical Reviews* **2014**, *114* (17), 8499-8541.
60. Gruner, F.; Blumendorf, F.; Schmutzler, O., et al., Localising functionalised gold-nanoparticles in murine spinal cords by X-ray fluorescence imaging and background-reduction through spatial filtering for human-sized objects. *Sci Rep* **2018**, *8* (1), 16561.
61. Bulte, J. W. M.; Daldrup-Link, H. E., Clinical Tracking of Cell Transfer and Cell Transplantation: Trials and Tribulations. *Radiology* **2018**, *289* (3), 604-615.
62. Accomasso, L.; Gallina, C.; Turinetto, V., et al., Stem Cell Tracking with Nanoparticles for

Regenerative Medicine Purposes: An Overview. *Stem Cells Int* **2016**, *2016*, 7920358.

63. Kopittke, P. M.; Lombi, E.; Wang, P., et al., Nanomaterials as fertilizers for improving plant mineral nutrition and environmental outcomes. *Environmental Science: Nano* **2019**, *6* (12), 3513-3524.
64. Athanassiou, C. G.; Kavallieratos, N. G.; Benelli, G., et al., Nanoparticles for pest control: current status and future perspectives. *Journal of Pest Science* **2018**, *91* (1), 1-15.
65. El-Saadony, M. T.; Abd El-Hack, M. E.; Taha, A. E., et al., Ecofriendly Synthesis and Insecticidal Application of Copper Nanoparticles against the Storage Pest *Tribolium castaneum*. *Nanomaterials* **2020**, *10* (3), 587.
66. Ahmed, B.; Rizvi, A.; Ali, K., et al., Nanoparticles in the soil–plant system: a review. *Environmental Chemistry Letters* **2021**, *19* (2), 1545-1609.
67. Ma, Y.; He, X.; Zhang, P., et al., Xylem and Phloem Based Transport of CeO₂ Nanoparticles in Hydroponic Cucumber Plants. *Environ Sci Technol* **2017**, *51* (9), 5215-5221.
68. Coccozza, C.; Perone, A.; Giordano, C., et al., Silver nanoparticles enter the tree stem faster through leaves than through roots. *Tree Physiol* **2019**, *39* (7), 1251-1261.
69. da Cruz, T. N. M.; Savassa, S. M.; Gomes, M. H. F., et al., Shedding light on the mechanisms of absorption and transport of ZnO nanoparticles by plants via *in vivo* X-ray spectroscopy. *Environmental Science: Nano* **2017**, *4* (12), 2367-2376.
70. da Cruz, T. N. M.; Savassa, S. M.; Montanha, G. S., et al., A new glance on root-to-shoot *in vivo* zinc transport and time-dependent physiological effects of ZnSO₄ and ZnO nanoparticles on plants. *Sci Rep* **2019**, *9* (1), 10416.
71. Spielman-Sun, E.; Lombi, E.; Donner, E., et al., Impact of Surface Charge on Cerium Oxide Nanoparticle Uptake and Translocation by Wheat (*Triticum aestivum*). *Environ Sci Technol* **2017**, *51* (13), 7361-7368.
72. Deng, H.-H.; Shi, X.-Q.; Wang, F.-F., et al., Fabrication of Water-Soluble, Green-Emitting Gold Nanoclusters with a 65 % Photoluminescence Quantum Yield via Host–Guest Recognition. *Chemistry of Materials* **2017**, *29* (3), 1362-1369.
73. Zhang, Y.; Li, M.; Niu, Q., et al., Gold nanoclusters as fluorescent sensors for selective and sensitive hydrogen sulfide detection. *Talanta* **2017**, *171*, 143-151.
74. Ding, C.; Xu, Y.; Zhao, Y., et al., Fabrication of BSA@AuNC-Based Nanostructures for Cell Fluorescence Imaging and Target Drug Delivery. *ACS Appl Mater Interfaces* **2018**, *10* (10), 8947-8954.
75. Hühn, J.; Carrillo-Carrion, C.; Soliman, M. G., et al., Selected Standard Protocols for the Synthesis, Phase Transfer, and Characterization of Inorganic Colloidal Nanoparticles. *Chemistry of Materials* **2016**, *29* (1), 399-461.
76. Sun, X.; Gamal, M.; Nold, P., et al., Tracking stem cells and macrophages with gold and iron oxide nanoparticles – The choice of the best suited particles. *Applied Materials Today* **2019**, *15*, 267-279.
77. Gordy, W., A New Method of Determining Electronegativity from Other Atomic Properties. *Physical Review* **1946**, *69* (11-12), 604-607.
78. Ma, B.; Lii, J.-H.; Schaefer, H. F., et al., Systematic Comparison of Experimental, Quantum Mechanical, and Molecular Mechanical Bond Lengths for Organic Molecules. *The Journal of Physical Chemistry* **1996**, *100* (21), 8763-8769.
79. Su, Y.; Ashworth, V.; Kim, C., et al., Delivery, uptake, fate, and transport of engineered nanoparticles in plants: a critical review and data analysis. *Environmental Science: Nano* **2019**, *6* (8), 2311-2331.
80. Yamanaka, S., Pluripotent Stem Cell-Based Cell Therapy-Promise and Challenges. *Cell Stem Cell* **2020**, *27* (4), 523-531.
81. Romano, M.; Fanelli, G.; Albany, C. J., et al., Past, Present, and Future of Regulatory T Cell Therapy in Transplantation and Autoimmunity. *Front Immunol* **2019**, *10*, 43.
82. Peng, R.; Ji, H.; Jin, L., et al., Macrophage-Based Therapies for Atherosclerosis Management. *J*

Immunol Res **2020**, 2020, 8131754.

83. He, W.; Kapate, N.; Shields, C. W. t., et al., Drug delivery to macrophages: A review of targeting drugs and drug carriers to macrophages for inflammatory diseases. *Adv Drug Deliv Rev* **2020**, 165-166, 15-40.
84. Krueger, T. E. G.; Thorek, D. L. J.; Denmeade, S. R., et al., Concise Review: Mesenchymal Stem Cell-Based Drug Delivery: The Good, the Bad, the Ugly, and the Promise. *Stem Cells Transl Med* **2018**, 7 (9), 651-663.
85. Conriot, J.; Silva, J. M.; Fernandes, J. G., et al., Cancer immunotherapy: nanodelivery approaches for immune cell targeting and tracking. *Front Chem* **2014**, 2, 105.
86. Lee, H. W.; Gangadaran, P.; Kalimuthu, S., et al., Advances in Molecular Imaging Strategies for *In vivo* Tracking of Immune Cells. *Biomed Res Int* **2016**, 2016, 1946585.
87. Edmundson, M.; Thanh, N. T.; Song, B., Nanoparticles based stem cell tracking in regenerative medicine. *Theranostics* **2013**, 3 (8), 573-82.
88. Yin, F.; Fan, Y.; Xu, L., et al., Macrophages loaded with dendrimer-entrapped gold nanoparticles as a theranostic platform for CT imaging-guided combinational therapy of orthotopic osteosarcoma. *Chemical Engineering Journal* **2021**, 417, 129273.
89. Ou, Y. C.; Wen, X.; Bardhan, R., Cancer Immunoimaging with Smart Nanoparticles. *Trends Biotechnol* **2020**, 38 (4), 388-403.
90. Wang, Q.; Ma, X.; Liao, H., et al., Artificially Engineered Cubic Iron Oxide Nanoparticle as a High-Performance Magnetic Particle Imaging Tracer for Stem Cell Tracking. *ACS Nano* **2020**, 14 (2), 2053-2062.
91. Endres, P. J.; MacRenaris, K. W.; Vogt, S., et al., Quantitative Imaging of Cell-Permeable Magnetic Resonance Contrast Agents Using X-Ray Fluorescence. *Molecular Imaging* **2006**, 5 (4), 7290.2006.00026.
92. Kornig, C.; Staufer, T.; Schmutzler, O., et al., In-situ x-ray fluorescence imaging of the endogenous iodine distribution in murine thyroids. *Sci Rep* **2022**, 12 (1), 2903.
93. Pelaz, B.; Alexiou, C.; Alvarez-Puebla, R. A., et al., Diverse Applications of Nanomedicine. *ACS Nano* **2017**, 11 (3), 2313-2381.
94. Jin, T.; Guo, S.; Zuo, J. L., et al., Synthesis and assembly of Pd nanoparticles on graphene for enhanced electrooxidation of formic acid. *Nanoscale* **2013**, 5 (1), 160-3.
95. Bastús, N. G.; Merkoçi, F.; Piella, J., et al., Synthesis of Highly Monodisperse Citrate-Stabilized Silver Nanoparticles of up to 200 nm: Kinetic Control and Catalytic Properties. *Chemistry of Materials* **2014**, 26 (9), 2836-2846.

Publications

[1] **Yang Liu**, Christian G. Körnig, Bing Qi, Oliver Schmutzler, Theresa Staufer, Carlos Sanchez Cano, Elisabeth Magel, Neus Feliu*, Florian Grüner*, Wolfgang J. Parak* *“Size-dependent transport of nanoparticles in matricaria chamomilla investigated with mass spectroscopy and X-ray fluorescence imaging” (currently prepared for publication)*

[2] Carlos Sanchez-Cano, Ramon A. Alvarez-Puebla, John M. Abendroth, Tobias Beck, Robert Blick, Yuan Cao, Frank Caruso, Indranath Chakraborty, Henry N. Chapman, Chunying Chen, Bruce E. Cohen, Andre L. C. Conceição, David P. Cormode, Daxiang Cui, Kenneth A. Dawson, Gerald Falkenberg, Chunhai Fan, Neus Feliu, Mingyuan Gao, Elisabetta Gargioni, Claus-C. Glüer, Florian Grüner, Moustapha Hassan, Yong Hu, Yalan Huang, Samuel Huber, Nils Huse, Yanan Kang, Ali Khademhosseini, Thomas F. Keller, Christian Körnig, Nicholas A. Kotov, Dorota Koziej, Xing-Jie Liang, Beibei Liu, Sijin Liu, **Yang Liu**, Ziyao Liu, Luis M. Liz-Marzán, Xiaowei Ma, Andres Machicote, Wolfgang Maison, Adrian P. Mancuso, Saad Megahed, Bert Nickel, Ferdinand Otto, Cristina Palencia, Sakura Pascarelli, Arwen Pearson, Oula Peñate-Medina, Bing Qi, Joachim Rädler, Joseph J. Richardson, Axel Rosenhahn, Kai Rothkamm, Michael Rübhausen, Milan K. Sanyal, Raymond E. Schaak, Heinz-Peter Schlemmer, Marius Schmidt, Oliver Schmutzler, Theo Schotten, Florian Schulz, A. K. Sood, Kathryn M. Spiers, Theresa Staufer, Dominik M. Stemer, Andreas Stierle, Xing Sun, Gohar Tsakanova, Paul S. Weiss, Horst Weller, Fabian Westermeier, Ming Xu, Huijie Yan, Yuan Zeng, Ying Zhao, Yuliang Zhao, Dingcheng Zhu, Ying Zhu, and Wolfgang J. Parak* *“X-ray-Based Techniques to Study the Nano–Bio Interface” ACS Nano* **2021**, *15*, 3, 3754. **(published)**

[3] Christian Körnig, Theresa Staufer, Oliver Schmutzler, Tanja Bedke, Andres Machicote, Beibei Liu, **Yang Liu**, Elisabetta Gargioni, Neus Feliu, Wolfgang J. Parak, Samuel Huber and Florian Grüner,* *“In-situ x-ray fluorescence imaging of the endogenous iodine distribution in murine thyroids” Sci Rep* **2022**, *12*, 2903. **(published)**

[4] Oliver Schmutzler, Sebastian Graf, Nils Behm, Wael Y. Mansour, Florian Blumendorf, Theresa Staufer, Christian Körnig, Dina Salah, Yanan Kang, Jan N. Peters, **Yang Liu**, Neus Feliu, Wolfgang J. Parak, Anja Burkhardt, Elisabetta Gargioni, Sabrina Gennis, Sarah Chandralingam, Finn Höeg, Wolfgang Maisson, Kai Rothkamm*, Florian Schulz* and Florian Grüner* *“X-ray Fluorescence Uptake Measurement of Functionalized Gold Nanoparticles in Tumor Cell Microsamples”* Int. J. Mol. Sci. **2021**, 22, 3691. **(published)**

[5] Yanan Kang, Leroy Marwin Nack, **Yang Liu**, Bing Qi, Yalan Huang, Ziyao Liu, Indranath Chakraborty, Florian Schulz, Abdullah A. A. Ahmed, Mirco Clavo Poveda, Fereshta Hafizi, Sathi Roy, Marina Mutas, Malte Holzapfel, Carlos Sanchez-Cano, K. David Wegner, Neus Feliu & Wolfgang J. Parak* *“Quantitative considerations about the size dependence of cellular entry and excretion of colloidal nanoparticles for different cell types”* ChemTexts **2022**, 8, 9. **(published)**

Acknowledgement

Sincerely thanks will be given to Prof. Wolfgang Parak and Dr. Neus Feliu for the valuable assistance on my doctorate studies in the Center for Hybrid Nanostructure (CHyN), Chemistry department in Hamburg University.

Firstly, I would like to show my thanks to Prof. Wolfgang Parak for offering the opportunity to work in his group for my PhD study. I appreciate his guidance and continuous support about the experiment and my research.

Secondly, I would like to thank Dr. Neus Feliu for her advice in my experiment. And her constructive suggestions always helped me solving the problem. Her patience and care always make me warm in foreign land.

Thirdly, I would like to thank all group members to let me work and study in a very pleasant and friendly atmosphere.

Besides, I would like to thank Marta Gallego for measuring TEM images in CIC biomaGUNE (Spain) and Dr. Indranath Chakroborty for helping me and teaching me with ICP-MS measurements. Many thanks for Prof. Florian Grüner and his group members Christian Körnig, Theresa Stauffer and Oliver Schmutzler for the XFI work. Thanks for Christian Körnig provides the XFI image.

Lastly, I sincerely appreciate China Scholarship Council for providing the scholarship to support my overseas studies.





Abbreviation





Au	gold
KI	potassium iodide
I	iodine
Pd	palladium
Cd	cadmium
Ag	silver
NPs	nanoparticles
NCs	nanoclusters
QDs	quantum dots
DLS	dynamic light scattering
TEM	transmission electron microscopy
ICP-MS	inductively coupled plasma mass spectrometry
A _{cell}	area of cell
FBS	fetal bovine serum
BSA	Bovine serum albumin
CLSM	phosphate buffered saline
XFI	X-ray fluorescence imaging
DTT	1-dodecanethiol
TOAB	tetraoctylammonium bromide
ACC	acetylcysteine
PMA	poly (isobutylene–alt–maleic anhydride)–graft–dodecyl
ATT	6-aza-2-thiothymine
d _c	core diameter
ζ	zeta potentials
LDA	laser Doppler anemometry
d _h	hydrodynamic diameter
N (d _h)	number hydrodynamic diameter



I (d _h)	intensity hydrodynamic diameter
MHS	macrophage
CTLL-2	T cell
μ-XRF	micro-X-ray fluorescence microscopy
XANES	X-ray absorption near edge structure
FM	fluorescence microscopy
EXAFS	extended X-ray absorption fine structure



List of hazardous substances


Substance	GHS pictograms	Hazard Sentences	Precaution Sentences
RPMI-1640 medium		Not hazardous substance	
Sodium pyruvate solution		Not hazardous substance	
Penicillin/streptomycin		Not hazardous substance	
Fetal bovine serum		Not hazardous substance	
Resazurin		Not hazardous substance	
Phosphate buffered saline		Not hazardous substance	
0.05 % trypsin/EDTA		Not hazardous substance	
Fluorescein Diacetate		Not hazardous substance	
Ethdium Homo Dimer		Not hazardous substance	




1			
Corning™ T-Cell Culture Supplement with ConA (IL-2 Culture Supplement), Rat	Not hazardous substance		
gold(III) chloride trihydrate	 GHS05, GHS07 Danger	H314-H317	P280-P305 + P351 + P338-P310
Sodium hydroxide	 GHS05 Danger	H290-H314	P260-P280-P303 + P361 + P353-P304 + P340 + P310-P305 + P351 + P338
β-mercaptoethanol	 GHS05, GHS06, GHS08, GHS09 Danger	H301 + H331-H310-H315-H317-H318-H373-H410	P261-P273-P280-P301 + P310-P302 + P350-P305 + P351 + P338
Calcein	 Warning	H302 + H312 + H315 + H319 + H332 + H335	P261+ P264 +P280
Trisodium citrate	Not hazardous substance		




Bovine serum albumin	 Warning	H302	P264, P270, P301+P312, P330, and P501
6-aza-2-thiothymine	 Warning	H302+H312+H315 +H319+H335	P261, P264, P270, P271, P280, P301+P312, P302+P352, P304+P340, P305+P351+P338, P312, P321, P322, P330, P332+P313, P337+P313, P362, P363, P403+P233, P405, and P501
Acetylcysteine	 Warning	H315+H319+H335	P261, P264, P271, P280, P302+P352, P304+P340, P305+P351+P338, P312, P321, P332+P313, P337+P313, P362, P403+P233, P405, and P501
Acetic acid	 Danger	H226+H314	P210, P233, P240, P241, P242, P243, P260, P264, P280, P301+P330+P331,



			P303+P361+P353, P304+P340, P305+P351+P338, P310, P321, P363, P370+P378, P403+P235, P405, and P501
Methanol	 <p>Danger</p>	H225+H301+H311 +H331+H370	P210, P233, P240, P241, P242, P243, P260, P261, P264, P270, P271, P280, P301+P310, P302+P352, P303+P361+P353, P304+P340, P307+P311, P311, P312, P321, P322, P330, P361, P363, P370+P378, P403+P233, P403+P235, P405, and P501
Tetraoctylam monium bromide	 <p>Warning</p>	H315+H319+H335	P261, P264, P271, P280, P302+P352, P304+P340, P305+P351+P338, P312, P321, P332+P313,

			P337+P313, P362, P403+P233, P405, and P501
Sodium borohydride	 <p>Danger</p>	H260+H301+H311 +H314+H318+H332+H360	P201, P202, P223, P231+P232, P260, P261, P264, P270, P271, P280, P281, P301+P310, P301+P330+P331, P302+P352, P303+P361+P353, P304+P312, P304+P340, P305+P351+P338, P308+P313, P310, P312, P321, P322, P330, P335+P334, P361, P363, P370+P378, P402+P404, P405, and P501
poly(isobutylene-alt-maleic anhydride)	Not hazardous substance		
1-dodecanethiol	 <p>Danger</p>	H302+H304+H312 +H314+H315+H317+H318+H319+H332+H334+H335+H400+H410	P260, P261, P264, P270, P271, P272, P273, P280, P285, P301+P310, P301+P312,

			<p>P301+P330+P331, P302+P352, P303+P361+P353, P304+P312, P304+P340, P304+P341, P305+P351+P338, P310, P312, P321, P322, P330, P331, P332+P313, P333+P313, P337+P313, P342+P311, P362, P363, P391, P403+P233, P405, and P501</p>
dodecylamine	 <p>Danger</p>	<p>H302+H304+H314 +H318+H335+H37 3+H400+H410</p>	<p>P260, P261, P264, P270, P271, P273, P280, P301+P310, P301+P312, P301+P330+P331, P303+P361+P353, P304+P340, P305+P351+P338, P310, P312, P314, P321, P330, P331, P363, P391, P403+P233, P405,</p>

			and P501
CHO-PEG-SH 2000	 Warning	H302	P264, P270, P301+P312, P330, and P501
Oleylamine	 Danger	H302+H304+H314 +H335+H373+H40 0+H410	P260, P261, P264, P270, P271, P273, P280, P301+P310, P301+P312, P301+P330+P331, P303+P361+P353, P304+P340, P305+P351+P338, P310, P312, P314, P321, P330, P331, P363, P391, P403+P233, P405, and P501
Oleic acid	 Warning	H315+H319+H335	P261, P264, P271, P280, P302+P352, P304+P340, P305+P351+P338, P312, P321, P332+P313, P337+P313, P362, P403+P233, P405, and P501

1-Octadecene	 Danger	H304	P301+P310, P331, P405, and P501
Borane-morpholine	 Danger	H228+H302+H312 +H314	P210, P240, P241, P260, P264, P270, P280, P301+P312, P301+P330+P331, P302+P352, P303+P361+P353, P304+P340, P305+P351+P338, P310, P312, P321, P322, P330, P363, P370+P378, P405, and P501
Palladium acetylacetonate	 Warning	H228+H315+H319 +H335	P210, P240, P241, P261, P264, P271, P280, P302+P352, P304+P340, P305+P351+P338, P312, P321, P332+P313, P337+P313, P362, P370+P378, P403+P233, P405, and P501

Silver nitrate	 <p>Danger</p>	H272+H314+H400 +H410	P210, P220, P221, P260, P264, P273, P280, P301+P330+P331, P303+P361+P353, P304+P340, P305+P351+P338, P310, P321, P363, P370+P378, P391, P405, and P501
Tannic acid	 <p>Warning</p>	H319+H412	P264, P273, P280, P305+P351+P338, P337+P313, and P501

Declaration on oath

I hereby declare on oath, that I have written the present dissertation by my own and have not used other than the acknowledged resources and aids.

Date, Signature

23.03.2022

Yang Liu